ISAS - INTERNATIONAL SCHOOL FOR ADVANCED STUDIES

From Interface Growth to Dynamics in Disordered Media and Self Organized Criticality

Thesis submitted for the degree of
"PhilosophiæDoctor"

CANDIDATE
Marsili Matteo

SUPERVISOR
Prof. Amos Maritan

October 1994

TRIESTE

SISSA - SCUOLA INTERNAZIONALE SUPERIORE DI STUDI AVANZATI
TRIESTE
Strada Costiera 11

Contents

Chapter 1

Introduction

After Boltzmann it has become more and more evident that the laws that govern many phenomena in Nature have a statistical origin. It is the collective behavior of large ensembles of random variables, rather than the detailed microscopic dynamics, that provides the understanding of macroscopic phenomena. This observation has grown, in the last century, into the discipline of statistical mechanics. One of the highest achievements in this field, the theory of second order phase transitions, finally led to recognize the importance of scale invariance for the understanding of critical phenomena. In equilibrium statistical mechanics criticality and scale invariant are the exception as they arise only for particular values of a continuously varying parameter (e.g. temperature, magnetic field, etc.).

B. Mandelbrot [1] and P. Bak [2] recently realized that scale invariance and criticality – i.e. long range correlations in space and/or in time – are the rule in Nature rather than the exception. The geometry of coastlines and natural river networks, the distribution of galaxies and of the magnitude of earthquakes, fluctuations in economy are all examples of phenomena that lack of a characteristic length or time scale. The same applies to systems at a second order phase transition, but there are two important differences: *1)* criticality arises *spontaneously*, there is no need to tune a parameter (like temperature) to a critical value and *2)* there is no obvious free energy minimization behind these phenomena. Long range correlations are likely to be dynamically built up by the system. Even when a stationary regime of evolution is reached, its statistical nature is often intrinsically related to the dynamics that has led to it. On the contrary, detailed balance guarantees that the dynamics of the kinetic Ising model will asymptotically sample the Boltzmann equilibrium distribution $\exp\{-\beta H\}$ irrespectively of the particular dynamical prescription used.

This thesis touches on three topics of non equilibrium statistical mechanics: interface growth, dynamics in disordered media and self organized criticality. The link between these subjects is of a personal nature. I will try to convince the reader, in this introduction, that these links form a path that is not a random walk, not

completely at least.

Interface growth occurs in a very wide variety of phenomena ranging from propagation of a fire front, to growth of bacterial colonies and crystal growth by Molecular Beam Epitaxy. The interfaces dealt with in this thesis are rough. Often the roughness is a result of a far from equilibrium dynamics rather than of thermal fluctuations. For an interface growing from a substrate, the equation usually takes on the form

$$\partial_t h = \mathcal{F}(h, \nabla h, \ldots) + \eta. \tag{1.1}$$

$h(x,t)$ is the height of the interface on the point x of the D dimensional substrate, ∂_t is the partial derivative with respect to time and ∇ is the spatial gradient. Finally $\mathcal{F}$ is a functional of h and of its derivatives and $\eta(x,t)$ is a random field, that is often assumed to be gaussian with zero average and delta correlated both in x and in t. Equation (1.1) also describes the thermal dynamics by which a system with an Hamiltonian $\mathcal{H}[h]$ reaches equilibrium. In this case $\mathcal{F}[h] = -\frac{\mathcal{H}}{\delta \mathcal{H}}$ [3].

Translation invariance in the h direction is expected to hold in modeling processes such as those previously mentioned. This implies that $\mathcal{F}$ cannot depend directly on h but only on its derivatives. As a result the fluctuations of h on a portion of linear size ℓ of the substrate are expected to diverge as $\delta h \sim \ell^{\alpha}$. Indeed, consider the familiar case of the Ginzburg–Landau Hamiltonian $\mathcal{H} = \int dx[(\nabla h)^2 - m^2 h^2 + u h^4]$. The statement $\delta \mathcal{F}/\delta h = 0$ clearly implies that the *mass* term is zero ($m = 0$) and also $u = 0$. Therefore the Langevin dynamics of eq. (1.1) will sample the system exactly at the Gaussian critical point. In this sense kinetically rough interfaces are a prototype of systems that naturally contain scale invariance and critical fluctuations.

Regarding interface growth, I will discuss a general method for the derivation of stochastic partial differential equations based on the requirement of reparametrization invariance [4]. This allows a panoramic of the most physically motivated terms that can appear in the equation for a growing interface. Next we will focus on a particular equation, derived from these considerations, and we will carry out the program of the dynamic renormalization group for this equation. This equation describes processes of growth in the presence of an inclined flux of particles. The relevant mechanism of relaxation is via surface diffusion; this is a physical situation which is actually realized in Molecular Beam Epitaxy experiments.

To move on to the dynamics in a disordered medium, it is natural to consider the situation of interface growth in a random media. This has been the subject of a extraordinary activity very recently. Growth in disordered environment is relevant for a wide variety of phenomena, from fluid flow in porous media and imbibition experiments, to domain wall dynamics in disordered magnets. We borrow again the description of equation (1.1) for the interface. A noteworthy difference now is that the random term in the equation does not depend on (x,t) as before but on x and h itself. It depends on the position (x,h) of the interface in the $D+1$ dimensional space. Even in the absence of a *mass* term this would destroy translation invariance. Indeed the behavior of eq. (1.1) with $\eta = \eta(x,h)$ is similar to that of a standard statistical

model, like the Ising model. If the driving force $F = \mathcal{F}(0, 0, \ldots)$ is smaller than a critical value, the interface finally gets *pinned* by the random potential and stops. If instead F is too large the interface overcomes any obstacle the random potential η may pose and the interface moves at a constant velocity. Thus $h(x,t) \sim t$ and one recovers the situation of eq. (1.1) with $\eta(x,t)$. The properties of the system at the depinning transition, that is at the critical value of F, are of great interest. This is not only academic since the situation is an experimentally realizable one. Frequently it is simpler to control the velocity of the interface rather than the force that pushes it. Naturally at the depinning transition translation invariance, and the resulting "generic" scale invariance [5], is recovered.

The dynamic at the depinning transition is very different from the Langevin dynamic considered so far. In order to realize a model for a surface that moves infinitely slowly it is natural to consider at each discretized time step the point on the interface with the smallest pinning force (i.e. with the largest $\partial_t h$). This will indeed be the first point to move under a slowly increasing F. After updating the interface in this point we shall consider the point with the next smallest pinning force, we will move it and so on. A similar situation is realized also in the metropolis dynamics [6] of driven disordered systems at zero temperature. These dynamics involve, in the end, a global search for the minimum of a random field and will be hereafter referred to as "quenched dynamics".

Quenched dynamics is the central subject of the second chapter of this thesis. The problem one faces in the analytic treatment of disordered system is that of quenched averages. The dynamics depends on the actual realization of the noise and at the end one should take the average over all possible configurations of the noise. The first part of the chapter shows that this difficulty can be circumvented in principle, by mapping the quenched process of evolution, that is deterministic for any realization of the disorder, into a stochastic process. The transformation, in a loose sense, performs the average over all realizations of disorder consistent with a given evolution history. In practice the transformation involves very heavy calculations that become prohibitive for large systems. The method however proves to be useful in connection with approaches devised to study critical systems, as the real space renormalization group and the Fixed Scale Transformation [7]. The following two sections indeed illustrate two applications of these ideas.

Finally we come to self organized criticality. This term is probably too much abused. In a strict sense it refers to models for earthquakes and sand piles [2]. Its broad sense has undefined limits. Growing interfaces are, maybe trivially, self organized critical systems. Also models with quenched dynamics self organizes into a critical state. In the latter there is more than just power law correlations, as in interface growth, to motivate this term: there is the statistics of avalanches. An avalanche is a sequence of events of evolution that are causally and spatially connected. These macro events can be defined in models with quenched dynamics and their distribution is seen to follow power laws just as in ordinary models of self organized criticality.

The transformation of the quenched dynamics to a stochastic dynamics offers a clue for the understanding of the emergence of the power law behavior in the avalanche distributions. This is because in the transformation to a stochastic dynamics memory effects are generated. Memory, as the sensibility of local dynamics to a large period of the past history of the process, extends in these models over times that diverge with the size of the system. The work presented in the previous chapter, suggests a general method to detect memory effects in a system. It also suggests a method to inquire whether self organization in quenched dynamic is a general consequence of memory effects or whether it is a peculiar characteristic due to the presence of disorder. This amounts in devising a model that contains only memory effects, without reference to the disorder, and in investigating whether this model can reproduce the self organized critical properties observed in the corresponding model with quenched dynamics. The response of numerical analysis is affirmative. If the the memory effect is "fine tuned" to that observed in quenched dynamics, the same behavior is found within numerical uncertainty. Moreover the model also uncovers a rich scenario of self organized critical behavior arising from memory effects that extends beyond that observed for dynamics in quenched disorder. This is the final point of the detour through non equilibrium statistical mechanics presented in this thesis.

Chapter 2

Interface Growth

The best way to start a discussion on kinetic roughening is probably to write down the celebrated Kardar Parisi Zhang (KPZ) equation [8]

$$\partial_t h = \nu_s \nabla^2 h + \frac{\lambda}{2}(\underline{\nabla} h)^2 + \eta. \tag{2.1}$$

Its fame, apart from its relations with the Burger equation for fluid dynamics [8, 9] and with directed polymers in random media [8, 10], is mainly due to its implications for growing surfaces. This is indeed a description at a coarse grained (mesoscopic) level of a growing interface in a $D+1$ dimensional space. The location of the surface is specified by its height $h(\underline{x}, t)$ on the points $\underline{x}$ of a D dimensional substrate. As previously mentioned ∂_t is the partial derivative w.r.t. time whereas $\underline{\nabla}$ is the spatial gradient and $\eta(\underline{x}, t)$ is a zero average delta correlated gaussian noise.

The KPZ equation describes a self affine interface: typical fluctuations of h over a region of linear size ℓ are of the order of $\delta h \sim \ell^{\alpha}$. Eq. (2.1) can be regarded as the lowest order expansion of a more complex nonlinear equation in powers of $\underline{\nabla} h$. As long as $\alpha < 1$, which is the case for $D > 0$, this expansion is legitimate since $\underline{\nabla} h \sim \ell^{\alpha - 1}$ is small for $\ell \gg 1$. In other words, the large scale ($\ell \gg 1$) fluctuations of the interface would not be affected by the presence in eq. (2.1) of higher order spatial derivatives of h. This statement, that can be made more precise by the dynamical renormalization group approach, explains why the KPZ equation is so relevant: the terms in eq. (2.1) are the first ones[1] that are expected to appear in the expansion of the local velocity $\mathcal{F}$ in small gradients of h. The KPZ universality class then enjoys of very large domain of application.

Note that eq. (2.1) is not invariant under the reflection transformation $h \to -h$. This means that, for a fixed sign of λ, the interface distinguishes between the occupied region and the region it is going to invade. Taking the integral on the whole space,

[1] A constant term and a term proportional to $\underline{\nabla} h$ are easily absorbed in the l.h.s. by a galileian transformation

the l.h.s. yields the time derivative of the volume enclosed by the interface while in the r.h.s. the integral of the λ term gives a nonvanishing term. This means that the equation describes a growing interface or that the dynamics does not conserve the volume. There are situations in which symmetries or conservation laws are instead expected to hold. These will exclude all the terms in the expansion of $\mathcal{F}$ in powers of $\underline{\nabla} h$ that are not consistent with them. For example a $(\underline{\nabla} h)^2$ term cannot appear in the equation for the fluctuations of a soap film where volume is conserved.

In view of these considerations, M. Kardar [5] has suggested a general method to derive stochastic partial differential equations much in the spirit of the Landau's construction of effective actions in static critical phenomena. This amounts to: *i)* expand the equation of motion for small gradients of h *ii)* retain only the lowest order terms (the relevant ones) that are consistent with the symmetries and the conservation laws of the process. This method has been successfully applied in many situations in connection with the dynamic renormalization group scheme [11].

The self affine nature of the fluctuations of h, that is verified *a posteriori*, is crucial in this approach. Moreover notice that eq. (1.1) is not the most general equation that one can write down for an interface. This is because it exploits a particular parametrization of the points on the surface, that is $\vec{r} = (\underline{x}, h)$, that we will hereafter call the Monge parametrization. In particular single–valuedness of $h(\underline{x}, t)$ excludes the possibility to deal with overhangs or handles. These observations motivates the work presented in the first part of this chapter. This concerns the derivation of equations for the interface in a generic parametrization. Guided by differential geometry and by the requirement that the equation has the same form in terms of the properties that characterize the intrinsic local geometry of the surface, namely reparametrization invariance, we derive and discuss the more important terms that can appear in the growth equation. The expression in the Monge parametrization is given along with the general form and its small gradient expansion is discussed. This procedure clarifies the geometrical origins of various terms. For example we find that the nonlinear term in eq. (2.1) arises either from a pressure term or by a deposition probability that depends on the local inclination of the surface; the sign of λ is found to be opposite in the two cases. Also we find that the term $\nabla^2(\underline{\nabla} h)^2$, which has been discussed in literature [12, 13, 14], has a rather obscure physical meaning in terms of the geometric invariants of the surface. This term would be relevant in equations with volume conservation, as those for Molecular Beam Epitaxy, and cannot be ruled out by symmetry considerations alone.

The second part of the chapter discusses the scaling behavior of an equation derived with the above method. The situation is that of an interface growing in the presence of an inclined flux of particles that relaxes through surface diffusion. The results should apply to experiments of Molecular Beam Epitaxy. We apply the dynamic renormalization group scheme to one loop order and find a rich scenario with a non trivial stable fixed point. In particular an exact scaling relation yields a value for the roughness exponent in the direction perpendicular to the beam, that is in excellent

agreement with experimental results.

Quite involved calculations are used in this chapter. In order not to obscure the physical description, these have been included in the appendix. This contains also a brief discussion of the necessary elements of differential geometry and of the dynamic renormalization group scheme.

2.1 Equations for a Growing Surface and Reparametrization Invariance

The most general Langevin equation for the evolution of a surface in a $D+1$ dimensional space has the form

$$\partial_t \vec{r}(\underline{s},t) = \hat{n}\mathcal{G}[\vec{r}(\underline{s},t)] + \vec{F}(\underline{s},t). \tag{2.2}$$

where the $D+1$ dimensional vector $\vec{r}(\underline{s},t) \equiv \{r_\alpha(\underline{s},t)\}_{\alpha=1}^{D+1}$ runs over the surface as $\underline{s} \equiv \{s^i\}_{i=1}^{D}$, varies in a parameter space. In Eq. (2.2) $\hat{n}$ stands for the versor normal to the surface at $\vec{r}$ while $\mathcal{G}$ contains a deterministic growth mechanism that causes growth along the normal $\hat{n}$ of the surface and is a functional of $\vec{r}$ itself. $\vec{F}$ is a random force acting on the interface. Eq. (2.2) derives from Newton laws in the limit of a massless surface when the inertial term, $\partial_t^2\vec{r}$, can be ignored with respect to the dissipative force. Independently on the kind of physical mechanisms entering the various terms of Eq. (2.2), which therefore specify the form of $\mathcal{G}$ and the properties of $\vec{F}$, this equation has to satisfy the fundamental requirement of reparametrization invariance (R–invariance). This requires that only quantities that are independent of the choice of the parameterization $\underline{s}$, such as those referring to the inner geometry of the surface, like the curvature, can appear in the equation. As any other symmetry, reparametrization invariance poses constraints on the possible forms the equation (2.2) can take. Unlike other symmetries however this has not a physical content. It is only a statement about mathematics. In the following we will focus mainly on the physical description. For detailed calculations and the basic elements of differential geometry used in this section, we will make reference to appendix A.

The deterministic part of Eq. (2.2), as well as the noise, can be further expressed as a sum of different terms

$$\mathcal{G} = \mathcal{G}_a + \mathcal{G}_b + \ldots \quad \text{and} \quad \vec{F} = \vec{F}_a + \vec{F}_b + \ldots.$$

The derivation of the equation can then be split in the derivation of the individual terms that are expected to appear in a real physical system.

When growth occurs from a flat substrate it is convenient to describe the interface in the Monge form, i.e. with $\vec{r} = (\underline{x}, h(\underline{x}))$. $h(\underline{x})$ is the coordinate in the direction

normal to the substrate and since it must be a single valued function of $\underline{x}$ the interface cannot have overhangs. In this form (2.2) becomes

$$\partial_t h(\underline{x},t) = \sqrt{g}\,(\mathcal{G}+\eta) \tag{2.3}$$

where $g = 1 + (\underline{\nabla} h)^2$ is the determinant of the metric tensor (see A.1). $\mathcal{G}$ and η, as before, are the amplitude of the deterministic force and the noise in the normal direction respectively (note indeed that $\partial_t h(\underline{x},t)/\sqrt{g}$ is the normal velocity).

2.1.1 Deterministic part $\mathcal{G}$

Reparametrization invariance requires that $\mathcal{G}$ may depend only on intrinsic geometric properties of the interface like the mean curvature H, or eventually on scalar products of the normal $\hat{n}$ with some fixed vector $\vec{v}$ (in this case $\mathcal{G}$ is not rotational invariant).

The physical meaning of $\mathcal{G}$ is particularly evident in the case in which it can be derived from a potential

$$\partial_t \vec{r}(\underline{s},t)|_{\rm det} = -\frac{1}{\sqrt{g(\underline{s})}}\frac{\delta \mathcal{H}[\vec{r}(\underline{s})]}{\delta \vec{r}(\underline{s})} \tag{2.4}$$

where $\mathcal{H}$ is an R–invariant functional of $\vec{r}$. In this case indeed this term induces a dynamic that tends to minimize the potential energy $\mathcal{H}$ of the surface. Moreover, if the random force is properly chosen, i.e. if it is not conservative, the system approaches a steady state whose distribution of $\vec{r}$ is given by $\exp\{-\beta\mathcal{H}[\vec{r}]\}$ where β is related to the correlations of the noise [3].

R–invariance of $\mathcal{H}$ guarantees that the functional derivative in Eq.(2.4) is a vector parallel to the normal and the $1/\sqrt{g}$ factor guarantees R–invariance of the functional derivative. Indeed R–invariance of $\mathcal{H}$ implies that $\mathcal{H}[\vec{r}(\underline{s}')] = \mathcal{H}[\vec{r}(\underline{s})]$ for any reparametrization $\underline{s}'(\underline{s})$. For an infinitesimal transformation $\underline{s}' = \underline{s} + \underline{\epsilon}(\underline{s})$,

$$\vec{r}(\underline{s}') = \vec{r}(\underline{s}) + \underline{\epsilon}\cdot\underline{\partial}\vec{r}(\underline{s}) + O(\epsilon^2)$$

so that

$$\mathcal{H}[\vec{r}(\underline{s}')] = \mathcal{H}[\vec{r}(\underline{s})] + \epsilon^i \partial_i \vec{r}(\underline{s})\cdot\frac{\delta\mathcal{H}}{\delta\vec{r}}.$$

Since $\partial_i\vec{r}$ is a vector in the tangent plane, the second term in this equation vanishes for any $\underline{\epsilon}\in\mathbf{R}^D$ only if the functional derivative is parallel to the normal $\hat{n}$.

In the Monge form, if $\mathcal{G}$ derives from a potential $\mathcal{H}$, we find (see A.3)

$$\mathcal{G} = -\hat{n}\cdot\frac{1}{\sqrt{g}}\frac{\delta\mathcal{H}}{\delta\vec{r}} = -\frac{\delta\mathcal{H}}{\delta h}. \tag{2.5}$$

In the following we list the simplest possible terms that can appear in Eq. (2.2). We first give the expression in a general parameterization and then discuss the Monge form and the expansion in small gradients of $h(\underline{x},t)$.

Surface tension

The simplest physically motivated term in the Hamiltonian of a surface is proportional to the total area $\mathcal{A} = \int d^D s\sqrt{g}$ and produces a force that tends to minimize the surface area. This term is usually referred to as coming from surface tension. The functional derivative yields

$$-\frac{1}{\sqrt{g}}\frac{\delta}{\delta\vec{r}(\underline{s})}\int d^D s\sqrt{g} = \frac{1}{\sqrt{g}}\partial_i\left(\sqrt{g}g^{i,j}\partial_j\right)\vec{r}(\underline{s}) = \underset{\sim}{\Delta}\,\vec{r}(\underline{s}) \tag{2.6}$$

where $\underset{\sim}{\Delta}$ is the Beltrami–Laplace operator (A.4). Equation (A.6), if $\mathcal{H}_s = \nu_s\mathcal{A}$, yields

$$\mathcal{G}_s = \nu_s\hat{n}\cdot\underset{\sim}{\Delta}\,\vec{r} = \nu_s H \tag{2.7}$$

where H is the mean curvature. In the Monge parameterization this reads

$$\sqrt{g}\mathcal{G} = \nu_s\sqrt{g}\underline{\nabla}\cdot\frac{\underline{\nabla}h}{\sqrt{g}} \simeq \nu_s\nabla^2 h(\underline{x},t) + \ldots \tag{2.8}$$

Pressure

The second, simplest, geometric property on which $\mathcal{H}$ may depend is the volume $\mathcal{V}$ enclosed by the surface. A linear dependence on the volume physically represents a pressure term. If $\mathcal{H}_v = -\lambda\mathcal{V}$ the pressure $\lambda > 0$ encourages volume increase, while if $\lambda < 0$ the force Eq. (2.4) acts to deflate the surface. The infinitesimal volume variation on the surface element $d\sigma = d^D s\sqrt{g}$ is given by $d\sigma\hat{n}\cdot\delta\vec{r}$ so the functional derivative of $\mathcal{H}_v$ in Eq. (2.4) gives

$$\mathcal{G}_v = -\hat{n}\cdot\frac{1}{\sqrt{g}}\frac{\delta\mathcal{H}_v}{\delta\vec{r}} = \lambda \tag{2.9}$$

that in the Monge form is

$$\sqrt{g}\mathcal{G}_v = \lambda\sqrt{g} = \lambda\left[1 + \frac{1}{2}(\underline{\nabla}h)^2 + \ldots\right]. \tag{2.10}$$

Equation (2.2) with $\mathcal{G} = \mathcal{G}_a + \mathcal{G}_v$ is the R–invariant form [4] of the KPZ equation. Indeed, to lowest order in the gradient expansion, eq. (2.1) is recovered (the constant

term λ can be absorbed by redefining $h \to h + \lambda t$). The complete R–invariant KPZ equation derives from the Hamiltonian $\mathcal{H}_{KPZ} = \int d^D x(\nu_s\sqrt{g} - \lambda h)$ which, however, is unbounded from below for $h \to \infty$ ($\lambda > 0$). The expression $\exp(-\beta\mathcal{H}_{KPZ})$ for the equilibrium distribution of h is then meaningless. This is not surprising and it is related to the presence of a pressure that makes the system grow forever. In a sense the interface growth is intrinsically irreversible. Note that λ couples only to the $k = 0$ mode of h in a Fourier expansion. This would suggests that the steady state correlation functions, like $\langle[h(\underline{x}) - h(\underline{y})]^2\rangle$, are independent of λ. A derivation of the KPZ equation from the functional derivative of a free energy with a volume and a surface term, was also obtained by Grossmann et al. [15] in a rather more complex way.

External potentials

Other dependencies on $\vec{r}$ in $\mathcal{H}$ can be introduced, as the effect of an external potential. The simplest example is that of a gravitational field. The variation $\delta\mathcal{H}_g$ of the gravitational energy, if $\vec{r} \to \vec{r} + \delta\vec{r}$, is proportional to the variation of the mass $\rho d^D s\sqrt{g}\hat{n} \cdot \delta\vec{r}$ times the acceleration a_g of the gravitational field times the "height" $\hat{z} \cdot \vec{r}$, where $\hat{z}$ is the direction of the gravitational field. Then

$$\delta\mathcal{H}_g = -\nu_g \int d^D s\sqrt{g}(\vec{r} \cdot \hat{z})\hat{z} \cdot \delta\vec{r}. \tag{2.11}$$

where $\nu_g = \rho a_g$. This equation generalizes to the case of potential $V(\vec{r})$ if this is substituted to $\vec{r} \cdot \hat{z}$ in Eq. (2.11). It is easy to see that such terms in Eq. (2.2) destroy translational invariance, i.e. the equation changes if $\vec{r}(\underline{s}) \to \vec{r}(\underline{s}) + \vec{r}_0$ (unless $V(\vec{r}) = const.$ that would coincide with a pressure term). Since translational invariance is expected to hold these terms are not considered. In the Monge parameterization the gravitational energy is proportional to $\int d^D x h^2(\underline{x})$ and it brings a linear term in h in the equation of motion.

Curvature energy

It is natural to expect that the Hamiltonian depends on the curvature H of the interface. In general this dependence can be expressed in a power expansion

$$\mathcal{H}_c = -\int d^D s\sqrt{g}(\kappa_1 H + \kappa_2 H^2 + \ldots) = \mathcal{H}_{c,1} + \mathcal{H}_{c,2} + \ldots. \tag{2.12}$$

The physics behind the first term reflects the difference in the mechanical properties of the media divided by the interface. Indeed for $\kappa_1 > 0$ large positive curvatures are encouraged while negative ones are depressed. The functional derivative is carried

out in the appendix (A.5) with the result

$$\mathcal{G}_{c,1} = -\frac{1}{\sqrt{g}}\hat{n}\cdot\frac{\delta\mathcal{H}_{c,1}}{\delta\vec{r}} = -\kappa_1\left(H^2 - \sum_{i=1}^{D}\lambda_i^2\right) \tag{2.13}$$

where λ_i are the eigenvalues of the matrix of the coefficients of the second fundamental form and express the principal curvatures of the surface. Since $H = \lambda_1$ in $D = 1$, $\mathcal{G}_{c,1}$ vanishes. This is a consequence of the Gauss–Bonnet theorem that states that the integral of the Gaussian curvature K on a closed surface is a constant. Since $H = K$ in $D = 1$, the variation of $\mathcal{H}_{c,1}$ is zero.

Equation (2.13), in terms of $h(\underline{x})$, takes the form (summation on repeated indices is assumed)

$$\sqrt{g}\mathcal{G}_{c,1} = \kappa_1\sqrt{g}\partial_i\frac{\partial_i h\partial_j^2 h - \partial_j h\partial_j\partial_i h}{g} \simeq \kappa_1\left[(\nabla^2 h)^2 - \sum_{i,j=1}^{D}(\partial_i h\partial_j h)^2 + \ldots\right]. \tag{2.14}$$

In the small gradient expansion no linear term arises. This term, as expected, breaks the symmetry $h \to -h$ in the equation.

Similarly higher powers of H are easily worked out (A.5). For the p^{th} term in Eq. (2.12) we find

$$\mathcal{G}_{c,p} = -\frac{1}{\sqrt{g}}\hat{n}\cdot\frac{\delta\mathcal{H}_{c,p}}{\delta\vec{r}} = \kappa_p\left(p\underset{\sim}{\Delta}H^{p-1} + pH^{p-1}\sum_{i=1}^{D}\lambda_i^2 - H^{p+1}\right). \tag{2.15}$$

This equation generalizes Eq. (2.7), that is the $p = 0$ case, and Eq. (2.13). The effect of these terms is more transparent in the Monge parameterization. Of particular interest is the κ_2 term in the expansion of the curvature potential:

$$\sqrt{g}\mathcal{G}_{c,2} = -\kappa_2\sqrt{g}\left\{2\partial_i\frac{\partial_i\sqrt{g}H}{\sqrt{g}} + \frac{\partial_j h}{\sqrt{g}}\partial_j\left[H^2 + 2\frac{(\partial_i\sqrt{g}H)\partial_i h}{g}\right]\right\} \tag{2.16}$$

$$= -2\kappa_2(\nabla^2)^2 h + \ldots \tag{2.17}$$

Orientation energy

Up to now all the terms we have considered, apart from being invariant under reparametrizations and translations, were also rotational invariant. The simplest term which would break this invariance is

$$\mathcal{H}_z = -\int d^D s\sqrt{g}\chi(n_z) \tag{2.18}$$

where $n_z = \hat{n}\cdot\hat{z}$, $\hat{z}$ is some fixed direction in the $D+1$ dimensional space and $\chi(x)$ is a generic function. Such a term would result, for example, by imposing a constraint

on the slopes of the surface with respect to a reference substrate plane. This is often realized in restricted solid on solid (RSOS) models for interface growth. These are lattice models in which the height of the surface from the reference plane on two neighboring sites can differ only by a given number of units. Clearly, at a coarse grained level, this constraint can be expressed by a term derived from Eq. (2.18) in a continuous description. The functional derivative is easily carried out observing that the variation of $\sqrt{g}\hat{n}\cdot\hat{z}$ vanishes. This is a consequence of the fact that integration of this in $d^D s$ results in the surface area of the substrate plane, that cannot change if $\vec{r}\to\vec{r}+\delta\vec{r}$. The resulting term in the equation for $\partial_t\vec{r}$ is

$$\begin{aligned}\mathcal{G}_z &= -\frac{1}{\sqrt{g}}\hat{n}\cdot\frac{\delta\mathcal{H}_z}{\delta\vec{r}} = \frac{1}{\sqrt{g}}\partial_i\sqrt{g}\left[n_z\frac{d\chi}{dn_z}-\chi(n_z)\right]\partial^i\vec{r} \\ &= \mathrm{div}\left(n_z\frac{d\chi}{dn_z}-\chi\right)\underline{\partial}\vec{r}. \end{aligned} \tag{2.19}$$

The constraint discussed above would result in a restoring force towards a flat surface. Indeed in this case we expect that $d\chi/dx>0$ and that $\chi(x)\geq 0$ is maximum for $x=1$. The first non trivial term is the quadratic one: $\chi(n_z)=\nu_z n_z^2$. A constant term would indeed be a surface energy while a linear term has no contribution. This has essentially the same effect than the surface tension term of Eq. (2.6). This is evident from the small gradient expansion of this term in the Monge parameterization

$$\sqrt{g}\mathcal{G}_z = \nu_z\nabla\frac{\nabla h}{\sqrt{g}} = \nu_z\nabla^2 h+\ldots \tag{2.20}$$

Different situations, in which $\chi(x)$ has a maximum at some $x<1$ or is decreasing, would result in a negative "surface tension" for some values of $\hat{n}\cdot\hat{z}$. Here and in the following, if not stated otherwise, we have assumed that the direction $\hat{z}$ is the same as that along which h is measured. The case in which a different direction is singled out can be dealt with similarly or by introducing an affine Monge parameterization (see later).

The flux of particles and geometric effects

Apart from forces that can be derived from an Hamiltonian, we can also think of purely geometric effects that result in an effective force in Eq. (2.2). The simplest, non conservative, such term is one deriving from a flux of particles, whose velocity is $\vec{\Phi}$, reaching the surface and sticking to it. The external flux of incoming particles is the basic source of non conservative noise in interface growth. For this reason we consider here only the effect of the average flux $\vec{J}=\langle\vec{\Phi}\rangle$ while the fluctuation term $\vec{F}=\vec{\Phi}-\vec{J}$ will be the subject of section 2.1.2. The growth rate $\mathcal{G}_J$ produced by $\vec{J}$ is proportional to the flux of $\vec{J}$ through the surface, that is exactly a measure of how many particles have been added to the surface

$$\mathcal{G}_J = -\hat{n}\cdot\vec{J} = -Jn_J \tag{2.21}$$

where n_J is the component of $\hat{n}$ in the $\vec{J}$ direction, $J = |\vec{J}|$ and the negative sign recalls that $\hat{n}$ and $\vec{J}$ have opposite directions. When growth occurs from a vapor $\vec{\Phi}$ is almost isotropically distributed and, having zero mean, gives a vanishing contribution whereas when particles arrive at the surface in a collimated beam this is different from zero. In most situations this term can be eliminated by a Galileian transformation, as it is obvious in the framework of Monge parameterization where

$$\partial_t h|_{\text{flux}} = \sqrt{g}\mathcal{G}_J = -J_z + \vec{J}_\perp \cdot \vec{\nabla} h \tag{2.22}$$

and $\vec{J}_\perp$ is the projection of $\vec{J}$ on the substrate plane. The first term is absorbed into $\partial_t h$ by the transformation $h \to h + J_z t$ while the second disappears once $\underline{x} \to \underline{x} + \vec{J}_\perp t$.

Let us go back to the height constraint used in some discrete lattice model for the growth of interfaces. Apart from producing a surface tension term, the constraint has an effect also on the flux term. This is because deposition can only occur in local minima of the discretized surface. In the coarse grained picture minima will be rare on steep portion of the interface. Thus deposition will be less probable in steep regions than in flatter ones. In other words the constraint should reduce the flux $d\phi = -n_J d^D s\sqrt{g}$ through the infinitesimal surface element $d^D s\sqrt{g}$ if n_J is small. This is easily accounted for by multiplying Eq. (2.21) by an increasing function of n_J

$$\mathcal{G}_J = -J n_J \, \Upsilon(n_J). \tag{2.23}$$

Independently of the choice of the function $\Upsilon(x)$, provided it is increasing, this term produces, in the small gradient expansion in h, the nonlinear term of the KPZ equation. Indeed, if $\vec{J} \parallel \hat{z}$, the first term in a power expansion of (2.23) is proportional to $n_z = 1/\sqrt{g} \simeq 1 - (\underline{\nabla} h)^2/2$ which contains the non linear term of the KPZ equation with a negative λ. This result was also found by other means [16, 17]. The effect of a constraint on height differences then produces both the surface tension and the non-linear term of the KPZ equation, and thus provides a physically different derivation than that discussed previously.

The applicability of equation (2.23) extends of course to any situation where the probability for an incoming particle to stick on the surface depends on the local inclination of the surface. This can also account for the relation between the ballistic deposition model and the KPZ equation. In this model particles from a ballistic beam attach at the first site they reach in their trajectories which has a nearest neighbor surface site. The result of this mechanism is a non compact cluster with a fixed density. Even though overhangs are present in the surface, the description of the process in terms of a single valued function $h(\underline{x}, t)$ is possible, at a mesoscopic level, by considering $h(\underline{x}, t)$ as the $\hat{z}$ coordinate of the highest occupied site for each $\underline{x}$. An incoming particle may either stick at the surface or penetrate in the voids of the structure. In the latter case the deposition process will not result in an increase of $h(\underline{x}, t)$. A correction of the flux term, such as Eq. (2.23), is expected since particles that arrive on a flat portion of the interface has more chances to penetrate into the structure than those arriving on steep ones. This situation would be modeled by a

function $\Upsilon(n_z)$ that should in this case be a decreasing function of n_z, in contrast to the previous case; this would finally result, in the small gradient expansion, in a non linear term of the KPZ type but now with a positive coefficient λ.

The flux term produces an other interesting effect in situations where the atoms cannot be approximated as point particles. Recently Mazor et al. [18] have shown that the finite size of particles is relevant in Molecular Beam Epitaxy (MBE) experiments in which thin films were grown at intermediate temperatures. The basic observation is that, if the atoms have a radius ξ deposition does not actually occur on the surface but at a distance ξ from it in the normal direction. The growth rate is then proportional to the flux of the beam through a surface $\vec{r}'(\vec{s}) \doteq \vec{r}(\underline{s}) + \xi\hat{n}$ that is displaced by an amount ξ, in the normal direction, from the actual surface. The growth rate on a surface element $d\sigma = d^D s\sqrt{g}$ is proportional to the flux $d\phi = -\hat{n}' \cdot \vec{J} d^D s\sqrt{g'}$ of $\vec{J}$ through the surface $\vec{r}'$. Here the primes refer to the displaced surface. Since $\hat{n}' = \hat{n}$ the only effect comes in the $\sqrt{g}$ factor. The metric tensor $g'_{i,j}$ obtained observing that $\partial_i\vec{r}' = \partial_i\vec{r} + \xi\partial_i\hat{n}$ so that $g'_{i,j} = \partial_i\vec{r}' \cdot \partial_j\vec{r}' = g_{i,j} - 2\xi b_{i,j} + O(\xi^2)$ (see A.1). Evaluating the determinant we find that Eq. (2.21) has to be modified as follows

$$\begin{aligned} \mathcal{G}_{J'} &= \mathcal{G}_J + \mathcal{G}_\xi = \frac{d\phi}{d\sigma} \\ &= -\hat{n} \cdot \vec{J}\sqrt{\frac{g'}{g}} = -\hat{n} \cdot \vec{J}(1 - \xi H) + O(\xi^2). \end{aligned} \tag{2.24}$$

In the equation for $h(\underline{x}, t)$ a term

$$\sqrt{g}\mathcal{G}_\xi = -\nu_\xi \underline{\nabla}\frac{\underline{\nabla} h}{\sqrt{g}} = -\nu_\xi \nabla^2 h + \ldots \tag{2.25}$$

must be included in the growth equation, with $\nu_\xi = J\xi$. It is interesting to note that, despite eqs. (2.20) and (2.25) differ only by a sign, $\mathcal{G}_\xi$ does not derive from a potential as $\mathcal{G}_z$.

Surface diffusion

In cases where the binding energy of particles on the surface are large compared to thermal energy fluctuations the motion of the particles at the surface is constrained into the tangent plane. This is actually the case in many experimental realizations of MBE. A force acting in the normal direction cannot displace particles. Its effect is to change the local chemical potential μ. Differences in chemical potential on the surface in their turn produces a current, proportional to the gradient of μ, onto the surface [19]. The evolution of the surface is given by the continuity equation that the particle density ρ and this current satisfy: $\partial_t\rho \propto \hat{n} \cdot \partial_t\vec{r}$ yield the l.h.s. of Eq. (2.2) while the divergence of the current gives the r.h.s..

The mathematical translation of this argument goes as follows. The constraint that the motion of particles occurs on the surface implies that the volume it encloses

cannot change. Since

$$\partial_t \mathcal{V} = \int d^D s \frac{\delta \mathcal{V}}{\delta \vec{r}(\underline{s},t)} \partial_t \vec{r}(\underline{s},t) = \int d^D s \sqrt{g} \hat{n} \cdot [\hat{n}\mathcal{G} + \vec{\eta}(\underline{x},t)], \tag{2.26}$$

the condition $\partial_t \mathcal{V} = 0$, for the deterministic part of Eq. (2.2), implies

$$\partial_t \mathcal{V} = 0 \quad \Leftrightarrow \quad \int d^D s \sqrt{g} \mathcal{G} = 0 \tag{2.27}$$

which is satisfied if

$$\mathcal{G} = \underset{\sim}{\Delta}\, \mathcal{F} = -\underline{\mathrm{div}} \underline{\mathcal{J}} \tag{2.28}$$

In other words volume conservation requires $\mathcal{G}$ to be the (covariant) divergence of a (contravariant) current $\mathcal{J}^i$ Here $\underline{\mathcal{J}}$ is the surface current of particles and $\mathcal{F}$ is proportional to the chemical potential. This relaxation mechanism is known as surface diffusion.

The chemical potential is proportional to the force the particles experience in the normal direction. If this force derives from a potential

$$\mathcal{F} = -\frac{1}{\sqrt{g}} \hat{n} \cdot \frac{\delta \mathcal{H}}{\delta \vec{r}} \tag{2.29}$$

Having derived in the previous section the forces coming from a the most simple potential energy of an interface it is straightforward to find what is the appropriate $\mathcal{G}^c$ term in the equation for $\partial_t \vec{r}$ under surface diffusion by applying the Beltrami Laplace operator to the terms derived previously. In the Monge form, the term appearing in Eq.(2.3) has the form

$$\sqrt{g}\mathcal{G} = -\sqrt{g}\, \underset{\sim}{\Delta}\, \mathcal{F} = \sqrt{g}\, \underset{\sim}{\Delta} \frac{\delta \mathcal{H}}{\delta h} \tag{2.30}$$

where the second equality holds for growth mechanisms that can be derived from a potential.

When surface diffusion occurs to minimize the surface area, the corresponding term in Eq. (2.2) reads

$$\mathcal{G}_s^c = \mu_s \underset{\sim}{\Delta}\, \hat{n} \cdot \underset{\sim}{\Delta}\, \vec{r} = \mu_s \underset{\sim}{\Delta}\, H. \tag{2.31}$$

this term has been widely used in numerical and analytical studies of the last years [18, 20, 21]. Its expression in terms of $h(\underline{x},t)$ is

$$\sqrt{g}\mathcal{G}_s^c = -\mu_s \underset{\sim}{\Delta}\, \underset{\sim}{\nabla} \cdot \frac{\underset{\sim}{\nabla} h}{\sqrt{g}} \simeq -\mu_s (\nabla^2)^2 h + \ldots \tag{2.32}$$

A pressure instead cannot produce any surface diffusion, as is evident since this conserves the volume. External potentials, that depend on $\vec{r}$, can produce surface

diffusion. In the simplest case of the gravitational potential (along the $\hat{z}$ direction) we have

$$\mathcal{G}_g^c = \nu_g \hat{z} \cdot \hat{n} H \tag{2.33}$$

where $\nu_g = \rho a_g$ is the mass density times the gravitational acceleration. The explicit $\hat{n} \cdot \hat{z}$ factor reminds that this term breaks rotational invariance. $\mathcal{G}_g^c$ has the same form as $\mathcal{G}_\xi$, but has the opposite sign. In actual experimental situation however the gravitational energy is negligible with respect to the binding energy. It can be estimated for example that, in MBE experiments of growth of thin films, ν_g is of the order of 10^{-14} of the corresponding coefficient in the $\mathcal{G}_\xi$ term. However terms of the form

$$\sqrt{g}\mathcal{G}_g^c = \nu_g \underset{\sim}{\Delta} h = \nu_g \underline{\nabla} \cdot \frac{\underline{\nabla} h}{\sqrt{g}} \simeq \nu_g \nabla^2 h + \dots \tag{2.34}$$

with a positive ν_g has been often used in recent literature. This is principally justified by RG considerations. Also if this term is not expected at a microscopic level, it is generated in the iteration of the RG equations from the non linear terms.

Surface diffusion can be induced also by curvature dependent Hamiltonian or by orientation dependent potentials in the same manner. The explicit expression is simply given by that for the non conserved case with the additional Beltrami Laplace operator. Since these are not very interesting terms we skip a detailed analysis.

2.1.2 The noise term

As already mentioned, the principal source of randomness in interface growth comes from a flux of particles that deposit on the surface. Another kind of noise is produced by thermal fluctuations of the surface. The main difference is that, while the latter conserves the total volume enclosed by the surface. In general we can take the random force $\vec{F} = \hat{n}\eta$ in the normal direction (see the last comment of A.1) with $\langle \eta \rangle = 0$. The properties of η will now be discussed for the two different cases of non conservative and conservative noise. Our main concern is the correlator $\langle \eta(\vec{s}, t)\eta(\vec{s}', t') \rangle$. In cases when the statistics of the noise is Gaussian, as is almost always assumed, the correlator specifies all the distribution of $\eta(\vec{s}, t)$.

Non conservative noise

For a flux of particles arriving at the surface with velocity $\vec{\Phi}$, the noise term is given by $\eta = \hat{n} \cdot \delta\vec{\Phi}$ where $\delta\vec{\Phi} = \vec{\Phi} - \langle\vec{\Phi}\rangle$, which is the fluctuation of the number of particles that arrive at the surface. The correlation of η is then given by

$$\begin{aligned} \langle \eta(\vec{s}, t)\eta(\vec{s}', t') \rangle &= n_\alpha(\vec{s}, t) n_\beta(\vec{s}', t') \langle \delta\Phi^\alpha(\vec{s}, t) \delta\Phi^\beta(\vec{s}', t') \rangle \\ &= n_\alpha(\vec{s}, t) n_\beta(\vec{s}', t') \Gamma^{\alpha,\beta} \frac{\delta(\vec{s} - \vec{s}')}{\sqrt{g}} \delta(t - t'). \end{aligned} \tag{2.35}$$

Here we choose $\delta\vec{\Phi}$ to be delta correlated both in space and time. The more general choice

$$\langle \delta\Phi^{\alpha}(\vec{s},t)\delta\Phi^{\beta}(\vec{s}',t')\rangle = \Gamma^{\alpha,\beta}C(\vec{s}-\vec{s}',t-t'),$$

where $C(\underline{s},t)$ is a R–invariant function, involves no further complication, so we will use the explicit expression (2.35). The coefficients $\Gamma^{\alpha,\beta}$ are symmetric in the indices and specify the geometric properties of the noise. We may distinguish two extreme cases:

- deposition processes that occur from the condensation of an isotropic vapor and
- deposition that occurs from a collimated beam of particles.

The difference between these two possibilities fully appears in the Monge parameterization. In order to discuss this it is useful to introduce the random field

$$\tilde{\eta}(\underline{x},t) = \sqrt{g}\eta(\underline{x},t) \tag{2.36}$$

that is the one that appears explicitly in the equation for $\partial_t h$. The correlation properties of $\tilde{\eta}(\underline{x},t)$ are derived directly from those of $\eta(\underline{x},t)$ discussed above.

The correlations of $\tilde{\eta}$ are easily read off from equation (2.35)

$$\langle \tilde{\eta}(\underline{x},t)\tilde{\eta}(\underline{x}',t')\rangle = \frac{\Gamma^{z,z} - 2\partial_i h\Gamma^{i,z} + \partial_i h\partial_j h\Gamma^{i,j}}{\sqrt{g}}\delta(\underline{x}-\underline{x}')\delta(t-t') \tag{2.37}$$

If growth occurs from condensation of an isotropic vapor, we expect that $\delta\vec{\Phi}$ is a random vector with uncorrelated components and[2] $\Gamma^{\alpha,\beta} = \Gamma\delta^{\alpha,\beta}$. In equation (2.37) we find

$$\langle \tilde{\eta}(\underline{x},t)\tilde{\eta}(\underline{x}',t')\rangle = \Gamma\sqrt{g}\delta(\underline{x}-\underline{x}')\delta(t-t') \tag{2.38}$$

For growth occurring from a directed flux, one may assume that all components of $\delta\vec{\Phi}$ are independent random variables so that $\Gamma^{\alpha,\beta} = \Gamma_{\alpha}\delta^{\alpha,\beta}$ (no summation on α is assumed here). If rotational invariance is expected for rotations in the substrate plane we have $\Gamma_i = \Gamma_{||}$ and

$$\langle \tilde{\eta}(\underline{x},t)\tilde{\eta}(\underline{x}',t')\rangle = \frac{\Gamma_z + \Gamma_{||}(\underline{\nabla}h)^2}{\sqrt{g}}\delta(\underline{x}-\underline{x}')\,\delta(t-t') \tag{2.39}$$

Note that in–plane correlations are enhanced in regions where h has steep derivatives. For a collimated beam perpendicular to the interface we have $\Gamma_{||} \ll \Gamma_z$ and

$$\langle \tilde{\eta}(\underline{x},t)\tilde{\eta}(\underline{x}',t')\rangle \cong \frac{\Gamma_z}{\sqrt{g}}\delta(\underline{x}-\underline{x}')\,\delta(t-t'), \tag{2.40}$$

[2]here we use use the Kronecker symbol with both upper indices which coincides with the metric tensor $g^{\alpha,\beta}$ in the $D+1$ dimensional space.

while if $\Gamma_{||} \cong \Gamma_z$ we recover eq. (2.38). If the randomness affects only the intensity of the beam $\Gamma^{\alpha,\beta} = \Gamma J^\alpha J^\beta$ and equation (2.37) becomes

$$\langle \tilde{\eta}(\underline{x},t)\tilde{\eta}(\underline{x}',t')\rangle = \Gamma \frac{(J_z - \underline{\nabla} h \cdot \underline{J}_\perp)^2}{\sqrt{g}} \delta(\underline{x}-\underline{x}')\,\delta(t-t') \tag{2.41}$$

where $\underline{J}_\perp$ is the component of $\vec{J}$ in the substrate plane $\vec{r} = \underline{x}$. In the case of a vertical rain $J_z \gg |\underline{J}_\perp|$ and we recover the previous result.

The physical meaning the prefactors of the delta functions is evident if we introduce $\eta_o(\underline{x},t)$ such that $\langle \eta_o(\underline{x},t)\eta_o(\underline{x}',t')\rangle = \Gamma'\delta(\underline{x}-\underline{x}')\delta(t-t')$. In condensation from a vapor, Eq. (2.38), we find that $\tilde{\eta}(\underline{x},t) = g^{1/4}\eta_o(\underline{x},t)$ in Eq. (2.3). The noise is enhanced in regions where h has steep derivatives since the exposed surface area in the substrate element $d^D x$, that is $\sqrt{g}d^D x$, is larger. The opposite case is that of growth from a perpendicular beam $\vec{J} = J_z\hat{z}$ in which case $\tilde{\eta}(\underline{x},t) = g^{-1/4}\eta_o(\underline{x},t)$. This comes because the flux of $\vec{J}$ through the surface is proportional to $\hat{n}\cdot\hat{z} = 1/\sqrt{g}$ and regions with high slopes receive less particles than those that are flatter.

Conservative noise

Another source of noise comes from thermal fluctuations and from internal degrees of freedom of the interface. In this case the noise is called conservative because it causes no increase of the volume enclosed by the interface. This requirement is translated in Eq. (2.26) in the condition

$$\partial_t \mathcal{V}|_{noise} = \int d^D s \sqrt{g}\eta = 0 \tag{2.42}$$

where again we have taken $\vec{F} = \hat{n}\eta$. This poses a condition on η. The more general way to make the noise contribution in Eq. (2.42) vanish is to take

$$\eta = \underline{\mathrm{div}}\underline{\zeta}$$

where $\underline{\mathrm{div}}$ is the covariant divergence acting on $\underline{\zeta}$ that is a delta correlated noise both in space and time and in components

$$\langle \zeta_i(\underline{s},t)\zeta^j(\underline{s}',t')\rangle = \Gamma\delta_i^{\,j}\frac{\delta(\underline{s}-\underline{s}')}{\sqrt{g'}}\delta(t-t').$$

Here reparametrization invariance has been satisfied and the delta function allows the use of $g' = g(s')$ instead of $g(s)$. The correlations of $\vec{\eta}$ readily follow:

$$\begin{aligned}\langle \vec{F}(\underline{s},t)\vec{F}(\underline{s}',t')\rangle &= \frac{1}{\sqrt{gg'}}\partial_i\sqrt{g}\partial'_j\sqrt{g'}\langle\zeta^i(\underline{s},t)\zeta^j(\underline{s}',t')\rangle \\ &= \Gamma\frac{1}{\sqrt{gg'}}\partial_i\sqrt{g}g^{i,j}\partial'_j\delta(\underline{s}-\underline{s}')\delta(t-t')\end{aligned}$$

$$
\begin{aligned}
&= -\Gamma \frac{1}{\sqrt{g}} \partial_i \sqrt{g} g^{i,j} \partial_j \frac{\delta(\underline{s}-\underline{s}')}{\sqrt{g'}} \delta(t-t') \\
&= -\Gamma \underset{\sim}{\Delta} \frac{\delta(\underline{s}-\underline{s}')}{\sqrt{g'}} \delta(t-t') \qquad (2.43)
\end{aligned}
$$

where primed quantities refer to $\underline{s}'$ and the presence of the delta function has been used repeatedly to change from primed to unprimed quantities (note that the operator $\underset{\sim}{\Delta}$ does not act on g'). This is the natural generalization in reparametrization invariant form of the correlator often used in dealing with conserved noise that contains the laplacian operator acting on the delta function. The expression of the correlator in the Monge parameterization is readily derived from the above expression and deserves no further comments.

2.1.3 Discussion

We are now in a position to make some considerations. First of all we have seen that there are four different mechanisms that produces a Laplacian term $\nu\nabla^2 h$ in the small gradient expansion of Eq.(2.3). Three of them, surface tension, a orientation dependent potential (or a constraint on n_z) and surface diffusion induced by gravity, lead to a positive ν coefficient and then drive the evolution towards flatter and flatter surfaces. Note that these effects could be distinguished only from higher order terms in the gradient expansion that however are irrelevant in the RG sense. The fourth one, that results from considering the finite size of incoming particles, has a negative coefficient in front of the Laplacian, so it leads to an instability. This is evident since Eq. (2.25) can be formally derived as a surface diffusion induced by a *negative* gravitational field. This also implies that this term, as well as Eq. (2.20), strictly conserve the volume enclosed by the surface (while surface tension, eq. (2.8), does not) even though they were not derived from conservation considerations.

Secondly we note that the non linear term of the KPZ equation (2.1), can be derived in either of two ways: from a pressure term in a potential, that gives a positive λ for a growing surface, or from an inclination dependent factor in the flux term. The latter may result as the effect of a constraint on n_z, yielding a negative λ, in agreement with known results. It has also been argued that such a term is expected in ballistic deposition but with the opposite effect, i.e. inhibiting growth on flat portions of the surface. A positive λ is expected in this case. The change of sign in this coefficient does not change the character of the process dramatically (as it is for ν). The value of λ however is a directly measurable quantity [17] since it is related to the inclination dependence of the velocity of growth $v(\underline{u})$. This is defined as the average of $\partial_t h(\underline{x}, t)$ over $\underline{x}$. Equation (2.1), for an interface growing from a flat substrate, yields

$$
v(0) = \frac{\lambda}{2} \langle (\underline{\nabla} h)^2 \rangle .
$$

If in this equation we substitute $h \to h + \underline{u} \cdot \underline{x}$, that would be appropriate for an opportune inclination of the substrate, we find that the inclination dependent growth velocity $v(\underline{u}) = v(0) + \lambda u^2/2$ from which

$$\lambda = \frac{1}{D} \nabla^2_{\underline{u}} v(\underline{u}).$$

Analyzing the behavior of $v(\underline{u})$ Krug were able to predict the presence of the non linear term of the KPZ equation in various models. In connection with our arguments we note that while this is a criterion based on the global behavior, our is based on the local properties of the growth process. Other derivations of the KPZ equations for these models were based on the relation with the polymer problem in a random environment [16].

Equation (2.17) provides a further physical derivation of a term $(\nabla^2)^2 h$ in the equation for a growing interface. This term has been usually associated with surface diffusion. This extends the validity of the results derived in the presence of this term to situations where the restoring force is derived from a potential surface energy proportional to H^2. However, while there are symmetry considerations for the absence of a linear term in the expansion of the potential in powers of H, this in general will contain the zero$^{\text{th}}$ order term, i.e. surface tension, that dominates the dynamics.

T. Sun et al. [12] studied an equation with a linear term proportional to $(\nabla^2)^2 h$ and a non linear term proportional to $\nabla^2(\underline{\nabla} h)^2$. The same equation was studied in refs. [13, 14]. This is in a loose sense the conserved version of the KPZ equation (also a conservative noise was considered). We note here that while the first term could be derived from surface diffusion or from a potential proportional to H^2, the non linear one is not related to one of the simple mechanisms discussed here. In particular a derivation of the *conserved* KPZ equation cannot follows the same lines described above. In one case because the KPZ equation comes out as a result of a process that does not conserve the volume. When the KPZ derives from the effect of a constraint on height gradients, one should motivate the rather odd choice $\Upsilon(n_z) = -\underset{\sim}{\Delta}\, \Upsilon(n_z)$. There are no R–invariant potentials that would lead to such term in the gradient expansion, neither under conservative or non conservative dynamics. It is still possible however that such a term is generated dynamically in a RG procedure.

It would be interesting to analyze the effect of the term resulting from a potential linear in H, eq. (2.14), in a RG scheme.

A point worth of discussion with respect to the noise term lies in the presence of prefactors in front of the random field. In a small gradient expansion these yield a nonlinear term of the KPZ type with a random valued λ, that could eventually be relevant in a RG calculation.

2.2 Renormalization Group Study of Growth Processes With an Oblique Incident Flux

The principal theme of this section is a renormalization group (RG) analysis of growth processes arising from an oblique flux of incident atoms. Such growth processes are commonly encountered in molecular beam epitaxy (MBE) experiments [22, 23] and growth arising from ballistic deposition processes [24]. MBE has been studied both by stochastic partial differential equations [25, 19, 26, 20, 27, 13] and by computer simulation [24, 26, 28, 29, 30]. Among the latter ballistic aggregation in the presence of an oblique incident flux was studied [24], but the effects of surface diffusion were not included. In the former, while including surface diffusion, only a normal incident flux was considered.

Our principal result is the elucidation of a rich behavior involving a novel growth regime that ultimately crosses-over to the familiar Edwards-Wilkinson (EW) universality class [31]. We calculate the scaling exponents of the new class of behavior to one-loop order in a $D = 6 - \epsilon$ calculation. Our results are obtained in the familiar no-overhang approximation (the Monge representation) in which the interface is described by a single-valued height function $h(\underline{x}, t)$ of the substrate $\underline{x}$ and time t. This approximation would be expected to be valid when the dominant relaxation mechanism, surface diffusion, is effective in eliminating overhanging configurations.

2.2.1 Stochastic Partial Differential Equation:

We study the equation

$$\frac{\partial h}{\partial t} = -\mu \nabla^4 h + (\underline{f} \cdot \underline{\nabla} h) \nabla^2 h + \eta \tag{2.44}$$

where $\eta(\underline{x}, t)$ is a stochastic Gaussian noise with a zero average and

$$\langle \eta(\underline{x}, t) \eta(\underline{x}', t') \rangle = 2\Delta \delta^D(\underline{x} - \underline{x}') \delta(t - t'). \tag{2.45}$$

The coefficient μ is a measure of the surface diffusion and $\underline{f}$ is proportional to the parallel component of the flux $\underline{J}_{||}$ (the incident flux is defined to be $\vec{J} \equiv (\underline{J}_{||}, J_z)$, where the z direction is normal to the substrate).

Equation (2.44) follows from straightforward physical considerations. As discussed in the previous section, in the Monge representation, the general form of the deterministic part of the growth equation is

$$\frac{\partial h}{\partial t} = \sqrt{g} \mathcal{G} \tag{2.46}$$

where $\mathcal{G}$ is a reparametrization invariant function [4]. If growth occurs due to an incident flux $\vec{J}$ of particles with surface diffusion being the principal relaxation mechanism, then

$$G = -\vec{J} \cdot \hat{n}(1 - rH) + \kappa \underset{\sim}{\Delta} \frac{\delta \mathcal{H}}{\delta h} \tag{2.47}$$

where $\hat{n} = (-\underline{\nabla} h, 1)/\sqrt{g}$ is the local normal to the interface; $H = \underline{\nabla} \cdot \left(\underline{\nabla} h/\sqrt{g}\right)$ is the mean curvature; $\underset{\sim}{\Delta}$ is the Beltrami-Laplace operator that incorporates the fact that the diffusion current is parallel to the interface and not to the substrate; r is the non-zero radius of the aggregating particles [25]; and $\mathcal{H} = \sigma \int d^d x \sqrt{g}$ represents the energy of the interface, that is proportional to its area. Equation (2.47) with $\underline{J} = J\hat{z}$ (i.e. $J_{||} = 0$) reduces to the r.h.s. of the equation of Mazor et.al. [25]. Near the upper critical dimension in the self-affine regime eq. (2.47) can be expanded in powers of $\frac{\partial h}{\partial x^i}$:

$$\frac{\partial h}{\partial t} = -J_z + \underline{J}_{||} \cdot \underline{\nabla} h + r J_z \nabla^2 h - r \underline{J}_{||} \cdot \underline{\nabla} h \nabla^2 h - \mu \nabla^4 h + \text{ higher order terms in power of } h \tag{2.48}$$

where $\mu = \kappa\sigma$.

The first term (note that $J_z < 0$) is just the average velocity of the interface, while the second describes a uniform shift of the fluctuations on the interface. Both can be eliminated by the galileian transformation

$$h(\underline{x}, t) = -J_z t + \tilde{h}(\underline{x} + \underline{J}_{||} t, t) \tag{2.49}$$

The new regime of behavior is obtained when the third term in the r.h.s. of (2.48) can be neglected with respect to the fifth one. This occurs for $r|J_z| << \mu\Lambda^2$ where Λ is the ultraviolet momentum cut-off. This is easily verified at nearly grazing incidence. Under a RG transformation, a $\nabla^2 h$ term will be generated in any case so that our results will hold at intermediate scales until such a term starts to become important (See also discussion in ref. [32]). Furthermore, since $J_z < 0$, the surface tension term is initially negative. Under the RG transformation a positive surface tension will be generated so that the coefficient of $\nabla^2 h$ diminishes in absolute value until it vanishes and after it grows positive, leading finally to the EW behaviour.

Notice, finally, that under the transformation

$$\tilde{h}(\underline{x}, t) = \tilde{\tilde{h}}(\underline{x}, t) - \frac{J_z}{J_{||}} \hat{J}_{||} \cdot \underline{x}$$

the equation for $\tilde{\tilde{h}}$ contains only the last two terms of (2.48). This transformation corresponds to a rotation of the z axis in the direction normal to the flux.

Thus including the noise due to fluctuations in the incident flux, equation (2.48) becomes (2.44) with $\underline{f} = r\underline{J}_{||}$.

Under RG, due to the anisotropy induced by $\underline{f}$, we are forced to generalize eq.(2.44) as follows:

$$\frac{\partial h}{\partial t} = -(\mu_{||}\partial_{||}^4 h + \mu_\perp \partial_\perp^4 h + \mu_d \partial_\perp^2 \partial_{||}^2 h) + \partial_{||} h(\lambda_{||}\partial_{||}^2 h + \lambda_\perp \partial_\perp^2 h) + \eta \tag{2.50}$$

Initially $\mu_{||} = \mu_\perp = \mu_d/2 = \mu$ and $\lambda_{||} = \lambda_\perp = f$. The deterministic part of eq.(2.50) is formally invariant under the transformation

$$h'(\underline{x}', t) = h(\underline{x}, t) - \epsilon x_{||} \tag{2.51a}$$

$$\underline{x}' = \underline{x} - t\epsilon(\lambda_{||}\hat{x}_{||}\partial_{||} + \lambda_\perp \underline{\partial}_\perp) \tag{2.51b}$$

In eqs. (2.50) and (2.51a,2.51b) we are using the following notations: $\underline{x} = (x_{||}, \underline{x}_\perp)$, $\underline{f} = (f, \underline{0})$ and $\underline{\nabla} = (\partial_{||}, \underline{\partial}_\perp)$. The Gaussian noise with a correlation given by (2.45) is not invariant under the transformation (2.51b) so that the symmetry of the deterministic part of (2.50) does not imply exponent equalities as in the Kardar-Parisi-Zhang [8] equation.

2.2.2 Sketch of the RG Calculation:

Following ref. [11] we integrate out fluctuations with wave numbers $\Lambda e^{-l} <| k_{||} |< \Lambda$ and $\Lambda e^{-\zeta l} <| \underline{k}_\perp |< \Lambda$ in order to determine the renormalized coefficients in eq. (2.50), $\mu_{||}(l)$, $\mu_\perp(l)$ etc (see appendix B.1 for more details). Λ^{-1} is proportional to a small length scale cut-off. The restoration of the original cut-off Λ in the renormalized equation follows from the subsequent rescaling

$$\begin{cases} x_{||} & \to & e^l x_{||} \\ \underline{x}_\perp & \to & e^{l\zeta}\underline{x}_\perp \\ h & \to & e^{l\alpha} h \\ t & \to & e^{lz} t \end{cases} \tag{2.52}$$

The exponent ζ is introduced due to the anisotropy present in our equation. Note that defining, $l\zeta = l_\perp$, α is changed into $\frac{\alpha}{\zeta}$ and z into $\frac{z}{\zeta}$. When the λ's are zero in eq. (2.50) the values of the exponents in eq.(2.52) are

$$\zeta_o = 1, \quad \alpha_o = \frac{4-D}{2} \quad \text{and} \quad z_o = 4 \tag{2.53}$$

leading to the bare scaling $\lambda_i \to \lambda_i l^{\frac{6-D}{2}}$, $i = ||, \perp$, induced by eq.(2.52). One then identifies $D_c = 6$ as the upper critical dimensional below which the λ's are relevant. The full renormalization is performed at 1-loop order. The calculations are quite involved. The essential details are presented in appendix B.1. In terms of the parameters

$$\rho = \left(\frac{\mu_\perp}{\mu_{||}}\right)^{\frac{1}{4}}, \quad r_\mu = \frac{\mu_d}{2\sqrt{\mu_{||}\mu_\perp}}, \quad r_\lambda = \frac{\lambda_\perp}{\lambda_{||}}\sqrt{\frac{\mu_{||}}{\mu_\perp}} \tag{2.54}$$

and

$$g = \frac{\lambda_{||}^2 \Delta}{16\sqrt{2} K_{D-1} \mu_{||}^3 \rho^5 (1+r_\mu)^{5/2}}$$

where $(2\pi)^D K_D$ is the surface area of the unit sphere in D-dimensions, the RG flow equations are

$$\frac{\partial \ln \Delta}{\partial l} = z - 2\alpha - 1 - (D-1)\zeta \tag{2.55a}$$

$$\frac{\partial \ln \lambda_\perp}{\partial l} = z + \alpha - 1 - 2\zeta \tag{2.55b}$$

$$\frac{\partial \ln \rho}{\partial l} = 1 - \zeta - g\Im_\rho(r_\mu, r_\lambda) \tag{2.55c}$$

$$\frac{\partial \ln r_\mu}{\partial l} = g\Im_\mu(r_\mu, r_\lambda) \tag{2.55d}$$

$$\frac{\partial \ln r_\lambda}{\partial l} = g\Im_\lambda(r_\mu, r_\lambda) \tag{2.55e}$$

$$\frac{\partial \ln g}{\partial l} = \epsilon - g\Im_d(r_\mu, r_\lambda) \tag{2.55f}$$

The g independent terms in eqs. (2.55a-f) arise from the rescaling (2.52). The functions $\Im_i$ introduced above are

$$\Im_\rho(r_\mu, r_\lambda) = \frac{1}{8}\left[3 + r_\mu - r_\lambda^2(3 + 7r_\mu + 10r_\mu^2 + 4r_\mu^3)\right]$$

$$\Im_\mu(r_\mu, r_\lambda) = \frac{1}{20 r_\mu}\left[5 - 20r_\mu - 2r_\lambda(5 + r_\mu) + r_\lambda^2(21 + 100r_\mu + 81r_\mu^2 + 50r_\mu^3 + 20r_\mu^4)\right]$$

$$\Im_\lambda(r_\mu, r_\lambda) = \frac{1}{4}\left[r_\mu - 3r_\lambda + r_\lambda^2(2 - 5r_\mu - 10r_\mu^2 - 4r_\mu^3) + 3r_\lambda^3(7 + 10r_\mu + 4r_\mu^2)\right]$$

and

$$\Im_g(r_\mu, r_\lambda) = \frac{1}{8(r_\mu + 1)}\left[1 - 6r_\mu - 7r_\mu^2 + 2r_\lambda(11 + 7r_\mu)\right.$$

$$\left. + r_\lambda^2(129 + 440r_\mu + 529r_\mu^2 + 238r_\mu^3 + 28r_\mu^4) - 12r_\lambda^3(1 + r_\mu)(7 + 10r_\mu + 4r_\mu^2).\right]$$

Notice that Δ and $\lambda_\perp$ do not renormalize apart from the rescaling (2.52). An inspection of the perturbative expansion shows that this holds at all orders. At the fixed point eqs. (2.55a-b) give the exponent equalities

$$z = 1 + \frac{3+D}{3}\zeta, \quad \alpha/\zeta = \frac{3-D}{3} \tag{2.56}$$

thus reducing the problem to the calculation of the anisotropy exponent ζ. Note that α/ζ is determined exactly. In the flow equations (2.55a-f) three exponents can be

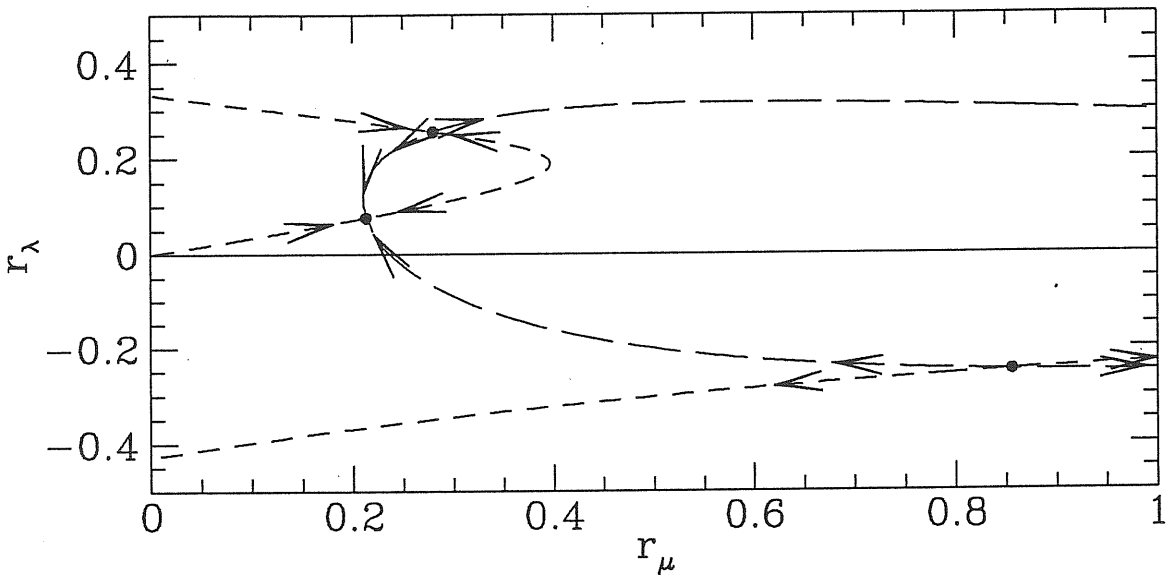

Figure 2.1: RG flow in the (r_μ, r_λ) plane. The short–dashed line is the locus where $\Im_\lambda$ vanishes while $\Im_\mu$ is zero on the long–dashed line. The signs of the various terms are such that the flow close to the fixed points is as shown by the arrows for $g > 0$.

eliminated fixing the scale of $x_{||}, t$ and h thus reducing the flow diagram to e.g. r_μ, r_λ and g. To leading order in ϵ we find three fixed points

$$\begin{aligned} r_\mu^{(1)} &= 0.855556 \quad r_\lambda^{(1)} = -0.24871 \quad g^{(1)} = -0.545298\epsilon \\ r_\mu^{(2)} &= 0.212544 \quad r_\lambda^{(2)} = 0.075748 \quad g^{(2)} = 0.113579\epsilon \\ r_\mu^{(3)} &= 0.279516 \quad r_\lambda^{(3)} = 0.254999 \quad g^{(3)} = 0.124125\epsilon \end{aligned}$$

The first fixed point is unphysical since $g^* < 0$. The analysis of the flow equations shows that only the second fixed point is physically relevant since it is stable and has a non–empty domain of attraction as seen in figure 2.1. The corresponding exponents are, to order ϵ,

$$\zeta = 1 - 0.0452\epsilon, z = 4 - 0.1800\epsilon \text{ and } \alpha = -1 + 0.0896\epsilon \tag{2.57}$$

One may attempt to estimate the lower critical dimension D_L defined by

$$\text{Max } (\alpha(D_L), \alpha(D_L)/\zeta(D_L)) = 1.$$

In the absence of nonlinearities, one obtains from eq. (2.53) that $D_L = 2$. The presence of nonlinearities leads to $D_L = 0$. A realistic estimate would entail the calculation of higher order corrections to the ζ exponent. We note in particular the coincidence of the result $\alpha/\zeta = 1/3$ in $D = 2+1$ with the experimental findings of ref.

[23] where such value of the wandering exponent was measured in a MBE experiment with an inclined flux.

In the presence of anisotropic scaling, for a sample of size $L_{||}$ in the direction parallel to $\underline{J}$ and $L_{\perp}$ in the other $D-1$, the steady state roughness has the general scaling form

$$w(L_{||}, L_{\perp}) = L_{||}^{\alpha(D)} f\left(L_{\perp}/L_{||}^{\zeta}\right). \tag{2.58}$$

If $L_{||} \sim 1$ this should reproduce the behaviour of the $D-1$ dimensional interface in the case in which the flux has normal incidence (and $\alpha_n(D-1)$ is its roughness exponent), so that $w(1, L_{\perp}) \sim f(L_{\perp}) \sim L_{\perp}^{\alpha_n(D-1)}$. This combined with eq. (2.58) yields $w(L, L) \sim L^{\tilde{\alpha}}$ with $\tilde{\alpha}(D) = \alpha(D) + [1 - \zeta(D)]\alpha_n(D-1)$.

In summary, we have studied the experimentally realizable case of a growing interface due to an oblique incident flux with surface diffusion being the dominant relaxation mechanism. Our renormalization group calculations indicate that while the long time behavior ought to be in the Edwards-Wilkinson universality class, a novel intermediate regime should be present. An exact expression for the exponent ratio α/ζ was found in this new universality class, whereas α itself was determined to lowest order in an ϵ expansion in (6-ϵ) dimensions.

Chapter 3

Dynamics in Disordered Media

A sheet of paper is held vertically and it is dipped into a basin filled with a suspension of ink. The paper starts absorbing the suspension and the interface between wet and dry paper advances [33]. The forces pushing the surface, namely capillary forces, acts in the normal direction, while evaporation tends to minimize the interface area. Thus the mechanism controlling the evolution of the surface is described by the first two terms ($\nu\nabla^2 h + \lambda(\nabla h)^2$) of the KPZ equation (2.1). This time however randomness comes in not from a beam of particles but from the inhomogeneities of the medium. Regions where the density of the paper is bigger will oppose more resistance to the flow than less compact regions. Instead of $\eta(\underline{x}, t)$, in equation (2.1), we have to take a random field that depends on the location of the interface, $\eta(\underline{x}, h)$, i.e. on the solution $h(\underline{x}, t)$ itself of the equation. A second difference with the equation with *annealed* noise (i.e. $\eta(\underline{x}, t)$) is that the average $f = \langle\eta\rangle$ cannot be eliminated as before. Indeed if $h \to h - ft$ the constant term is eliminated but it reappears in the argument of $\eta' = \eta(\underline{x}, h - ft) - f$. $f = \langle\eta\rangle$ is indeed a relevant parameter of the problem: it is the driving force. If it is too small the interface soon stops on a barrier of *pinning centers* whereas if it is too large we expect to recover the behavior of the KPZ with *annealed* noise. In fact if the interface moves at a constant, large speed $v \simeq f$, the argument h in η can be approximated by vt so that $\eta(\underline{x}, h) \to \eta(\underline{x}, t)$ for $v \gg 1$. The two behaviors are separated by the depinning transition that occurs for a critical value of f and has many typical aspects of a second order phase transition.

The situation at the depinning transition, where the interface moves at a vanishing speed and critical fluctuations of all sizes occur, has an interest that is not only academic. Let us return to the imbibition experiment. The interface ultimately will stop when the rate of evaporation will balance the effect of capillary forces. The final configuration will then be a realization of a typical interface at (or very close to) the depinning transition. It has also been argued [34] that, in actual experiments, it is often easier to control the velocity of the interface than the driving force. Thus driven interfaces in a disordered media are often at the depinning transition. Fortunately, for the problem at hand [33, 35], exactly *at* the depinning transition, geometrical

considerations allow to relate the exponents to those of directed percolation [36, 34]. For our purposes it is important to observe that the interface, at the depinning transition, advances by subsequent breaks through in the points with least resistance, i.e. with the largest $\partial_t h$ or the smallest $\epsilon_{\underline{x}} = -\partial_t h(\underline{x}, t)$.

A depinning transition is also observed in charge density waves [37] dynamics in quasi one dimensional metals. A mesoscopic description of this phenomenon [38] involves a Langevin equation

$$\partial_t h = (\nu \nabla^2 h + f + \eta)\theta(\nu \nabla^2 h + f + \eta)$$

Now $h(x,t)$ has the meaning of a phase, but the equation is very similar: f is a driving (electric) external field and $\eta(x)$ is a random field with short range correlations. The θ function allows h to "move" only forward. The noise term here does not depend on h and, were it not for the θ function, the solution would be very easy[1]. The non linear effects of the θ functions combined with those of the quenched noise $\eta(x)$ result in a large number of interesting phenomena like a depinning transition, stretched exponential relaxation in the pinned phase and memory effects. Also in this case, at the depinning transition the region where the local field (the argument of the θ) is positive consists in one point: that for which the sum $\nu \nabla^2 h + \eta = -\epsilon$ of the elastic potential and the pinning potential is largest.

Let us now consider the random field Ising model

$$\mathcal{H} = -\sum_{i,j} J_{i,j} s_i s_j - \sum_i (\eta_i + H) s_i \tag{3.1}$$

where η_i is a random field with zero average and standard deviation Δ, H is an external magnetic field and $J_{i,j}$ is the usual nearest neighbor coupling. Much recent interest has focused on aspects related to the $T = 0$ athermal dynamics of this system, which occurs as a response to a slow varying, driving magnetic field $H(t)$ Hysteresis loops [39] and domain wall dynamics [40] are two phenomena where this model provides a reliable description. Leaving aside a more detailed discussion of these phenomena, let us examine the process more carefully. The adiabatic condition means that the field is varied so slowly that the system jumps from a state to another state which differs only by one spin flip. Flipping spin i leads to a gain in energy of $\epsilon_i = 2s_i(\sum_j J_{i,j} s_j + \eta_i + H)$. The move of flipping the spin i will be accepted with probability $\min[1, \exp(-\epsilon_i/T)]$ for a general T [6]. In the limit $T \to 0$, however, only the spins with $\epsilon_i \leq 0$ will have a chance to flip. In practice the spin with the smallest value of ϵ_i will be the next one to be flipped.

In these examples the evolution implies a global search for the point with the extreme value of a random field ϵ_i (the extreme statistics) where the evolution will occur. This mechanism is also present in other widely studied models, like invasion

[1] In the fourier space the equation is diagonal. The solution is a uniformly "sliding" rigid charge density wave, which is indeed what happens for large positive values of f, where the theta function has no effect.

percolation [41], models for fracture propagation [43] and dielectric breakdown [44], and in more recently proposed models [35, 45].

Suppose we wish ultimately to monitor the behavior of a quantity $\mathcal{A}$ and evaluate its "quenched" average $A(t)$ that is the average on the disorder configurations. For a given realization of the random disorder, the process is deterministic of course. This means that all quantities of interest are functions of the random field η_i and $A(t) = \langle \mathcal{A}(t, \{\eta_i\}) \rangle$. If the functional dependence of $\mathcal{A}$ on the disorder configuration $\{\eta_i\}$ were known analytically the evaluation of the average would pose no problem. Usually however this dependence is accessible only by evolving the process with disorder $\{\eta_i\}$. Not even a zero order approximation is available in most cases so an analytic approach appears hopeless.

This chapter is devoted to the derivation and to some applications of a general method to deal with quenched dynamics, namely with processes whose evolution is based on the extreme statistics of a random field. The main idea, which was introduced by L. Pietronero and W. R. Schneider in the study of invasion percolation [46], consists in a transformation of the quenched process to an *annealed* one, i.e. to a stochastic process. While the former is deterministic, for each realization of the disorder, the latter is stochastic in the sense that individual evolution events are *independently* selected from a given distribution at each time. This probability distribution embodies the *screening* effect which is the origin of the interesting behavior of these systems. It also provides the probability of a given realization and allows in principle to perform averages on the space of all realizations. The condition for this process to be *statistically* identical with that evolving selecting the extremes of the disorder, specifies the evolution of the *effective* distribution of the random field ϵ_i on which the extremum is taken. The effective distribution of ϵ_i, which we will call *run time statistics* (RTS), is the distribution of ϵ_i that is statistically consistent with (or conditional to) the actual evolution of the process.

A simple illustration of the ideas behind the transformation is briefly discussed in section 3.1.1 for a model of diffusion in a random potential. Then we derive, in section 3.1.2 the transformation for the dynamics driven by the extreme statistics. The resulting set of transformations allows for an approximate solution for a general class of models (sect. 3.1.3, 3.1.4 and 3.1.5). The key quantity is the histogram of the values of the random field over which the search of the minimum is performed. From this a qualitative insight in the general properties of these processes can be gained (sect. 3.1.6). The use of the alternative description of the process based on the RTS in numerical studies would provide a wider information on the process. However the practical implementation of the transformation implies the heavy numerical task of performing a rather large amount of integrals. For this reason, the best application of the RTS is probably in connection with other theoretical methods devised to study critical phenomena. Examples of these applications are given in the two subsequent sections. In section 3.2 the RTS is used in the Fixed Scale Transformation [7] approach to uncover the fractal properties of invasion percolation with and without trapping

[47]. For simple invasion percolation[41] we find a lower bound of the fractal dimension which is within 0.5 % of the exact value. Including trapping [48], we find a fractal dimension which is in excellent agreement with numerical results. A natural extension of this approach is the computation of the fractal dimension for models where the random field is coupled to a local field. This occurs in models for fracture propagation [43] and for dielectric breakdown [44] in random media.

Finally, in section 3.3, we discuss the application of the RTS in connection with the real space renormalization group for a recently proposed model of biological evolution [49]. Also in this case, while unravelling aspects of the large scale behavior of the model, we find numerical results in excellent agreement with numerical findings [45].

3.1 The Run Time Statistics

A process with quenched dynamics evolves in a "cognitive" way: it acquires more and more information on the random environment by testing it. This section is devoted to the translation of this observation into a mathematical formalism, using the rules of conditional probability. The output of this formalism is the rule by which the *run time statistics* evolve. This is the *effective* probability distribution in which the information on the history of the process is stored in a conditional way. These ideas are briefly illustrated in a simple example, the random random walk, in the next subsection. Then we turn to growth processes with quenched dynamics, in which the growth occurs where the random environment attains its extreme value. The above approach provides a general mapping of a quenched growth process, that is deterministic with a space dependent randomness, to an annealed stochastic process, that is a process with a time dependent randomness. The latter is specified by a probability distribution for the individual growth events at each time, that contains the average on all realization of the disorder with that given history.

Having defined the models we deal with and set some notations, in section 3.1.2, we discuss the mapping of the quenched growth process to a stochastic process. The basic equations are then solved for the empirical distribution of the random field, using a simple approximation. This solution provides qualitative information on all the quantities that characterize the process. The case of invasion percolation [41] is discussed first (sect. 3.1.3) to illustrate the method, the approximations involved and how these can be controlled. The solution of the general case is worked out in section 3.1.4 extending the results on invasion percolation. A general relation for the critical threshold, that marks the location of the discontinuity in the empirical distribution, is derived. This extends a known rigorous result for invasion percolation [50] to the general model. A particular limit of the model, that is realized in recently proposed models for interface growth [35] and biological evolution [45], is analyzed in some detail in section 3.3. There the relaxation to the stationary state is investigated providing an explicit expression for the relaxation time. We discuss also the corrections

induced in the dynamics by a small non–zero temperature. Finally, in section 3.1.6, we discuss the asymptotic limit of an infinite cluster.

3.1.1 An example: The RTS in the Random Random Walk

Consider a one dimensional random walk with hopping probabilities x_i and $1-x_i$ for jumps to the left and the right respectively, on each site i. x_i are independent uniform random variables in $[0,1]$. This "random" random walk is a model for diffusion in a disordered media and has been widely studied [51]. We borrow this model to illustrate the general idea behind the transformation of a process in quenched disorder to a stochastic process.

Imagine to observe the walker in his motion in the random environment. The statistical properties of x_i are known (it is uniform in $[0,1]$), however we have no access to the actual values of the hopping probabilities that characterize the particular realization we are looking at. The only information available is what we see: the number of visits n_i on each site i and the number k_i of times the walker has moved from site i to site $i-1$ with a jump to the left. This is a sufficient information to describe, at a probabilistic level, the future evolution of the walker.

The probability that the random random walker has jumped to left k_i times out of its n_i visits to site i (and that $n_i - k_i$ times it has jumped to the right) is

$$P_{n_i,k_i}(x_i) = \binom{n_i}{k_i} x_i^{k_i}(1-x_i)^{n_i-k_i}.$$

This equation relates the statistics of the number of left jumps on each site, to the value of the hopping probability x_i. About x_i however we know only that it was drawn from a uniform distribution and that k_i left jumps have occurred out of n_i trials. These informations are easily combined, using the rules for conditional events, to derive the distribution density of x_i that is consistent with a fraction k_i/n_i of left jumps

$$p_{n_i,k_i}(x_i) = (n_i+1)\binom{n_i}{k_i} x_i^{k_i}(1-x_i)^{n_i-k_i}. \tag{3.2}$$

This distribution, in its turn, allows to evaluate the probability that the next jump will occur to the left

$$\mu_{n_i,k_i} = \mathbf{E}(x_i) = \int_0^1 x p_{n_i,k_i}(x)dx = \frac{k_i+1}{n_i+2} \tag{3.3}$$

which is the expected value of x_i. We could then simulate diffusion in a disordered environment, without making any reference to the disorder, by assigning from the beginning the rule (3.3) to evaluate jump probabilities in terms of the dynamical variables $n_i(t)$ and $k_i(t)$. Our simulation, by construction, will be statistically indistinguishable from the diffusion process in a random media. This is because the

condition that the future evolution be *statistically* consistent with the past history, has been properly satisfied.

The two processes, that based on x_i and the one that uses eq. (3.3), are related by the distribution $\rho_{i,t}(x) = p_{k_i(t),n_i(t)}(x)$ of x_i of eq. (3.2). $\rho_{i,t}(x)$ evolves conditionally subject to the information the process accumulates on x_i. For this reason we call it *run time statistics.*

This simple example uncovers some relevant aspects of dynamics in quenched disorder. As time goes on, the process samples the random environment and accumulates statistical informations about it. In this sense it might be seen as a cognitive process. Note indeed that the distribution (3.2), for $n_i \gg 1$ tends to

$$p_{n_i,k_i}(x_i) \cong \sqrt{\frac{n_i}{2\pi x_i(1-x_i)}} \exp\left\{-\frac{(x_i - k_i/n_i)^2}{2x_i(1-x_i)/n_i}\right\}.$$

As already stated, the expected value of x_i is $(k_i+1)/(n_i+2)$. The most probable value is instead k_i/n_i. The standard deviation diminishes as $1/\sqrt{n_i}$ as $n_i \to \infty$. As time goes on the information about x_i gets more and more precise. For a finite lattice of L sites with periodic boundary condition the distribution of x_i will approach a delta function more and more closely as time goes on. As the distributions of x_i get narrower and narrower, the process singles out all the realizations of the disorder that are consistent with the history of the process. In a strict sense the process will never reach a stationary state. This is related to the occurrence of aging [52] phenomena in this simple model [53].

In evaluating some quantity, like the mean square displacement of the random random walk, one faces the problem of quenched averages. The quantity must be averaged over the different realizations of the disorder and to do this one must repeat many times three operation: *i)* fix the disorder $\{x_i,\ i = 1,\ldots,L\}$, *ii)* perform the walk and *iii)* evaluate the quantity. With the use of the run time statistics instead one has direct access to the statistical weight of all the configuration of the disorder for a given history of the process: this is indeed given by the product over time of the probabilities $\mu_{n(t),k(t)}$ of the jump event occurred at time t.

The dependence of the jump probability $\mu_{n,k}$ on the past history of the process, i.e. on the number n of visits to the site and on the number k of times a jump to the left has occurred, implies the presence of memory effects. These will be the subject of the next chapter.

3.1.2 The RTS for Quenched Growth Models

Let us consider a model defined on a lattice. A random variable $\epsilon_i \in [0,1]$ is assigned to every site of the lattice. These are all independent and they are drawn from the same distribution $P_{0,0}(x) = \text{Prob}(\epsilon_i < x)$. Here and in the following we will use

lower case letters for probability densities while upper case letters stand for the corresponding distribution (e.g. $F(x) = \int_0^x f(y)dy$). Both ϵ_i and the their distributions can be defined in $[0,1]$ without loss of generality. We will refer to site models, the extension to the bond version being trivial. Once the disorder is assigned the process is deterministic. This is best explained by the example of site invasion percolation [41, 50] (IP), a model for fluid displacement in porous media [42]. One seed site i_0 is initially chosen. Among its nearest neighbor the one with the smallest random variable i_1 is added to i_0 at the $t = 1$ time step. Next the site with the smallest random variable, among the perimeter sites of the two sites cluster $\mathcal{C}_1 \equiv \{i_0, i_1\}$, is selected and added to the cluster. At a generic time t the next site to be added to $\mathcal{C}_t = \{i_0, \ldots, i_{t-1}\}$ is the one with the smallest ϵ_i where i labels one of the sites on the perimeter $\partial\mathcal{C}_t$ of the cluster $\mathcal{C}_t$.

This model is generalized as follows: growth starts from a set of seed sites $\mathcal{C}_0$. This defines also a corresponding set of active sites $\partial\mathcal{C}_0$, usually on the perimeter of $\mathcal{C}_0$. Among these the one with the smallest random variable, i.e. $\epsilon_{i_0} = \min\{\epsilon_j;\ j \in \partial\mathcal{C}_0\}$, is selected as the initiator of the growth event at time 0. A deterministic rule then specifies the set of sites $\mathcal{G}_0$ that, along with i_o, become part of the new cluster $\mathcal{C}_1 = \mathcal{C}_0 \bigcup \mathcal{G}_0 \bigcup \{i_0\}$. In the IP case $\mathcal{G}_0 \equiv \emptyset$. The same mechanism is repeated at later times: given the cluster set $\mathcal{C}_t$, the set of active sites $\partial\mathcal{C}_t$ is identified. Among these the one, i_t, with the smallest variable initiate the growth event by which a set $\mathcal{G}_t$, together with i_t, is removed from $\partial\mathcal{C}_t$ and is added to the cluster $\mathcal{C}_{t+1} = \mathcal{C}_t \bigcup \mathcal{G}_t \bigcup \{i_t\}$.

In section 3.1.5 we will discuss some recently proposed models for interface growth [35] in a disordered media that fit this general definition of the model. Here along with i_t also sites from the close neighborhood of i_t are allowed to grow to mimic the effect of surface tension. Also a recent model of biological evolution [45] exploits the same mechanism.

This class of models are simple prototype of systems that display a Self Organized Critical behavior. Indeed IP is known [41, 50] to reproduce the geometrical properties of standard percolation right at criticality without fine tuning any temperature like parameter.

At any time step, all the variables ϵ_i, for $i \in \partial\mathcal{C}_t$, are tested to decide which is the minimum, ϵ_{i_t}. For the one ($i = i_t$) that "wins" we acquire the information that it has been the smallest among all. For the others we know that they were not the smallest at that time. This can be directly translated in a formula for the effective probability density $\rho_i(x,t)$ of the variables ϵ_i at time t, that we will call Run Time Statistics (RTS). Before doing this it is essential to note that the distribution of ϵ_i for $i \in \partial\mathcal{C}_t$ depends only on the number τ_i of times it has been tested or, that is the same, on the time τ_i it has been in the set of active sites. We then choose the notation $p_{\tau,t}(x)$ for the RTS of variables that have been tested τ times and $n_{\tau,t}$ for the number of these sites. $N_t = \sum_\tau n_{\tau,t} = |\partial\mathcal{C}_t|$ is the total number of sites in $\partial\mathcal{C}_t$. Once the distribution $n_{\tau,t}$ and the RTS $p_{\tau,t}(x)$ are given the probability that a variable ϵ_i

with $\tau_i = \tau$ initiate growth is

$$\mu_{\tau,t} = \int_0^1 dx\, p_{\tau,t}(x) \prod_k [1 - P_{k,t}(y)]^{n_{k,t} - \delta_{k,\tau}} \tag{3.4}$$

This is indeed the probability that $\epsilon_j > \epsilon_i$ for all $j \neq i$. Here the Kronecker delta $\delta_{k,\tau}$ comes because the contribution of the variable ϵ_i itself has not to appear in the product. The normalization of this growth probability distribution (GPD) is easily proved introducing the function

$$Z_t(x) = \prod_\tau [1 - P_{\tau,t}(x)]^{n_{\tau,t}} \tag{3.5}$$

and observing that $\sum_\tau n_{\tau,t}\mu_{\tau,t} = -\int_0^1 \partial_x Z_t(x)dx = 1$.

Once a site i_t with $\tau_{i_t} = \tau$ is selected according to this GPD, its density is updated in a conditional way with the information that $\epsilon_{i_t} < \epsilon_j$ for all $j \neq i_t$. So it becomes

$$m_t(x|\tau) = \frac{1}{\mu_{\tau,t}} p_{\tau,t}(x) \prod_k [1 - P_{k,t}(x)]^{n_{k,t} - \delta_{k,\tau}} \tag{3.6}$$

The distribution of the other ϵ_j for $j \in \partial\mathcal{C}_t$ is updated with the information that $\epsilon_j > \epsilon_{i_t}$. The rules of conditional probability, if $\tau_j = \theta$, yield

$$p_{\theta+1,t+1}(x) = \frac{M_t(x|\tau)}{\int_0^1 p_{\theta,t}(y) M_t(y|\tau) dy} p_{\theta,t}(x). \tag{3.7}$$

that also expresses the fact that now the variable ϵ_j has been tested $\tau_j + 1$ times. The sites in $\mathcal{G}_t$ are added to the cluster. Their RTS does not evolve any more. The other ones remain in the set $\partial\mathcal{C}_{t+1}$ of active sites. Finally $n_{0,t+1}$ sites eventually enter the interface $\partial\mathcal{C}_{t+1}$ as they are reached by the growing cluster. Their probability distribution is of course the original one $p_{0,t+1}(x) = p_{0,0}(x)$.

Accordingly the distribution $n_{\theta,t}$ is updated: $n_{\theta+1,t+1} = n_{\theta,t} - g_{\theta,t} - \delta_{\tau,\theta}$ where $g_{\theta,t}$ is the number of sites in $\mathcal{G}_t$ with $\tau_i = \theta$.

The evolution of the process is completely specified by the initial conditions $\mathcal{C}_0$, $\partial\mathcal{C}_0$ and $p_{0,0}(x)$, the above set of equations and by the deterministic rules used to identify the set $\mathcal{G}_t$. Equations (3.4,3.5,3.6,3.7) provide a general mapping of a quenched process, i.e. a deterministic process in a random environment, to an *annealed* stochastic process with a time dependent randomness. The GPD, Eq.(3.4), as well as the RTS, depends in general on the whole history of the process. This memory is stored in the distributions of individual variables and generally makes it less likely for an *old* variable to grow than for a *younger* one. The memory effect extends over a time $T = \max_{i,j\in\partial\mathcal{C}_t}\{\tau_i - \tau_j\}$. Indeed if all variables have experienced the same history, no memory effect at all is present and $\mu_{\tau,t} = 1/N_t$.

A mapping between quenched and annealed models was proposed in Ref. [44] for the Dielectric Breakdown Model. This was actually in the direction opposite to

that discussed here: a stochastic model was mapped to a quenched model. As a result a spatial correlation in the disorder was induced. It is interesting to note that the reverse path discussed here produces a time correlation, i.e. a memory, in the stochastic model. Moreover in Ref. [44] it was found that this correlation is not present when growth is allowed on all sites (i.e. if $\partial\mathcal{C}_t$ contains all sites that are not in $\mathcal{C}_t$) and results in a disconnected cluster. This is consistent with the evident fact that, in our formalism, no memory is produced in the reverse transformation. This is because the distributions of all sites are conditioned on the same history in disconnected growth. Actually this argument is not rigorous in the case of the quenched version of the Dielectric Breakdown Model since there the random potential is coupled to the Laplace field [44].

The choice of the initial probability density $p_{0,0}(x)$ is clearly unessential. One can safely restrict attention to the uniform density in $[0,1]$, since the GPD is invariant under the transformation $x \to \int_{-\infty}^{x} p_{0,0}(y)dy$ that maps any density to the uniform one.

The probability densities $p_{\theta,t}(x)$ and $m_t(x|\tau)$ are themselves random. Iteration of equation (3.7) implies that

$$p_{\theta,t}(x) = A \prod_{k=t-\theta}^{t-1} M_k(x|\tau_k) \tag{3.8}$$

where A is the normalization constant and τ_k is the τ value of the smallest variable at time k. The noise acts in a multiplicative fashion on the distributions and this may be related to the occurrence of multiscaling in quenched processes [35].

3.1.3 The Empirical Distribution for Invasion Percolation

The starting point of the analysis of the set of equations (3.4,3.5,3.6,3.7) is the relation

$$\sum_{i\in\partial\mathcal{C}_t} \rho_{i,t}(x) + \sum_{i\in\mathcal{C}_t} \rho_{i,t}(x) = |\partial\mathcal{C}_t| + |\mathcal{C}_t| = N_t + \sum_{k=0}^{t-1}(G_k + 1) \tag{3.9}$$

where $\rho_{i,t}(x)$ is the RTS of the variable ϵ_i, $G_t + 1 = \sum_\tau g_{\tau,t} + 1 = |\mathcal{G}_t| + 1$ is the total number of sites that grow at time t and $p_{0,0}(x) = 1$ was used. This identity is, in a sense, a "law of conservation of information". The history of the process up to time t gives only information on how the probability is distributed among the two sums in Eq.(3.9), but it cannot affect the value of their sum. Eq.(3.9) also introduces the empirical distribution $h_t(x) = \sum_{i\in\partial\mathcal{C}_t} \rho_{i,t}(x)$ that is the histogram of the random variables on the interface (note that the same name in the literature was used for different quantities [50, 45]). This is a directly accessible quantity in a computer simulation. Our aim is to derive an analytic expression for $h_t(x)$ under simple and controllable approximations. It will be shown that $h_t(x)$ provides also information on the other quantities that characterize the growth process like $\mu_{\tau,t}$ and $n_{\tau,t}$. We start

from the case of IP ($\mathcal{G}_t \equiv \emptyset$ and $G_t = 0$), for which our scheme can be compared with rigorous results [50], and later we will turn to the general case.

The first step to derive an equation for the empirical distribution consists in taking the difference of Eq.(3.9) for $t+1$ and t. Since $\mathcal{C}_{t+1} = \mathcal{C}_t \bigcup \{i_t\}$ and $\rho_{i_t,t} = m_t(x|\tau)$, this is $h_{t+1}(x) = h_t(x) - m_t(x|\tau) + N_{t+1} - N_t + 1$ This contains still random quantities so we take the average $\langle\cdot\rangle$ over realizations and we define $\Omega_t = \langle N_t \rangle$ and $\omega_t = \partial_t \Omega_t = \langle N_{t+1} - N_t \rangle$. For a fixed realization of $\mathcal{C}_t$, the average over the realizations $\mathcal{C}_{t+1}$ of $m_t(x|\tau)$ yields $\langle m_t(x|\tau)\rangle_{\mathcal{C}_t} = \sum_\tau n_{\tau,t}\mu_{\tau,t} m_t(x|\tau) = -\partial_x Z_t(x)$. This gives

$$\langle h_{t+1}(x)\rangle = \langle h_t(x)\rangle + \partial_x \langle Z_t(x)\rangle + \omega_t + 1 \tag{3.10}$$

which is still an exact relation. The *boundary* conditions for this equation are (with the usual convention on uppercase notation)

$$\langle H_t(1)\rangle = \Omega_t \tag{3.11}$$

$$\langle H_{t+1}(1)\rangle = \langle N_{t+1}\rangle = \Omega_t + \omega_t \tag{3.12}$$

$$\langle h_{t+1}(0)\rangle = \omega_t + 1 \tag{3.13}$$

here the first two are statements on the total number of sites in $\partial\mathcal{C}_t$ and $\partial\mathcal{C}_{t+1}$ while the last one derives from the observation (see Eq.(3.7)) that $p_{\tau,t}(0) = \delta_{\tau,0}$ for any t and that $\langle h_t(0)\rangle = -\partial_x \langle Z_t(x)\rangle|_{x=0} = n_{0,t}$.

In order to obtain a closed equation for $\langle h_t(x)\rangle$ we have to express both $\langle Z_t(x)\rangle$ and $\langle h_{t+1}(x)\rangle$ as functions of $\langle h_t(x)\rangle$. These are the two main sources of approximations in the solution for the histogram. The second is controllable since once a solution for $\langle h_t(x)\rangle$ is found the approximation used for $\langle h_{t+1}(x)\rangle$ can be checked by power expansion in the time variable around t.

The approximation for $\langle Z_t(x)\rangle$ comes from expanding $(1-P_{\tau,t})^{n_{\tau,t}} = \exp[n_{\tau,t}\log(1-P_{\tau,t})] \simeq \exp[-n_{\tau,t}P_{\tau,t} + O(P_{\tau,t}^2)]$ in Eq. (3.5). When x is small the terms of higher order are small compared to the first. On the other hand when x is close to 1 $Z_t(x)$ is exponentially small in N_t. These considerations justify the approximation of retaining only the first term: $\langle Z_t(x)\rangle \cong \langle \exp[-H_t(x)]\rangle$. The same approximation is obtained in another way with the use of a Poisson transformation [54] in the appendix. Note that from Eq.(3.5) $Z_t(1) = 0$ while in the above approximation $\langle Z_t(1)\rangle = \exp(-N_t)$.

Since $h_t(x)$ is an histogram the number of sites whose variable is found in the x^{th} bin (i.e. $x \le \epsilon_i < x + dx$) should follows a binomial law with mean $\langle h_t(x)\rangle dx$ and variance $\langle h_t(x)\rangle dx(1 - \langle h_t(x)\rangle dx/\Omega_t) \cong \langle h_t(x)\rangle dx$. This would suggest that $\langle \exp[-H_t(x)]\rangle = \exp[-\beta\langle H_t(x)\rangle]$ where $\beta < 1$ should account for the first two cumulants while the central limit theorem should rules out the higher ones. If

$$Z_t(x) \cong \frac{\exp\left[-\beta\left\langle H_t(x)\right\rangle\right] - \exp\left[-\beta\Omega_t\right]}{1 - \exp\left[-\beta\Omega_t\right]} \tag{3.14}$$

is put in Eq. (3.10) we easily find that the conditions (3.11,3.12,3.13) are satisfied only if β is the solution of

$$\beta = 1 - e^{-\beta\Omega_t}. \tag{3.15}$$

The solution $\beta \neq 0$ is exponentially close to 1, which would be consistent with the case in which also the second cumulant of $h_t(x)$ is negligible. From another point of view, $\beta = 1$ would result also if the $n_{\tau,t}$ were all independent variables distributed with a Poisson law (see Appendix). We will return later on this point when comparing the results to numerical data. For the moment being we take $\langle Z_t(x) \rangle$ as given by Eq.(3.14,3.15) so that equation (3.10) becomes

$$\langle h_{t+1}(x) \rangle = \langle h_t(x) \rangle \{1 - \exp[-\beta \langle H_t(x) \rangle]\} + \omega_t + 1. \tag{3.16}$$

We now introduce the function $\phi_t(x) = \langle h_t(x) \rangle / \Omega_t$ and expand $\langle h_{t+1} \rangle$ in the time variable around t: $\langle h_{t+1}(x) \rangle = \Omega_t \phi_t(x) + \omega_t \phi_t(x) + \Omega_t \partial_t \phi_t(x) + \ldots$. Our strategy is to retain only the term proportional to $\phi_t(x)$ and to check on the solution whether the other terms are relevant. Eq. (3.11) implies that $\int_0^1 \phi_t(x) = 1$. The choice $\langle h_{t+1}(x) \rangle = (\Omega_t + \omega_t)\phi_t(x)$ satisfies Eqs. (3.12,3.13) implies that

$$\phi_t(0) = \frac{\omega_t + 1}{\Omega_t + \omega_t} \tag{3.17}$$

In this approximation, after some algebra, Eq. (3.16) yields

$$\partial_x \phi_t(x) = \beta \Omega_t \phi_t^2(x) \left[1 - \frac{\omega_t}{\omega_t + 1} \phi_t(x)\right] \tag{3.18}$$

that is readily integrated to give $\phi_t(x)$ in implicit form

$$\frac{\omega_t}{\omega_t + 1} \log\left(\frac{\Omega_t \phi_t}{\omega_t + 1 - \omega_t \phi_t}\right) - \frac{1}{\phi_t} = \beta \Omega_t \left(x - x_c(t)\right) \tag{3.19}$$

where

$$x_c(t) = \frac{1}{\beta \Omega_t \phi_t(0)} = \frac{\Omega_t + \omega_t}{\beta \Omega_t (\omega_t + 1)} \tag{3.20}$$

and Eq. (3.17) was used for $\phi_t(0)$. It is a matter of algebra to verify that $\int_0^1 \phi_t(x) dx = 1$ is satisfied. $\phi_t(x)$ is monotonously increasing (see (3.18)). For $x = 0$ its value is of order $1/\Omega_t$ while at $x = x_c(t)$ it attains a finite value $\phi_c \cong 0.7822(1 + \omega_t^{-1})$. $x_c(t)$ is also very close to the point where the second derivative of ϕ_t vanishes (and $\phi_t = 2(1 + \omega_t^{-1})/3$). Finally at $x = 1$ it reaches the value $\phi_t(1) = (1 + \omega_t)/[\omega_t + \Omega_t \exp(-\beta \Omega_t)] \cong 1 + \omega_t^{-1}$. Some algebra shows that for $0 < x_c(t) - x \sim 1/\log \Omega_t$ the function ϕ_t is still close to $\phi_t(0)$ and is of the order of $\log \Omega_t / \Omega_t$. It is of the order $\phi_t \sim 1/\log \Omega_t$ for $0 < x_c(t) - x \sim \log\log \Omega_t / \Omega_t$. Above $x_c(t)$ we find that $\phi_t(1) - \phi_t(x) \sim 1/\Omega_t$ for $0 < x - x_c(t) \sim \log \Omega_t / \Omega_t$. So there is a small interval in which $\phi_t(x)$ changes rapidly from $\phi_t(0)$ to $\phi_t(1)$ (in this interval indeed its derivative, Eq. (3.18), is large).

Equation (3.19) also allows to evaluate $\partial_t \phi_t(x)$ and check the validity of the approximation. This can be cast in the form $F(\phi_t, \Omega_t) = 0$ where the dependence on t comes in Ω_t. Then $\partial_t \phi_t = -\omega_t \partial_{\Omega_t} F / \partial_{\phi_t} F$ that reads

$$\partial_t \phi_t(x) = \beta \omega_t \phi_t^2(x) \left[1 - \frac{\omega_t}{\omega_t + 1} \phi_t(x)\right] [x - x_c(t)] = \frac{\omega_t}{\Omega_t} (x - x_c) \partial_x \phi. \tag{3.21}$$

From the above estimates of ϕ_t we find that $\Omega_t \partial_t \phi_t$ is small in absolute value. At most it has a sharp peak of the order of $\log\log\Omega_t/(\log\Omega_t)^2$ close to x_c. Thus it is vanishingly small w.r.t. $(\Omega_t + \omega_t)\phi_t$ as $\Omega_t \to \infty$ which supports the validity of the approximation. Higher time derivatives of ϕ_t, that can be explicitly calculated in the same way, also yield a negligible contribution as $\Omega_t \to \infty$.

Note that $\Omega_t \partial_t \phi_t$ is of the same order of $\omega_t \phi_t$ up to $x \sim x_c - 1/\log\Omega_t$. $\phi_t(x)$ decreases below x_c and it increases above x_c. $\partial_t \phi_t$ vanishes very rapidly over a length of the order of $1/\Omega_t$ for $x > x_c$ and $\int_0^1 \partial_t \phi_t(x) dx = 0$, apart from exponentially small terms. So the total loss of $\phi_t(x)$ below x_c is compensated by its increase in a small region above x_c.

One unpleasant feature of the approximation used is that $\langle h_t(0)\rangle$ is fixed by the boundary conditions. The undesired consequence of this is that, since $\langle h_t(0)\rangle = \langle N_t - N_{t-1}\rangle = \omega_{t-1}$, Eq. (3.17) yields a recurrence relation for Ω_t that implies $\lim_{t\to\infty} \omega_t = \infty$. The simplest way to overcome this problem is to take $\langle h_{t+1}(x)\rangle = (\Omega_t + \tilde{\omega}_t)\phi_t(x) + \omega_t - \tilde{\omega}_t$ from the beginning. The only effect of this different choice is to replace ω_t by $\tilde{\omega}_t$ in Eqs. (3.17–3.21). Using the expansion $\langle h_{t+1}(x)\rangle = \langle h_t(x)\rangle + \partial_t\langle h_t(x)\rangle + \ldots$ we can control the approximation requiring that the L_2 norm of the error $\Delta\langle h_{t+1}(x)\rangle = \langle h_t(x)\rangle + \partial_t\langle h_t(x)\rangle - [(\Omega_t + \tilde{\omega}_t)\phi_t(x) + \omega_t - \tilde{\omega}_t]$ is minimum. This condition fixes the value of $\tilde{\omega}_t$ that, once the calculations are worked out, is

$$\tilde{\omega}_t = \omega_t + \frac{3\omega_t}{2\Omega_t x_c(t)} + O(\Omega_t^{-2}\log\Omega_t) \tag{3.22}$$

Thus, in the end, this refinement of the approximation implies only a shift of ω_t by an amount of order $1/\Omega_t$.

Figure 3.1 displays the histogram from 10^6 realizations of $t = 100$ IP clusters compared to the solution $\phi_t(x)$. The values of $\Omega_t \simeq 106$ and $\omega_t \simeq 0.853\ldots$ were computed in the simulation. The accuracy of the solution, as expected, gets worse as x_c is approached[2]. The accuracy improves as Ω_t increases. Note that $\phi_t(x)$ has a sharper character than the numerical histogram that may be indicative of a too large value of Ω_t or β. The weak point in our scheme, that is also the hardest to deal with, is the approximation on $\langle Z_t(x)\rangle$. The same assumption that $\langle Z_t(x)\rangle$ depends on the RTS through $\langle h_t(x)\rangle$ is by no mean obvious.

The histogram $\phi_t(x) = \langle h_t(x)\rangle/\Omega_t$ converges to a step function as $t \to \infty$. This is the behaviour that is actually observed for empirical distributions in quenched growth models. In IP the location of the discontinuity coincides with the critical threshold p_c and we find:

$$p_c = \lim_{t\to\infty} x_c(t) = \lim_{t\to\infty} \frac{1}{\omega_t + 1}. \tag{3.23}$$

The limit of ω_t as $t \to \infty$ in IP is the surface to volume ratio of the cluster. In Ref. [50] this relation was derived rigorously for IP. The last relation is very similar to

[2]The discrepancy for $x > x_c(t)$ is required by the normalization condition.

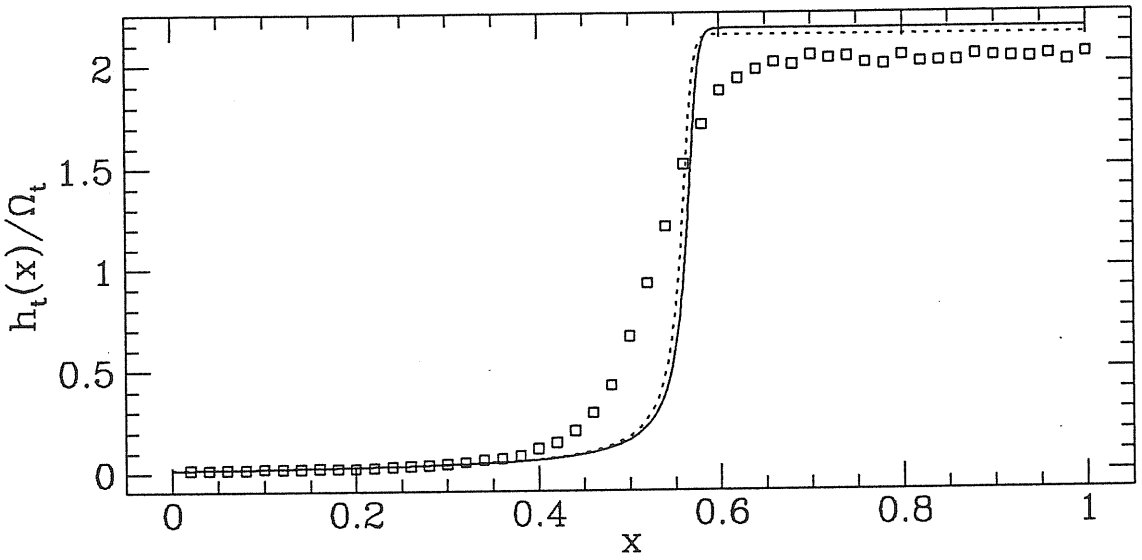

Figure 3.1: Empirical distribution $h_t(x)$ evaluated in a computer simulation ($\Box$) compared to $\phi_t(x)$. 10^6 clusters of size $t = 110$ were generated. The parameters in $\phi_t(x)$, computed in the simulation, are $\Omega_t \simeq 106$, $\omega_t \simeq 0.853$ (full line) and $\tilde{\omega}_t \simeq 0.875$ (dotted line).

the one that results from a partition function approach for the Self Avoiding Walk [55] where the critical step fugacity k_c is related to the average number b_t of bonds that can be added to a walk of t steps: $k_c = \lim_{t\to\infty} 1/b_t$. The similarity is even more suggestive in terms of $n_{0,t} = \omega_t + 1$. The relation $p_c = \lim_{t\to\infty} 1/n_{0,t}$ implies that asymptotically the average number of the newly added random variables that are smaller than p_c is one.

Figure 3.2 shows that Eq.(3.23) is satisfied quite well in IP. The motivation for the choice of the variable $t^{-1/D\nu}$ in Fig. 3.2 comes from scaling relations in ordinary percolation. The size $\xi(p)$ of the typical cluster is connected with the deviation from p_c as $\xi(p) \sim (p_c - p)^{-\nu}$. This is also related to the mass t via the fractal dimension D: $\xi(p) \sim t^{1/D}$. These scaling relations together imply that $p_c - (1+\omega_t)^{-1} \sim t^{-1/D\nu}$. The slow convergence to p_c makes it hard to use this method to evaluate the critical threshold: to get $(1+\omega_t)^{-1}$ within 1% of p_c clusters of the size of $t \sim 10^5$ are needed.

Once $\langle h_t(x)\rangle$ is known, we can also evaluate the distribution of the minimum variable in $\partial\mathcal{C}_t$: $\langle m_t(x)\rangle = -\partial_x\langle Z_t(x)\rangle = \omega_t + 1 - \omega_t\phi_t(x)$. $\langle M_t(x)\rangle = \int_0^x \langle m_t(x)\rangle$ in its turn provides an approximate expression for $p_{\tau,t}(x)$ through Eq. (3.7). Actually we cannot evaluate the average of the product of $M_k(x)$ in Eq. (3.8), but only the product of the average values $\langle M_t(x)\rangle$. Using Eq. (3.21), and expanding $\langle M_{t-k}(x)\rangle$ in the time variable around t, we easily find that $\langle M_{t-k}(x)\rangle$ can be replaced by $\langle M_t(x)\rangle$ at the expense of errors of the order of k/Ω_t. Within these approximations the RTS

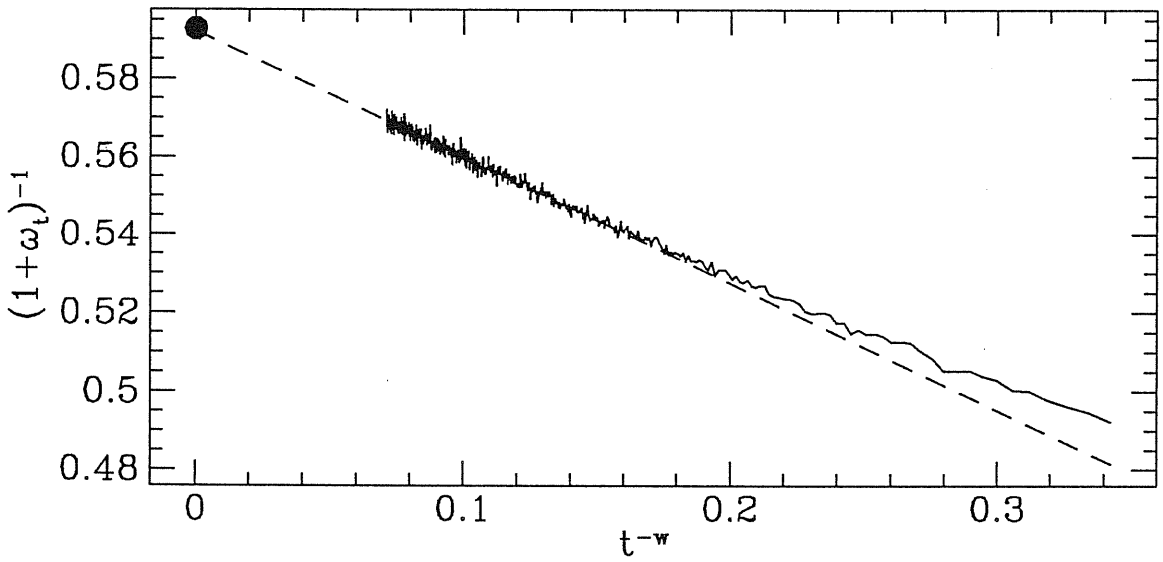

Figure 3.2: Effective threshold $p_c(t) = 1/(\omega_t + 1)$ from numerical simulation (10^6 cluster of size $t = 800$) for site invasion percolation on the square lattice. The form $p_c(t) = p_c(\infty) + At^{-w}$ with $w = 1/D\nu$ is extrapolated (dashed line) in the range $150 < t < 800$ to $p_c(\infty) = 0.5924 \pm 0.0010$.

$p_{\tau,t}(x) \simeq A\langle M_t(x)\rangle^\tau$ can be used in Eq. (3.4) to get an estimate of the GPD:

$$\mu_{\tau,t} = \int_0^1 \frac{M_t^\tau(x)}{\int_x^1 M_t^\tau(y)dy}\,[1 - M_t^\tau(x)]\,dx \tag{3.24}$$

where a factor $Z_t(x) = 1 - M_t(x)$ has been singled out in the integrand of Eq. (3.4) and we have suppressed the average symbol. The above integral is easily evaluated numerically[3]. Since the limit $\lim_{t\to\infty} \mu_{\tau,t} = \mu_{\tau,\infty}$ is finite and $\mu_{\tau,t} = \mu_{\tau,\infty} + O(\Omega_t^{-1})$ we leave the discussion of the GPD for a later paragraph where $\mu_{\tau,\infty}$ is analyzed.

Finally from the estimate of $p_{\tau,t}(x)$ we can also find an approximated expression for $n_{\tau,t}$. This is achieved expanding both sides of

$$\Omega_t\phi_t(x) = \sum_{\tau=0}^{\infty} n_{\tau,t}p_{\tau,t}(x) = \sum_{\tau=0}^{\infty} n_{\tau,t}\frac{M_t^\tau(x)}{\int_0^1 M_t^\tau(y)dy}, \tag{3.25}$$

which defines $\langle h_t(x)\rangle$, in powers of x for $t \to \infty$. All the derivatives of ϕ_t and $M_t(x)$, as well as the integral of $M_t^\tau(x)$, can be evaluated explicitly so that equating the coefficients of x^k on both sides yields a system of linear equations for $n_{\tau,t}$. We just mention here the leading term in $1/\Omega_t$ that is

$$n_{\tau,t} = \omega_t + \frac{1}{\tau+1} + O(\Omega_t^{-1}). \tag{3.26}$$

[3]The integrand can be expressed as a function of $M_t(x)$ alone and then a change of integration $M_t(x)dx = dM$ leads to a definite integral in M.

This concludes the exposition of the results for the IP model. In summary we have been able to give an estimate of all the quantities appearing in Eqs. (3.4–3.7). Due to the approximations used, that are too severe with respect to time correlations, our results, specially those concerning the RTS, the GPD and $n_{\tau,t}$, are not expected to meet more than qualitative agreement with the actual quantities.

3.1.4 The Solution for the General Case

The extension to the case $\mathcal{G}_t \neq \emptyset$ of the procedure outlined for the IP model follows the same guidelines. The only difference is that in taking the difference of Eq. (3.9) for $t+1$ and t the new term $\sum_{i\in\mathcal{G}_t} \rho_{i,t}(x)$ appears. The origin of this new term is model dependent. The way in which the sites in $\mathcal{G}_t$ are chosen in $\partial\mathcal{C}_t$ may depend on geometric properties of the interface in a neighbourhood of the site with the minimum RV. Examples of this sort will be discussed in the next section. One could also think to a mechanism of growth independent of the location of the smallest RV. Think for example to a modification of IP in which the sites in $\mathcal{G}_t$ are chosen randomly with equal probability in $\partial\mathcal{C}_t$. This generalization would include IP and the Eden model, when $G_t = |\mathcal{G}_t| \gg 1$, as particular cases. For this model

$$\left\langle \sum_{i\in\mathcal{G}_t} \rho_{i,t}(x) \right\rangle = \frac{\gamma_t}{\Omega_t} \langle h_t(x) \rangle \tag{3.27}$$

where $\gamma_t = \langle G_t \rangle$. We will discuss later how to improve this equation to account for the situation in which the growth events of $\mathcal{G}_t$ and of i_t are not independent.

The boundary conditions (3.11,3.12) still apply while that on $\langle h_{t+1}(x) \rangle$ must be modified to

$$\langle h_{t+1}(0) \rangle = \gamma_t + \omega_t + 1. \tag{3.28}$$

The same approximation Eq. (3.14) for $\langle Z_t(x) \rangle$ is used, but now the same algebra shows that Eqs.(3.11,3.12,3.28) implies that β is a solution of

$$\beta = \left(1 - \frac{\gamma_t}{\Omega_t}\right)\left(1 - e^{-\beta\Omega_t}\right) \tag{3.29}$$

and the equation for the histogram finally becomes

$$\langle h_{t+1}(x) \rangle = \left(1 - \frac{\gamma_t}{\Omega_t}\right) \langle h_t(x) \rangle \left(1 - e^{-\beta\langle H_t(x)\rangle}\right) + \gamma_t + \omega_t + 1. \tag{3.30}$$

As before, $\langle h_t(x) \rangle = \Omega_t \phi_t(x)$ and we take $\langle h_{t+1}(x) \rangle = (\Omega_t + \omega_t)\phi_t(x)$. Then Eq.(3.17) generalizes to

$$\phi_t(0) = \frac{\gamma_t + \omega_t + 1}{\Omega_t + \omega_t} \tag{3.31}$$

while the solution is given by

$$\frac{\gamma_t + \omega_t}{\gamma_t + \omega_t + 1} \log\left[\frac{(\Omega_t - \gamma_t)\phi_t}{\gamma_t + \omega_t + 1 - (\gamma_t + \omega_t)\phi_t}\right] - \frac{1}{\phi_t} = \beta\Omega_t\,[x - x_c(t)] \tag{3.32}$$

with $x_c(t) = [\beta\Omega_t\phi_t(0)]^{-1}$. The same considerations discussed for the IP case are readily translated to this general case. Again we can control the approximation on $\langle h_{t+1}(x)\rangle$ and eventually refine it with a "renormalized" value $\tilde{\omega}_t$ of ω_t. Also the evaluation of the RTS, of the GPD (that refers only to the site with the smallest RV) and of $n_{\tau,t}$ follows the same guidelines and does not need further discussion.

As a final remark we discuss a refinement on the approximation of Eq. (3.27) when the G_t sites are chosen in a way that depends on the site i_t. To improve the approximation on $\sum_{i\in\mathcal{G}_t}\rho_{i,t}(x) = \sum_\tau g_{\tau,t}p_{\tau,t}(x)$ we note that Eq. (3.27) implies that $\gamma_t n_{\tau,t} = \Omega_t g_{\tau,t}$. This means that the probability of a site in $\partial\mathcal{C}_t$ to be in $\mathcal{G}_t$ is the same for all sites (i.e. γ_t/Ω_t) irrespective of their τ value. Often the mechanism to select the sites in $\mathcal{G}_t$ involves only the close neighbourhood of i_t. It is then likely that in this case $g_{\tau,t}$ will be larger for τ small than for $\tau \gg 1$. Within our scheme we can enhance in a simple way the importance of the $\tau = 0$ term in the sum on $\mathcal{G}_t$. This is accomplished taking $g_{\tau,t} = \tilde{\gamma}_t n_{\tau,t}/\Omega_t + (\gamma_t - \tilde{\gamma}_t)\delta_{\tau,0}$ so that Eq. (3.27) becomes

$$\left\langle \sum_{i\in\mathcal{G}_t}\rho_{i,t}(x)\right\rangle = \frac{\tilde{\gamma}_t}{\Omega_t}\langle h_t(x)\rangle + \gamma_t - \tilde{\gamma}_t. \tag{3.33}$$

This is easily seen to provide the same solution outlined above but with γ_t replaced by $\tilde{\gamma}_t$. So finally this refinement only implies a shift in the threshold value. The magnitude $\delta\gamma_t = \gamma_t - \tilde{\gamma}_t$ of this shift is a parameter that must be supplied by consideration of the actual mechanism of growth, however, if $g_{0,t}$ is of the same order of $g_{\tau,t}$ for $\tau > 0$, the shift is expected to be $\delta\gamma_t \sim \gamma_t/\Omega_t$ that is vanishingly small as $\Omega_t \to \infty$. This argument can also be applied to the $\tau = 1$ term. This indeed would yield in Eq. (3.33) a term which is proportional to $\langle M_t(x)\rangle = 1 - \langle Z_t(x)\rangle$ that can also be expressed as a function of $\langle h_t(x)\rangle$. In principle this procedure could be extended further to deal with $\tau = 2, 3, \ldots$. The extension is straightforward, but since it depends on the specific mechanism of growth it will not be discussed here.

3.1.5 The case $\omega_t = 0$

A particular case worth of mention is that of $\gamma_t > 0$ and $\omega_t = 0$. Models recently introduced for interface growth [35] and for biological evolution [45] are exactly of this type. We briefly mention about the former. In $d = 1 + 1$ dimensions, the interface grows along an infinitely long lattice whose transverse size is L. Cylindrical boundary conditions apply in this direction. The surface is pinned by a random force modeled assigning a RV to every site of the lattice. The second ingredient of the model is surface tension that tends to minimize the extension of the interface. In the extreme case (infinite surface tension) the length of the interface is fixed to its minimum possible value (i.e. L) by an height difference constraint that forces the interface on one column to be at the same height or one unit above or below the interface on neighbouring columns. When the site i_t with the smallest random variable among those on the interface grows, also all the sites that are necessary to recover the single

step constraint are forced to grow. Since the number of sites in the interface is always fixed to L we are exactly in the case $\omega_t = 0$ while γ_t is the average number of other sites that have to grow to recover the constraint. Other models of the same sort may involve a milder mechanism for the minimization of the interface length, allowing for a stochastic readjustment of the interface in the region close to i_t.

The peculiarity of these models is that since $\Omega_t = L$ is fixed, they evolve in a stationary regime of growth. The guess $\langle h_{t+1}(x)\rangle = \Omega_t \phi_\infty = \langle h_t(x)\rangle$ in Eq. (3.30) is exact for the steady state empirical distribution (note indeed that $\partial_t \phi_t(x) \propto \omega_t$). This forces us to change slightly the notation: for L fixed we define $\gamma_{_L}$ as the steady state average value of γ_t. The discontinuity in the empirical distribution appears in this case in the $L \to \infty$ limit: $p_c = \lim_{L\to\infty}(1+\gamma_{_L})^{-1}$. In Ref. [45] a derivation of the empirical distribution was given. The result coincide essentially with our $\phi_\infty(x)$ but the derivation was based on the assumption that all the variables in $\partial\mathcal{C}_t$ have the same probability density $\phi_\infty(x)$. This is a misleading assumption, in our opinion, since the difference in the probability densities of the variables in $\partial\mathcal{C}_t$ is actually the origin of the non–trivial behaviour of these models.

The Approach to the Stationary State

Apart from the discussion of the solution, that again follows the same guidelines outlined for IP, we are also in a position to analyze the dynamics of relaxation to the stationary solution $L\phi_\infty(x)$. This is usually characterized by a relaxation time Γ^{-1} that depends on the size of the system through the dynamical exponent z: $\Gamma \sim L^{-z}$[4]. A suggestion in this respect comes from the fact that Eq. (3.30) is mapped into that for the IP model, Eq. (3.16), if $\Omega_t = L - \gamma_t$ and $\omega_t = \gamma_t$. At $t = 0$, in both models, $\langle h_0(x)\rangle$ is a constant and the same function, apart an overall factor, at time t is obtained iterating t times Eqs. (3.30,3.16). Since in IP the number of iterations needed to get an interface of $\Omega_t = L$ sites is proportional to $\Omega_t/\omega_t = L/\gamma_t$ we expect $\Gamma^{-1} \propto L/\gamma_t$ and $z = 0$.

A more rigorous procedure is to consider Eq. (3.30) as a functional relation that yields $\phi_{t+1}(x)$ in terms of $\phi_t(x)$: i.e. $\phi_{t+1} = \hat{\mathbf{T}}_{\gamma_t}\{\phi_t\}$. In the following we consider the situation in which the value of γ_t is fixed to $\gamma_t = \gamma_{_L}$. In situations were [35] this parameter is not fixed from the beginning γ_t reaches its steady state value with a relaxation law that may be independent of that of the histogram. Here we suppose that γ_t relaxes faster than the histogram to $\gamma_{_L}$ or else that it relaxes so slowly that $\phi_t = \phi_\infty^{(\gamma_t)}$ evolves with γ_t adiabaticlly[5].

The operator $\hat{\mathbf{T}}_{\gamma_{_L}}$ has the fixed point $\phi_\infty^{(\gamma_{_L})}$. The dynamical relaxation is related to the damping of a small perturbation in $\phi_t = \phi_\infty^{(\gamma_{_L})} + \delta\phi$ at the fixed point: $\hat{\mathbf{T}}_{\gamma_{_L}}\{\phi_\infty^{(\gamma_{_L})} +$

[4]Usually z is defined with respect to a Montecarlo time step that corresponds to L individual events.

[5]The dependence on γ_t is made explicit in ϕ_∞ in this section.

$\delta\phi\} = \phi_\infty^{(\gamma_L)} + e^{-\Gamma}\delta\phi$ to linear order in $\delta\phi$. Actually such a simple relation for the evolution of perturbations does not hold in our case since

$$\hat{\mathbf{T}}_{\gamma_L}\{\phi_\infty^{(\gamma_L)} + \delta\phi\} = \phi_\infty^{(\gamma_L)} + \delta\phi - \frac{\gamma_L + 1}{L}\partial_x \frac{1}{\phi_\infty^{(\gamma_L)}} \int_0^x \delta\phi(x')dx' \tag{3.34}$$

and it is not possible to find $\delta\phi \neq 0$ such that the last term is proportional to $\delta\phi$ itself. A solution is instead possible if we require that

$$\partial_x \frac{1}{\phi_\infty^{(\gamma_L)}} \int_0^x \delta\phi(x')dx' = \alpha\delta\phi + \eta(1 - \phi_\infty^{(\gamma_L)}) \tag{3.35}$$

where α and η are parameters. The solution of this equation reads

$$\delta\phi(x) = \frac{\eta}{\gamma_L(1 - \alpha\phi_\infty)^2}\left\{(\gamma_L x_c - x)\partial_x\phi_\infty - \phi\left[1 + \gamma_L\alpha\phi_\infty(1 - \phi_\infty)\right]\right\}. \tag{3.36}$$

The relation $\hat{\mathbf{T}}_{\gamma_L}\{\phi_\infty^{(\gamma_L+\delta\gamma_L)}\} = \phi_\infty^{(\gamma_L+\delta\gamma_L)} + (1 - \phi_\infty^{(\gamma_L+\delta\gamma_L)})\delta\gamma_L$ explains the meaning of Eqs. (3.35, 3.36). These state that the operator $\hat{\mathbf{T}}_{\gamma_L}$ cannot be linearized at the fixed point $\phi_\infty^{(\gamma_L)}$ but around the "fixed point" $\phi_\infty^{(\gamma_L+\delta\gamma_L)}$ where $\delta\gamma_L = (1 - \gamma_L/L)(\gamma_L + 1)\eta$. Both $\delta\phi$ and $\delta\gamma_L$ are proportional to η and, as $\eta \propto e^{-\Gamma t} \to 0$, the fixed point $\phi_\infty^{(\gamma_L)}$ is reached. This is a physically sound effect: the steady state empirical distribution is reached by eliminating the excess of small random variables in $\partial\mathcal{C}_t$. Indeed $\delta\gamma_L > 0$ implies that $\delta x_c(t) < 0$; then $x_c(t) \to x_c(\infty)^-$ as $\delta\gamma_L \to 0$. We finally note that α has to be smaller than $\phi_\infty(1) \cong \gamma_L/(\gamma_L + 1)$ to avoid divergencies in (3.36) for $x \simeq 1$. Taking $\alpha = c\gamma_L/(\gamma_L + 1)$ with $c \leq 1$, we get in the end

$$\hat{\mathbf{T}}_{L,\gamma_L}\{\phi_\infty^{(\gamma_L+\delta\gamma_L)} + \delta\phi\} = \phi_\infty^{(\gamma_L+\delta\gamma_L)} + \left(1 - c\frac{\gamma_L}{L}\right)\delta\phi \tag{3.37}$$

that readily yields $\Gamma \simeq \gamma_L/L$ and $z = 0$. This result was also obtained by different methods in ref. [56] where however the relaxation of the histogram function to the steady state was not examined. Note that the characteristic time diverges as $\gamma_L \to 0$. This limit is achieved in a model of interface growth with no surface tension. At each time step the smallest RV is selected among those on top of L adjacent columns and the corresponding column advances of one lattice spacing. The process has clearly no steady state since every column is pinned by always increasing random variables.

The order statistics and $T \neq 0$ Dynamics

Let us consider in more detail the column invasion model we have just mentioned. This model belongs to the phase diagram of a random filed Ising model with asymmetric couplings. Imagine indeed the $T = 0$ Metropolis dynamics with the Hamiltonian of eq. (3.1). Imagine we are interested in the domain wall dynamics in $D = 2$ dimensional lattice that has infinite extent in one dimension and has a width of L sites

in the other. We prepare the system in a initial state in which all the spins are $+1$ up to a fixed height along the strip and above it all spins are -1. As we turn on the magnetic field H some spin becomes unstable (that with the highest local field) and flips. This event may cause other spins to become unstable and to flip, if this does not occur the external magnetic field H is raised until the first one becomes unstable. As a result, the interface advances along the strip. This model has a rather trivial behavior[6]: depending on the competition between the strength J of the coupling and the width Δ of the noise (for which we take a uniform distribution) the growth occurs either layer by layer ($J > \Delta$) or as in invasion percolation ($J < \Delta$), thus generating a fractal cluster.

The situation changes if we consider asymmetric couplings. If $J_{i,j} = J_{||}$ between neighbors along the strip and $J_{i,j} = J_{\perp}$ in the transverse direction, there is a third regime where overhangs are not allowed and the domain wall is a solid on solid (SOS) interface. This occurs if $J_{\perp} < \Delta < J_{||}$. To understand this imagine the situation where a spin on a vertical wall tries to flip. Its gain in energy comes only from the competition between $J_{||}$ and Δ because the final configuration will have one $\perp$ bond satisfied and one not just as in the initial state. However, since $J_{||} > \Delta$, there will be no field h_i for which the move leads to a gain in energy. In a sense, while the model is in the layer by layer phase w.r.t. $J_{||}$ it is in the invasive phase w.r.t. $J_{\perp}$. If we now imagine to let $J_{\perp} \to 0$ we recover exactly the column invasion model mentioned at the end of the last section. As previously mentioned this model never reaches a steady state since every column, independently of the others, is entangled in the endless search for the largest possible random number. The situation changes of course if we raise the temperature: the sites are selected on the interface[7] according to the Boltzmann weight $\exp\{-\epsilon_i/T\}$. However, for a very small temperature $T \ll \Delta$ we can imagine that the evolution is still based on the search of the smallest ϵ_i but the system makes a fault from time to time. Sometime it is not the smallest variable ϵ_i to be selected. If this is a very rare event we can qualitatively describe the system within our model with $\omega_t = 0$. The parameter γ_t will be the average number of "faults" (selection of RV's which are not the smallest) in the time interval between two growth events in which the minimum was actually selected. In brief an estimate of γ is given by the ratio of the contributions of the minimum $\epsilon_{\min}$ and all the other random variables to the partition function, that is

$$\gamma = \sum_{i \neq \min} \exp\left[(\epsilon_{\min} - \epsilon_i)/T\right] \tag{3.38}$$

where $\epsilon_{\min}$ is the smallest variable and we have suppressed the t index on γ since we are interested in its steady state value. The simplest way to deal with this average is to introduce the order statistics $\check{\epsilon}_i$. These are defined as $\check{\epsilon}_k = \check{\epsilon}_{\pi_k}$ where π_k is the

[6]We only consider the range of parameters where the random field cannot overcome the strength of four J couplings so that spin inside the sea of -1 can never flip and the evolution occurs only on the interface

[7]Also in this case events in which a spin in the sea of down spins flips can be neglected by taking $J_{||} \to \infty$.

permutation of the indices for which $\tilde{\epsilon}_k < \tilde{\epsilon}_{k+1}\ \forall k < L$. The distribution density of the k^{th} order statistics $\tilde{\epsilon}_k$ is derived in the appendix and it is

$$\theta_k(x) = -\partial_x \left| (-1)^{k-1} \frac{\partial_\lambda^{k-1}}{(k-1)} Z_\lambda(x) \right|_{\lambda=1}$$

where $Z_\lambda(x) = \frac{1}{\lambda} \prod_{i=1}^{L} [1 - \lambda P_i(x)]$. Then eq. (3.38) can be approximated by

$$\gamma = \frac{\sum_{k>1} \langle \exp[-\tilde{\epsilon}_k/T] \rangle}{\langle \exp[-\tilde{\epsilon}_1/T] \rangle}.$$

For the purposes of evaluating

$$\langle \exp(-\tilde{\epsilon}_k/T) \rangle = (-1)^k \frac{\partial_\lambda^{k-1}}{(k-1)} \int_0^1 e^{-x/T} \partial_x Z_\lambda(x)\, dx \tag{3.39}$$

it is sufficient, in order to uncover the qualitative behavior of γ, to consider the power expansion in x. The x^j term in the expansion of $\partial_x Z_\lambda(x)$ yields a term proportional to T^{j+1}. The expansion is easily examined by observing that

$$-\partial_x Z_\lambda(x) = \sum_{\tau=0}^{\infty} n_\tau P_\tau(x) - \lambda \sum_{\tau,\tau=0}^{\infty} n_\tau (n_\tau - \delta_{\tau,\tau}) P_\tau(x) P_\tau(x) + O(\lambda^2). \tag{3.40}$$

and that the expansion of $P_\tau(x)$ starts with $x^{\tau+1}$. Moreover notice that the λ^{k-1} term in eq. (3.40) contains k factors $P_\tau(x)$ which are at least of order x and on differentiating $k-1$ times w.r.t. λ, the terms of order smaller than $k-1$ in λ vanish. These considerations suggest that the contribution of the k^{th} order statistics to the statistical sum is at least of order T^k. This is however not true because of the Kronecker δ in eq. (3.40); The T^k term results by taking all τ's equal to zero but $n_0 = 1 + \gamma$ is very close to one. For this reason one must take the k smallest τ values in the term with k P_τ factors. This finally leads to conclude that the contribution of the k^{th} order statistics is of order $k(k+1)/2$ in T. Our final conclusion is then

$$\gamma \simeq \frac{\langle \exp(-\tilde{\varepsilon}_2/T) \rangle}{\langle \exp(-\tilde{\varepsilon}_1/T) \rangle} \sim T^3 + O(T^4).$$

In particular note that, even though as $L \to \infty$ the number of sites diverge, γ remains finite because a series of powers with exponent $k(k+1)/2$ converges if $T < 1$ and the coefficients are all of order L^0. A finite temperature introduces a relaxation time in this problem that diverges as $T \to 0$ as T^{-3} and as L as $L \to \infty$. The situation for a model whose dynamic at $T = 0$ is characterized by $\omega_t = 0$ and a finite $\gamma_0 > 0$ is a little bit different. From the above considerations we expected the k^{th} order statistics to contribute a term of order T^k and then to have a correction of order $\delta\gamma \sim T$ in γ_0.

3.1.6 Asymptotics

This paragraph is devoted to the analysis of the asymptotic behaviour of the quantities appearing in Eqs. (3.4,3.6,3.5,3.7) as $\Omega_t \to \infty$. This is the asymptotic time limit when $\omega_t > 0$ while it is the limit $\Omega_t = L \to \infty$ for $\omega_t = 0$. The empirical distribution, as already discussed, tends to a step function with a discontinuity at $p_c = \lim_{t\to\infty}(1+\omega_t+\gamma_t)^{-1}$. The distribution of the minimum instead tend to

$$M_\infty(x) = \min(1, x/p_c) \tag{3.41}$$

that is also evident from power expansion of $M_t(x) = [1-(\gamma_t+\omega_t)/\Omega_t]y + (\gamma_t + \omega_t)y^2/(2\Omega_t) + \ldots$ with $y = x/p_c$. The function $M_\infty(x)$ is the starting point for the calculations in this section. This will be used to evaluate the RTS $p_{\tau,t}(x)$ from Eq. (3.8) and then of the GPD and of $n_{\tau,t}$ with a procedure already sketched for the IP case. These quantities are relevant in the study of the statistics of "avalanches". Avalanches and self organized criticality in these models will be analyzed in the next chapter. For the moment, with this introductory outline we wish to make explicit from the beginning the approximations involved in this section. This is actually severe with respect to time correlations since the average of the product of $M_t(x)$ in the evaluation of the RTS, Eq. (3.8), is substituted by the product of the average. Furthermore we take $M_{t-k}(x) \cong M_t(x)$ for $k \leq \tau$ and

$$p_{\tau,t} = \frac{M_t^\tau(x)}{\int_0^1 M_t^\tau(x')dx'} \tag{3.42}$$

that is a more controllable approximation since, as discussed in 3.1.3, it only introduces an error of order τ/Ω_t. The results derived within these approximation are however expected to give qualitative information on the actual behaviour of the models considered.

With this proviso, taking $M_t(x) = M_\infty(x)$ in Eq. (3.42) and using the resulting RTS in Eq. (3.4), we find the following expression for the GPD

$$\mu_{\tau,\infty} = \int_0^1 \frac{(\tau+1)y^\tau(1-y)}{1+(\tau+1)(\gamma_t+\omega_t)-y^{\tau+1}}dy. \tag{3.43}$$

This is easily evaluated numerically, but a simple closed expression is not available. The fact that $\lim_{\Omega_t\to\infty}\mu_{\tau,t} = \mu_{\tau,\infty}$ is finite excludes the possibility of a multifractal behaviour of the GPD, that is observed in other growth models that, as IP, produce fractal patterns. Moreover we note that $\mu_{\tau,\infty} \simeq \tau^{-2}/(\gamma_t+\omega_t) + O(\tau^{-3})$ for $\tau \gg 1$. We can next investigate the asymptotic distribution of times that is $n_{\tau,\infty} = \lim_{t\to\infty} n_{\tau,t}$. This is done by taking the limit on both sides of Eq.(3.5) and using the above approximation for the RTS. It is easy to realize that, for $x > p_c$, both limits yield zero. Instead for $y = x/p_c < 1$ this reads

$$1-y = \exp\left\{\sum_{\tau=0}^{\infty} n_{\tau,\infty}\log\left[\frac{1+(\tau+1)\omega_t - y^{\tau+1}}{1+(\tau+1)(\gamma_t+\omega_t)}\right]\right\}$$

Differentiation of both sides yields

$$1 = (1-y)\sum_{\tau=0}^{\infty} n_{\tau,\infty}\frac{(\tau+1)y^{\tau}}{1+(\tau+1)(\gamma_t+\omega_t)-y^{\tau+1}}.$$

The normalization of the asymptotic GPD $\sum_{\tau=0}^{\infty} n_{\tau,\infty}\mu_{\tau,\infty} = 1$ is indeed recovered integrating between 0 and 1 this equation. For $y = 0$ we again find $n_{0,\infty} = \gamma_t + \omega_t + 1$. A system of linear equations for $n_{\tau,\infty}$ results equating the coefficients of y^k in the expansion of the r.h.s. to zero for $k > 0$. A simple expression is not possible for any τ. If $\tau - 1$ is a prime integer we find $n_{\tau,\infty} = [\gamma_t + \omega_t + 1/(\tau+1)][1 + (\gamma_t + \omega_t + 1)^{-\tau}]$. For general values of τ more terms appear in the second bracket while the first factor (the leading one for $\tau \to \infty$) remains unchanged. The result $n_{\tau,\infty} = \gamma_t + \omega_t + 1/(1+\tau)$ derives easily from the same procedure if $Z_t(x) \simeq \exp[-\beta H_t(x)]$ instead of equation (3.5) is used. This agrees with the estimate of $n_{\tau,t}$ given in 3.1.3 but it does not yield the normalization of the asymptotic GPD.

3.2 The RTS and the Fixed Scale Transformation Approach to the Fractal Dimension of Invasion Percolation

This section is devoted to the calculation of the fractal dimension of clusters of invasion percolation with and without trapping. For the second model the result is known exactly, since it coincides with the fractal dimension of the infinite percolating cluster $D_f = 91/48$ while only numerical results are available for the former. The calculation of the fractal dimension for these models, within the Fixed Scale Transformation (FST) approach has been already discussed in ref. [46] using the idea of describing the quenched process by a stochastic one. The equations for the evolution of the RTS in ref. [46] were however incomplete. The results of the calculations, even though in spectacular agreement with exact and numerical results, are then questionable. We propose here to repeat these calculations using the correct evolution of the RTS. Again we find excellent results but a much slower convergence with the order of the calculation which is consistent with the general properties of quenched dynamics.

3.2.1 The Fixed Scale Transformation Approach

The Fixed Scale Transformation (FST) is a theoretical scheme which provides a systematic description of the scale invariant properties of fractal growth models. It focuses on the dynamics at a given scale and it examines accurately the nearest–neighbour correlations at this scale by suitable *lattice path integrals*. The use of scale invariant growth rules allows then to generalize these correlations to coarse grained cells of any size and therefore to compute the fractal dimension. The basic point is to split the long time limit ($t \to \infty$) for the dynamical process at a given scale, from the large scale limit ($r \to \infty$) in which the scale invariant dynamics is defined. In addition, by working at a fixed scale with respect to the dynamical evolution, it is possible to include the fluctuations of boundary conditions and to reach a remarkable level of accuracy for a real space method. This new framework is able to explain the self–critical nature and the origin of self–similar structures in irreversible growth models and to compute their fractal dimension analytically.

The Parametrization of the Structure

Focusing on a fractal structure we want to find a simple way to describe its essential properties. This can be done more easily by choosing a lower dimensional subset with which we can fully characterize the whole structure. For a fractal structure of dimension D_f embedded in two dimension this is clearly the intersection set with a line. The intersection set is also a fractal and its dimension is $D_I = D_f - 1$. For

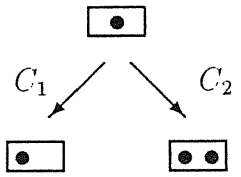

Figure 3.3: The fragmentation process which defines the dyadic random Cantor set of the intersection.

homogeneous self-similar structures the intersection can be done in any direction. Dealing with a structure generated by a growth process, for reason that will be clear in the following, we will prefer to take an intersection perpendicular to the growth direction. We can analyze the set of points generated by the intersection with a procedure of box-covering. A box is characterized by a black dot if it contains some points belonging to the structure. Conversely, a box is characterized by a white dot if it does not contain any point of the structure. First we consider a box of the size of our maximum length scale along the intersection. This box contains the whole set of points, so it is black. We then subdivide this box into two sub-boxes considering length scales half of the previous length. By continuing this subdivision process white boxes begin to appear corresponding to regions in which there is no part of the structure. Then the process of subdivision continues only for the occupied boxes. Clearly, voids (empty boxes) are generated at all scales if the structure is fractal. One can obtain the fractal dimension D_f by the scale invariant statistics of the occupation of the intersection. To look at the scale invariant statistics of this set we focus on the elementary process by which a black (occupied) box is subdivided into two as shown in fig. 3.3. We start by defining the n-n pair correlation configurations along the intersection. The possible configurations of site pairs generated by the growth process are:

i) A configuration of type 1 with an occupied (black) site and an empty (white) site.

ii) A configuration of type 2 with both sites occupied (black).

The probabilities of occurrence of these configuration in the fragmentation (fine graining) process are C_1 and C_2 respectively (see fig. 3.3), with the normalization requirement $C_1 + C_2$=1. These probabilities, strictly speaking, characterize only the n-n transverse correlation at a given scale. If C_i are scale invariant, they characterize correlation between cells of any size. In such a situation our pairs of cells correspond to the generators of the box covering process of the intersection set. In the asymptotic limit, the number of occupied boxes at scale $\ell/2$ can be related to the number at scale ℓ. It is easy therefore to show that the (box counting) fractal dimension of

the intersection set, and then D_f, is is directly related to the value C_1, C_2 by:

$$D_f = 1 + D_I = 1 + \frac{\ln(C_1 + 2C_2)}{\ln 2}. \tag{3.44}$$

The problem of the calculation of the fractal dimension is then shifted to the calculation of the asymptotic distribution $\{C_i\}$. The Fixed Scale Transformation provides a systematic way to evaluate the C_i's considering the generators of the fragmentation process as the basic diagrams of the dynamics of the system.

The Matrix of the Fixed Scale Transformation

Structures produced in fractal growth have two types of invariance:

a) The structure is invariant under scale transformations in the sense that the values of $\{C_i\}$ that we obtain via a fine graining from scale ℓ to scale $\ell/2$ are the same as those obtained from scale ℓ' to scale $\ell'/2$.

b) The structure is invariant with respect to the dynamical evolution at the same scale. This means that if one considers two different intersections of the original structure and performs a fine graining analysis for the two different sets one obtains the same distribution $\{C_i\}$.

The FST method uses this second type of invariance to relate the statistics of occupation ($\{C_i\}$) of two successive intersections in the growth direction. The Fixed Scale Transformation can be thought of as an "equation of motion" for C_i in the growth direction of the intersection, that is a Master Equation for the $\{C_i\}$ under translation. Since C_i is a two dimensional vector, we can write in full generality the Fixed Scale Transformation as an iterative equation of type:

$$\begin{pmatrix} C_1^{k+1} \\ C_2^{k+1} \end{pmatrix} = \begin{pmatrix} M_{1,1} & M_{2,1} \\ M_{1,2} & M_{2,2} \end{pmatrix} \begin{pmatrix} C_1^{k} \\ C_2^{k} \end{pmatrix} \tag{3.45}$$

where k denotes the order of iteration, corresponding to the height of the intersection. The Fixed Scale Transformation matrix elements $M_{i,j}$ are the conditional probabilities that in the asymptotic structures, a configuration of type i will be followed by a configuration of type j in the growth direction. As such they are normalized as $M_{i,1} + M_{i,2} = 1$. Clearly the asymptotic invariant distribution $\{C_i^*\}$ will be given by the fixed point of the FST:

$$C_1^* = \frac{M_{2,1}}{1 + M_{1,2}}. \tag{3.46}$$

The above relation in combination with eq.(3.44) allows one to compute the fractal dimension D_f of the structure. Actually, taking into account the fluctuations of boundary conditions, the matrix elements $M_{i,j}$ will be non-linear functions of the

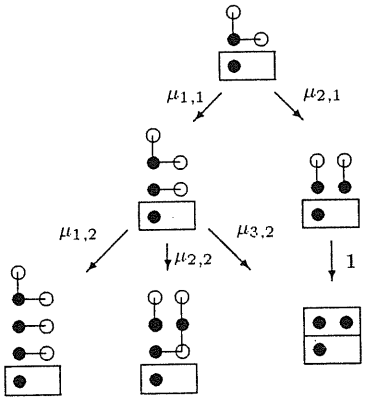

Figure 3.4: The growth processes for the calculation of the matrix element $M_{1,j}$. The probabilities refer to the bonds which join black to white dots. These bonds are labeled by the first index i of $\mu_{i,s}$, from left to right and from the top to the bottom of each configuration. The second index refer to the order of the graph.

distribution C_i itself. Eq. (3.46) is in general a self consistent equation whose solution is the fixed point distribution.

The FST is then a sort of transfer matrix for the probability of occurrence C_1, C_2 of the elementary configurations. It is important to remark in this respect that it relates the statistics of the structure on different intersections at the same scale. This is different from the real space renormalization group approach where the critical behavior is extracted by relating the properties of the same local process at two different scales. If the matrix elements are scale invariant, the resulting value of C_i will be the same at all scales and therefore will yield the fractal dimension D_f. In order to have such a situation one should use the scale invariant dynamics in the calculation of the matrix elements, which is not necessarily the microscopic one, and it has to be found using different methods.

The dynamics of the system is then the essential point of the FST approach and it is contained in the matrix elements $M_{i,j} = \text{prob.}(i \to j)$ which define the conditional probability to have a cell of type i followed by a cell of type j on the next line adjacent to it. The matrix elements are defined by the lattice path integrals corresponding to the various growth processes $i \to j$. It should be noticed that this whole construction refers to the "frozen structure", which has already grown to its asymptotic state and for which no further evolution will occur. This implies that the lattice path integrals should be extended until the growing interface is far enough from the starting configurations, so that they can be considered asymptotic (large time limit).

In order to calculate explicitly the matrix elements we develop a diagrammatic graphical method. We start with a configuration of type i and then we consider a "growth" column above it. We have then to consider all the graphs linking the

occupied sites in the initial cell to the sites of the next cell in the column. By the order of graph we will mean the number of bonds occupied by the path, excluding the trivial starting one on top of the cell. We have also to enforce the connectivity of the column, therefore each path consists of a connected sequence of bonds. The matrix elements are evaluated by summing up the weight of each graph of a given order which leads from a configuration of type i to a configuration of type j. In this sense the calculation of the matrix elements corresponds to a lattice path integral defined by the growth process. It is very simple to assign the weight of each path, following the dynamical evolution inside the growth column. Consider for example the figure 3.4 where the starting cell is of type 1. We can not consider growth in the initial cell because it is conditionally "frozen". Therefore we have only two possible paths indicated by the bonds of the corresponding growth events. The probability of the growth events are indicated by $\mu_{i,s}$ where the first index "i" refers to the growth bond and the second one "s" refers to the order of the graph to which it will give rise. At the second order the resulting graphs are five as shown in fig. 3.4. Each of them has a weight given by the product of the probability of the first order path $\mu_{i,1}$ and the probability of the growth process which leads to the corresponding second order path $\mu_{i,2}$. We can now evaluate the matrix elements at the first two orders. At first order only the process $\mu_{2,1}$ will lead to the occupation of both sites in the cell on top of the starting one, therefore $M_{1,2}^{(I)} = \mu_{2,1}$. At second order all the paths generated from the growth process $\mu_{2,1}$ belong to the matrix element $1 \rightarrow 2$. In addition the other first order path of fig. 3.4 can generate a double occupation in the first growth cell with probability $\mu_{3,2}$. We have then at first and second order

$$\begin{aligned} M_{1,2}^{(I)} &= \mu_{2,1} \\ M_{1,2}^{(II)} &= \mu_{2,1} + \mu_{1,1}\mu_{3,2} \end{aligned} \tag{3.47}$$

We can repeat all the previous steps starting with a cell of type 2 obtaining similar results for $M_{2,2}^{(I)}$ and $M_{2,2}^{(II)}$. The relation $M_{i,1} = 1 - M_{i,2}$ provides the other matrix elements.

Clearly the values of the growth probabilities $\mu_{i,s}$ necessary to define the matrix elements are defined through the growth rules of the model considered and depend upon the graph order, the boundary conditions and the type of starting configuration.

The asymptotic matrix elements are those evaluated at the infinite order: $M_{i,j} = \lim_{n\to\infty} M_{i,j}^{(n)}$ but in practice the series (3.47) can be truncated when the probability of occupation of the second site of the configuration j is virtually negligible. This is called the "freezing condition". In fact, if there is a screening effect in the dynamic process, the higher order terms of the series correspond to configurations in which the second site of configuration j is strongly screened by growth which has occurred at other sites. Such a fact is crucial because it allows the rapid convergence of the series of $M_{i,2}$ to a value smaller than one. This is a key point for the formation of fractal structures. In fact, if the $M_{i,2}$ converges to a number smaller than one this implies that $M_{1,1} = 1 - M_{1,2} > 0$ asymptotically. Therefore there is a finite probability that

growth will leave empty sites even asymptotically and, for the scale invariance of the problem, holes of all scales are generated. The FST then states a precise condition to distinguish between compact and fractal structures. Given the growth rule of a model it is possible looking at the FST matrix elements, to decide if it will give rise to a fractal structure or not. In this sense the FST illuminates the key point for the generation of fractal structures as the screening effect of the growth dynamics of the model.

As already mentioned, the growth process, the probabilities $\mu_{i,s}$ and therefore the matrix elements $M_{i,j}$, depend on the configuration of boundary conditions considered. To include the effect of fluctuations in the boundary conditions, the generic matrix element $M_{i,j}$ should be interpreted as the convolution over all possible boundary conditions around the growth column. In this way we define an effective average dynamics with respect to the fluctuations of boundary conditions. The simplest non trivial method to include the effect of different boundary conditions consists in assuming that the matrix elements are not too sensitive to the distance of the next branch unless it is very close. In this sense we can consider mainly two different types of matrix elements. The first type, $M^{\rm cl}_{i,j}$, is evaluated with "closed" boundary conditions (one cell period) for which the next branch is very close. The second type, $M^{\rm op}_{i,j}$, of matrix elements are instead calculated with open boundary condition (infinite period). Without entering the details of the distribution of boundary conditions (the interested reader may consult ref. [57] for an exhaustive discussion), we report here the fixed point solutions in this approximated scheme:

$$C^*_1 = \frac{M^{\rm cl}_{1,2} + M^{\rm cl}_{2,1} - \frac{3}{2}M^{\rm op}_{2,1} - [(\frac{3}{2}M^{\rm op}_{2,1} - M^{\rm cl}_{1,2} - 2M^{\rm cl}_{2,1})^2 + -4M^{\rm cl}_{2,1}A]^{1/2}}{2A} \qquad (3.48)$$

where $A = M^{\rm cl}_{1,2} + M^{\rm cl}_{2,1} - \frac{3}{2}(M^{\rm op}_{1,2} + M^{\rm op}_{2,1})$.

This scheme of calculus, called "open–closed", gives very good results in all two dimensional problems, and could be improved by the introduction of intermediate boundary conditions.

3.2.2 Asymptotic Scale Invariant Dynamic in Invasion Percolation

We have seen that the correlation properties calculated with the FST correspond to the asymptotic structure only if the scale invariant dynamics is used. This is a crucial and not obvious point on which is based the FST. In the growth rules which give the dynamics of the model are defined at the smallest scale considered (the microscopic scale), and it is not obvious that exactly the same growth rules hold also for coarse grained variables. The identification of the effective growth rules which apply to coarse grained variables is necessary for the definition of the FST. In this sense the scale invariant dynamic is an external input that has to be provided with some of the

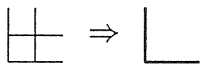

Figure 3.5: The coarse graining procedure for the bonds.

various methods like mean field, cluster expansion, series expansion, renormalization group or even by numerical determination. A general features of the scale invariant dynamics is that it applies to bond variables [58]. The question we have to address here is then what is the scale invariant dynamics of bond invasion percolation.

At the smallest scale, the dynamic variables ϵ_i are the RV's defined on each bond. The dynamic rule applied to these variables is: select the minimum RV among those on the perimeter $\partial\mathcal{C}_t$ of the cluster $\mathcal{C}_t$ and add the corresponding bond to the structure. This simple mechanism produces self similar structures and memory effect: indeed the presence of a finite threshold p_c implies [50] that the structure has a surface to volume ratio $|\partial\mathcal{C}_t|/|\mathcal{C}_t|$ which tends to a constant ω_∞ as $t \to \infty$. This can only be consistent with a fractal structure, since for all compact objects in two dimensions this ratio would vanish as $t^{-1/2}$ ($t = |\mathcal{C}_t|$ is the volume). Next we saw that the probability of selection of a bond depends on the time τ it has been on the perimeter and it vanishes as a power law for $\tau \to \infty$. The possibility to account for these critical properties, at a qualitative level, using the microscopic dynamics alone, suggests that the relevant features of the scale invariant dynamics are already present in the microscopic dynamics.

Let us try to figure out how the dynamics can change under a scale dilatation. The first important point is the coarse graining procedure: the prescription by which the process at one scale is described at the larger scale. The geometry of coarse graining is given in figure 3.5. The set of 8 bonds at the smaller scale (on the left) is replaced by two bonds at the larger scale. Correspondingly we shall define two coarse grained variables $\epsilon_i^{(1)}$, $i = 1, 2$, on these bonds. These will in general be a function of the 8 RV at the smaller scale. The only requirement on this function is that it has to retain the relevant details which allow a description of the process at the larger scale. If these condition is satisfied, in the scale transformation we have eliminated only small scale irrelevant details. For the problem at hand, where the extreme values of the bond variables decide the evolution, the information we want to preserve from one scale to the other is: irrespectively of the path inside the cell, in what direction (vertical or horizontal) will the process evolve. Avoiding the details of the explicit construction of this function, we assume there is a function $\epsilon_i^{(1)} = F(\epsilon_j,\ j = 1, \ldots, 8)$ which is such that the minimum RV among $\epsilon_i^{(1)}$ identifies the direction where the process will evolve. We also make the additional hypothesis that, as for RV at the smaller scale, the two coarse grained variables are independent. Once the function F is known, from the distribution of small scale RV, we can evaluate that of $\epsilon_i^{(1)}$. We now observe that coarse grained RV are defined up to an increasing function. Indeed, as long as $\partial_x f_1(x) > 0$, the variables $\varepsilon_i^{(1)} = f_1(\epsilon_i^{(1)})$ will also enable us to know in what direction

the process is evolving by selecting the coarse grained bond with the minimum $\varepsilon_i^{(1)}$. This additional freedom in the definition of coarse grained cells can be used to fix the distribution of coarse grained RV which are just reached by the cluster ($\tau = 0$). In particular we can choose the uniform distribution for these variables. Isotropy guarantees that the distribution of the two coarse grained variables will be the same. By this hand waving argument, we conclude that the dynamics at scale 1 of invasion percolation is the same as the dynamics at the smallest scale. This same argument can be iterated to any scale thus suggesting that the microscopic dynamic is indeed the scale invariant dynamic in invasion percolation.

The crucial assumption is that of independence of the coarse grained variables. A careful analysis of its validity implies the direct construction of the transformation and the evaluation of the joint distribution of $\epsilon_i^{(1)}$. Even though the transformation might build up a correlation between the variables, the crucial point is whether this correlation vanishes under repeated application of the coarse graining transformation or not. Research in this direction is in current progress.

Having defined the coarse grained variables and their dynamics, we want now to explicitly evaluate the probabilities $\mu_{i,s}$ which enter the calculations of the FST matrix elements. In this respect it is important to note that we will focus on the local dynamics of large scale coarse grained bond variables. We are interested in the asymptotic ($t \to \infty$) behavior of the growth process. This implies that the local growth process, we will focus on, occurs on an infinite cluster. The dynamics we have discussed up to now is not the scale invariant local dynamics but the global one. This is a very important observation.

To understand the difference between the rules of global and local dynamics, let us follow the evolution for a while. At time t the bond with the smallest RV $\epsilon_{i^*} = p(t)$ is selected on the whole perimeter $\partial\mathcal{C}_t$ and it is added to the cluster. In this event new perimeter bonds are reached by the cluster. These are the bonds adjacent to i^* which were neither in $\mathcal{C}_t$ nor in $\partial\mathcal{C}_t$. In the successive global search for the minimum, one of these bonds can be selected. This will happen surely if the smallest among the new RV is smaller than $p(t)$. This is simply because the previous event has shown that all other variables in $\partial\mathcal{C}_t$ are larger than $p(t)$. The global selection will occur on the set of bonds generated by the growth event on bond i^*, at later times $t + s$, as long as the smallest RV $p(t + s)$ will be smaller than $p(t)$. Instead when all "descendants" of the initiator bond i^* have a bond variable larger than $p(t)$, the global dynamics will choose a different region where a new local process will occur. The first conclusion we have reached is that: the global dynamics is based on the selection of the minimum RV on the whole infinite cluster. The local dynamics is instead based on the selection of the minimum RV *in the local environment of the initiator with the additional constraint that the value of the minimum is smaller than the value of the initiator of the local process.* In other words, the cluster globally grows by a series of casually connected local events. These macro events, that we will call avalanches, are characterized by the fact that the minimum RV selected inside the avalanche

at time $t+s$ is smaller than the value of the initiator RV. This condition, namely $p(t+s) < p(t)$, guarantees, at the same time, that all events, inside the avalanche, are spatially and causally connected.

The run time statistics allows to compute explicitly the probabilities $\mu_{i,s}(p)$ of the local growth events inside an avalanche. As shown, this depends on the value $p = p(t)$ of the initiator RV. To compute $\mu_{i,s}(p)$ we will repeat the derivation outlined in section 3.1.2 with the additional constraint that the minimum RV is smaller than p. Imagine to know all the distributions densities $p_{i,s}(x)$ (i.e. the RTS) of the RV ϵ_i generated by the selection of the initiator after s selection events. The probability that the j^{th} RV is the smallest one, being smaller than p, is

$$\mu_{j,s}(p) = \int_0^p dx\, p_{j,s}(x) \prod_{i \neq j} \int_x^1 dy\, p_{i,s}(y). \tag{3.49}$$

With this probability the event at time $t+s$ happens on site j. In this case the distribution of the j^{th} RV becomes

$$p_{j,s}(x) \to m_{j,s}(x) = \frac{\theta(p-x)}{\mu_{j,s}(p)} p_{j,s}(x) \prod_{i \neq j} \int_x^1 p_{i,s}(y) dy \tag{3.50}$$

that is just the density of ϵ_j conditional to the events $\epsilon_j = \min_i(\epsilon_i)$ and $\epsilon_j < p$. The same information acts conditionally on the distribution of other RV's (that were not the smallest at that time) that become

$$p_{i,s+1}(x) = A p_{i,s}(x) \int_0^x m_{j,s}(y) dy \tag{3.51}$$

where A is the normalization constant. The density of each RV, when it is first reached by the cluster, is the uniform one. The equations (3.49)–(3.51), with these initial condition, completely specify the local dynamics.

There are two remarkable points in this dynamics:

- *a)* the local dynamics is defined only in terms of local variables. The presence of an infinite cluster enters only through the value p of the initiator RV. In particular the knowledge of the RTS of all the other RV in the perimeter $\partial \mathcal{C}_t$ is not necessary.
- *b)* the growth probability distribution $\mu_{i,s}(p)$ is not normalized. There is a finite probability $Z_s(p) = \prod_i \int_p^1 p_{i,s}(y) dy$ that the local event stops at time s. This, as we are going to see, is a relevant aspect of the local avalanche dynamics.

How long will the local avalanche event last? The answer to this question depends on the value p of the initiator. If the initiator has a very large bond variable it is

very likely that the local process will never stop. On the other hand, if $p(t)$ is very small it will be very unprobable for the "descendants" to supply at each time a RV $p(t+s)$ smaller than $p(t)$. The probability the local process will survive a time s will drop exponentially to zero as $s \to \infty$ with a characteristic time s_0. Clearly none of the these two local processes is characterized by a scale invariant dynamics. This is evident if we remember that we are dealing with invasion percolation. The initiator site will sample the duration of its local growth process from the cluster size distribution of standard percolation at a concentration $p(t)$. There is only one value p_c for which the cluster size distribution has scale invariant properties. This leads to the conclusion that *the scale invariant dynamics we should use to evaluate the FST matrix elements, is given by the equations* (3.49)–(3.51) *with* $p = p_c$. This is the dynamics of local avalanche events starting from an initiator bond with a random variable $\epsilon_i = p_c$.

In the application of the FST scheme, the freezing condition is usually enforced by normalizing the growth probability inside the column and letting the interface of growth evolve far from the considered region. The region of the cluster one is interested in is that of the *bulk* of the *infinite* cluster. This is important because the fractal properties of the growing interface of the cluster are often different from those of the bulk, which is the case for Diffusion Limited Aggregation [7], and because one is not interested in the properties of finite clusters, which could be sampled for example by the scale invariant dynamics in percolation or Potts models [57]. These two problems can be both solved with the normalization of the growth probability in the growth column. In invasion percolation none of these two problems arise: *1)* the cluster is by definition infinite and connected, and *2)* when a local process stops in a region it leaves a structure with the statistical properties of the bulk of the infinite cluster. Indeed, after a local event with this dynamics has finished no further evolution will ever occur in that region in the asymptotic $t \to \infty$ limit. This is because the scale invariant dynamics will leave only RV larger than p_c in this region. Any further local event in this region will therefore be not scale invariant. Moreover the probability that a second local event will start in the same region vanishes as the size of the cluster $t \to \infty$. The structure produced by the local, scale invariant dynamics is that of the asymptotic cluster.

The above mentioned lack of normalization in the growth probability is totally consistent with the FST scheme. This is a relevant aspect of the scale invariant dynamics in invasion percolation. Events in which growth stops in the column must be included in the statistics because the local growth processes must be sampled from a scale invariant distribution, the cluster size distribution of percolation at p_c. Imposing normalization on this distribution is the same as sampling this distribution for $p = 1$. We have checked that the FST result for the fractal dimension is, accordingly, $D = 2$: a compact cluster.

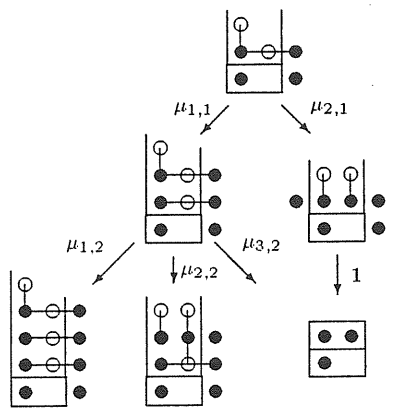

Figure 3.6: The growth processes for the calculation of the matrix element $M^{\rm cl}_{1,j}$. The closed boundary conditions are denoted by the lines on the sides of the growth column. The structure is repeated in the nearby columns as shown.

3.2.3 The Fractal Dimension of Invasion Percolation

Having defined the scale invariant dynamics we should use to study invasion percolation, we can evaluate the fractal dimension following the project of the FST. The bond percolating probability on the square lattice is known exactly: $p_c = 1/2$. This value will be used in the following thus suppressing the dependence on p in $\mu_{i,s}$.

The most relevant technical point lies in the fluctuations of boundary conditions. In the present application the open closed approximation is a very good one. This is because the growth probability $\mu_{i.s}(p_c)$ does not depends on how far is the next branch of the structure, as long as this is not close to the growth column (as for closed boundary conditions). An eventual near branch would have no effect since the local dynamics allows only paths directly connected with the initiator RV.

The calculation is performed using the graphical expansion of the matrix elements shown in figure 3.4. The situation depicted there refers to open boundary conditions, so we will start with the evaluation of $M^{\rm op}_{i,j}$. In the top graph of figure 3.4 the initiator RV, that is relative to the bond which connects the two black sites, has just been selected. The value of its bond random variable was p_c. Therefore the distributions of the RV's on the two bonds that can grow is the original one, that is uniform. The first growth event then occurs with a probability $\mu_{i,1} = \int_0^{1/2}(1-x)dx = 3/8$. Already at the first step, there is a probability $1/4$ that the process will stop. With probability $\mu_{2,1}$ the second site on the upper intersection gets occupied. so the first contribution to $M^{\rm op}_{1,2}$ is $3/8$. The other growth event results in the first order configuration on the left in figure 3.4. The bonds connected to the top black site have a uniform distribution $p_{i,2}(x) = 1$, $i = 1, 2$, while the distribution of bond 3 is obtained with eq.

n	$M_{1,2}^{\rm op}$	$M_{2,2}^{\rm op}$	$M_{1,2}^{\rm cl}$	$M_{2,2}^{\rm cl}$
3	0.43869730	0.59135136	0.65073384	0.72864921
4	0.50334684	0.65782821	0.72777563	0.80269596
5	0.52879759	0.68399751	0.75083084	0.82503358
6	0.55085940	0.70538634	0.77611005	0.84851797
7	0.56151848	0.71594246	0.78531358	0.85716702
8	0.57084028	0.72485091	0.79621307	0.86704406
9	0.57576926	0.72967473	0.80058298	0.87106235

Table 3.1: The Fixed Scale Transformation matrix elements for invasion percolation. n is the order of the calculation, that is the number of bonds that have to grow to enforce the freezing condition. The matrix elements are listed for $j = 2$. The normalization condition $M_{i,1} = 1 - M_{i,2}$ yields the $j = 1$ elements.

(3.51) using the distribution of the minimum $m_{1,1}(x) = 8\theta(x - 1/2)(1 - x)/3$:

$$p_{3,2}(x) = \frac{9}{7} \min\left[\frac{4x(2-x)}{3}, 1\right].$$

Again eq. (3.49) yields $\mu_{3,2} = \frac{31}{140}$ which allows the determination of $M_{1,2}^{\rm op}$ to second order

$$M_{1,2}^{\rm op} = \frac{3}{8} + \frac{3}{8} \cdot \frac{31}{140} + \ldots = \frac{513}{1120} + \ldots$$

It is clear that as the order of the calculation grows, the iteration of the equations (3.49)–(3.51) involves functions of increasing complexity. Moreover the convergence of the matrix elements is very slow. Usually in the applications of the FST, $M_{i,j}$ converges exponentially to an asymptotic value as a consequence of screening. In the present case the convergence is of power law type. This is because stopping the calculation at the order n involves neglecting a contribution $\mu_{i,n}$ to $M_{1,2}$ which is the growth probability of a bond RV that has been tested, unsuccessfully, $n - 1$ times in the search for the smallest variable. We have seen in the previous sections that $\mu_{i,n}$ vanishes as a power law as $n \to \infty$. The same behavior is then expected for $M_{i,j}^{(n)}$.

For these reasons the calculation of the FST has to be pushed to high orders. Some approximations involved in the FST may seem questionable when the order is as high as 8 or 10. These subjects has been analyzed in detail in the past years [57]. In any case the FST scheme provides a systematic prescription to evaluate the fractal dimension to any desired order. A prescription that has well defined physical basis. Extending this procedure to an arbitrarily large order can be done in the same spirit of, say, the standard ϵ expansion for critical phenomena. In the latter scheme one will eventually evaluate exponents for $\epsilon = 2$ or 3, neglecting higher powers of ϵ. In the FST, apart the reliability the method has shown in numerous application, we might have more confidence since in any case the method will provide a lower bound to the fractal dimension [57].

The complexity of the distribution functions generated in the process, forced us

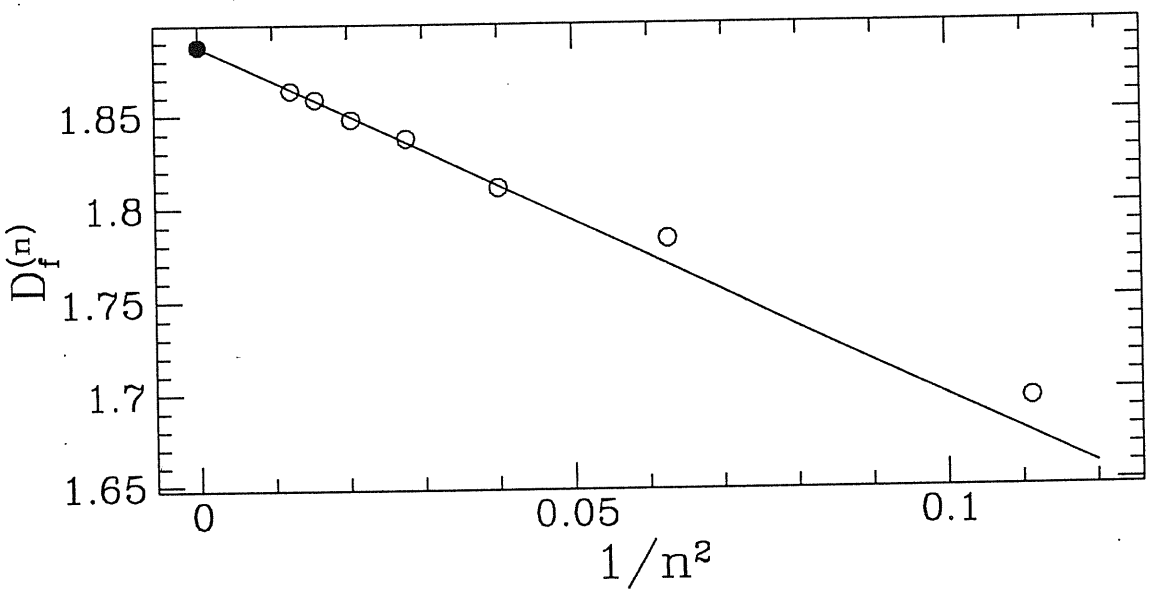

Figure 3.7: Values of the fractal dimension (o) for invasion percolation from the FST at order $n = 3, \ldots, 9$. These are plotted versus $1/n^2$. The linear fit yielding the extrapolation $D_f^{(\infty)} = 1.8879\ldots$ (•) is also shown as the full line.

to resort to numerical techniques. The integrals were performed using Gaussian integration on 100 points in the interval $[0, 1/2]$ (all the distributions have a constant value for $x > 1/2$). A Fortran code was developed to automatically generate the configurations occurring in the growth process and to evaluate the distributions of each bond variable and then the growth probability distribution. The results for the matrix elements with open boundary conditions are reported in table 3.1.

The same method was used to compute the matrix elements for closed boundary conditions. The graphs occurring in the first two steps of the process are shown in fig 3.6. This is the same as figure 3.4 apart from the presence of the adjacent structure mirrored by the periodic boundary conditions. The only technical difference with the previous case is that growth can occur on both horizontal bonds at any height of the structure. This simply amounts in a double counting of the events occurring on the horizontal bonds. The results for the matrix elements $M_{i,j}^{\mathrm{cl}}$ are displayed in table 3.1.

Using these values in equation (3.48), we finally obtain estimates $D_f^{(n)}$ of the fractal dimension of invasion percolation at any given order n. These are plotted in figure 3.7 versus $1/n^2$. As expected the convergence is of power law type. Moreover the figure shows that the convergence nicely fits with the behavior $\mu_{\tau,\infty} \sim \tau^{-2}$ found in section 3.1.6. The extrapolation to infinite order can be performed by a linear fit. The result of this is $D_f^{(\infty)} = 1.8879\ldots$ which is a lower bound between 0.5 % of the fractal dimension of the infinite cluster of percolation $D_f = 91/48 = 1.89583\ldots$.

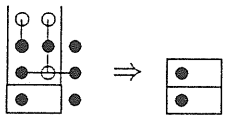

Figure 3.8: The inclusion of trapping in the FST calculation. The second site of the configuration above the frozen one is surrounded by the structure. Then it will asymptotically remain empty. All the paths that are generated in the successive evolution will contribute to $M^{\rm cl}_{1,1}$.

3.2.4 The Extension to Invasion Percolation with Trapping

The same calculation is easily extended to the invasion percolation with trapping. The growth mechanism of invasion percolation may produce voids in the cluster. Actually, since the cluster is a fractal, it will produce voids, or holes, of any size. In the version of invasion percolation that includes trapping, the growth process is not allowed to continue inside the voids. Once a region has been closed by the structure it remains asymptotically empty (or trapped). This is a more realistic model, than invasion percolation, for various situations involving fluid flow in porous media. This additional constraint in the model poses great problems on the theoretical side. L. Pietronero and W. R. Schneider [46] have shown that the FST can account for the nonlocal effects introduced by this constraint in a rather simple and natural way.

Let us start from the problem of identifying the scale invariant dynamics. Assuming statistical independence of the coarse grained RV the scale invariant dynamics is totally specified by the value of p_c. This, for invasion percolation with trapping, is the same as that of the model without trapping. This can be argued as follows: Imagine to set up a real space renormalization group method to evaluate the threshold p_c for invasion percolation with and without trapping. We would certainly rely on the coarse grained procedure of figure 3.5. All the processes on this configurations will have the same statistics in the two cases, since no trapping event can occur in the left hand configuration. Our fixed point value of p_c will therefore be the same in both cases. An alternative way of finding the same result is based on the observation that once a region gets trapped, in invasion percolation, the growth events inside the region and outside it become statistically independent. This means that, the fact that growth occurs inside the trapped region or not, has no consequence on the growth process on the external perimeter. So the scale invariant dynamics will be exactly the same.

A direct consequence of these observation is that the FST matrix elements with open boundary conditions will coincide with that found previously for the case without trapping. The only difference then comes in the calculation of $M^{\rm cl}_{i,j}$. Indeed trapping events occur only for this kind of boundary conditions. The first graph where such an event occur is the second order graph of figure 3.6 that is reported

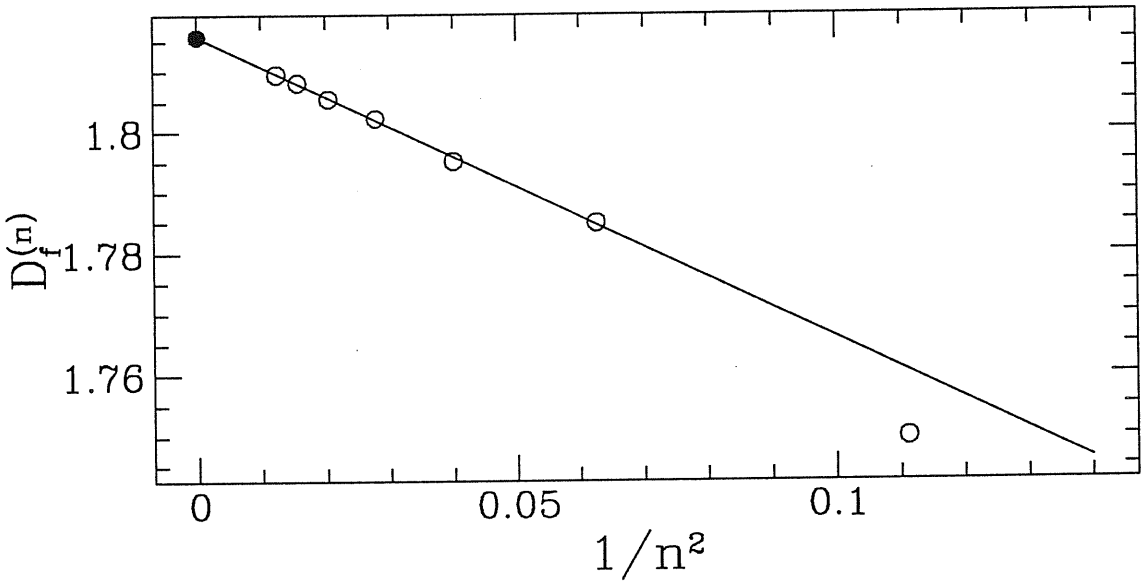

Figure 3.9: The results of the FST for the fractal dimension of invasion percolation with trapping. The line is a linear fit of $D_f^{(n)}$ (o) versus $1/n^2$ and yields the asymptotic value $D_f^{(\infty)} = 1.8157\ldots$ (•).

in fig. 3.8. In this graph the second site of the configuration above the frozen one is surrounded by the structure. Trapping is fully taken into account if we forbid further growth on this site. Then, as shown in figure 3.8, this graph and all these generated by the successive growth will contribute to $M^{\rm cl}_{1,1}$. Trapping occurs also in higher order graphs, whenever both sites, at a given height larger than 1, get occupied. It is very easy to account for these events. The matrix elements $M^{\rm cl}_{i,j}$ were also obtained iterating numerically the equations for the RTS. The resulting estimates for the fractal dimension is plotted in figure 3.9 again versus $1/n^2$. The extrapolated value $D_f^{(\infty)} = 1.8157\ldots$ is totally consistent with known numerical results [41, 48].

3.3 The RTS and the Real Space Renormalization Group Approach to a Simple Model of Biological Evolution

This section discusses the critical properties of a model recently proposed by P. Bak and K. Sneppen, for biological evolution [45]. This is probably the simplest model which combines both the effects of irreversible dynamics and quenched disorder and displays a non–trivial self organized critical behavior. Our goal is not to discuss its implications in biology but rather to propose a new method to tackle a wider class of models. This approach is based on two elements: *i)* the transformation, based on the run time statistics, of a quenched quenched process into a stochastic one; *ii)* the identification of the scale invariant dynamics of avalanche events through a real space renormalization group (RSRG) approach along the same general lines of ref. [59]. This allows to unravel the self organized nature of the process and to compute the critical exponents that agree fairly well with available numerical data on the Bak–Sneppen (BS) model [45].

The BS model [45] is defined as follows: to every site i of a 1–d lattice is associated a random variable (RV) ϵ_i extracted from a uniform distribution. At time step t the smallest RV and k of its neighbors are selected and *refreshed*, i.e. they are substituted with a new uniformly distributed random variable (UDRV). The system self organizes to a "critical" steady state in which almost all RV's are above a certain threshold value ρ. This state is characterized also by long range correlations, both in space and in time.

We focus on the critical behavior of avalanche events. An avalanche is initiated at time t on the site with the smallest RV $\epsilon_i = \rho$ and lasts until the smallest RV in the system becomes bigger than ρ. If this happens at time $t + s$ we say that s is the duration of the avalanche while ξ is the size of the region it has covered. The statistics of avalanche events is characterized by two exponents: that of the avalanche size distribution

$$P(\xi) \sim \xi^{-\tau} \tag{3.52}$$

that yields the probability $P(\xi)d\xi$ that the avalanche size is between ξ and $\xi + d\xi$, and the dynamic exponent of these local events, that relates the duration of an avalanche s to its size ξ

$$s \sim \xi^{z}. \tag{3.53}$$

Often the critical behavior is analyzed in terms of the avalanche *duration* distribution which defines the probability $P_d(s)ds$ that an avalanche lasts a time between s and $s + ds$. Also this distribution has a power law behavior $P_d(s) \sim s^{-\tau_d}$ and its exponent follows directly from eqs. (3.52) and (3.53):

$$\tau_d = 1 + \frac{\tau - 1}{z}. \tag{3.54}$$

In order to set up the RSRG approach, we have to focus on a coarse grained description of the process both in space and in time. This amounts to the identification of cell variables at a generic scale and of the dynamic rule for these variables. The coarse grained variables $\epsilon_i(k)$ in the i^{th} box $B_i(k)$ of 2^k sites, will in general be a function of all the RV $\epsilon_j = \epsilon_j(0)$ at scale 0 inside the box $B_i(k)$. At any scale k the activity will occur in the box that contains the smallest RV. The most general functional dependence that conserves this information at all scales is $\epsilon_i(k) = F_k(\min\{\epsilon_j,\ j \in B_i(k)\})$. Indeed, if $F_k(x)$ is a monotonic increasing function, the relative order of cell random variables is preserved. In particular the box $B_i(k)$ with the minimum RV at scale k will automatically contain the minimum RV at smaller scales. Note that this definition of coarse grained RV has a simple decomposition from scale k to scale $k+1$: $\epsilon_j(k+1) = f_k(\min\{\epsilon_{2j-1}(k), \epsilon_{2j}(k)\})$. Thus the RV at scale k result from the successive applications of the selection of the minimum among two RV at scale j and the function f_j for $j \leq k$. This structure, that for $f_j = 1$ amounts simply in the dyadic search of the minimum among 2^k RV's, is particularly suited to applications in the spirit of the renormalization group.

With respect to the dynamics, again it will rely on the selection of the minimum cell RV. As at the microscopic scale, the avalanche event, started from a box $B_i(k)$, will modify the RV's of neighboring cells. In order to define the dynamics at scale k, we can choose $f_k(x)$ in such a way that the distribution of the new cell RV in the box $B_i(k)$ that had the minimum RV, is uniform. However the new cell RV on the neighbor box $B_{i\pm1}(k)$, that has been updated along with the minimum one, will not be a UDRV in general. Thus we have to allow for a slight generalization of the dynamic rules:

1. the smallest cell RV $\epsilon_m(k)$ is selected and replaced by a UDRV;
2. one of its neighbors (chosen with equal probability) is replaced by a RV distributed with density $b_k(x)$, i.e. $b_k(x)dx = \text{Prob}\{x \leq \epsilon_{m\pm1}(k) < x + dx\}$.

Note that the original Bak Sneppen model [45] in which the smallest RV and its $k = 2$ neighbors were updated with UDRV's, after one scale transformation is of the type described here.

Our goal is to find a transformation that relates the dynamics at scale $k+1$ to that at scale k. More precisely, having parametrized the dynamics with the distribution $b_k(x)$, we will search for the transformation that gives the density $b_{k+1}(x) = \Re\{b_k(x)\}$ in terms of the density $b_k(x)$ at the smaller scale. The fixed point solution $b_\infty(x)$ of the transformation will yield the scale invariant dynamics and then the exponents. This in practice can be achieved by monitoring all histories that start from a *critical* initiator site at scale k and that finally update the RV's of two neighboring cells of size 2^{k+1} (i.e. four RV's at scale 2^k). The renormalization group procedure consists in a mapping of this process in a single burst event at scale 2^{k+1} that has updated two neighbor sites (see fig.3.10).

The first important observation concerns the initiator site. Its RV must be critical in the sense that it initiates an avalanche that belongs to the statistic described by eq.(3.52). In order for this to happen the value ρ of the initiator RV, being the smallest RV in the system, must not be too small, otherwise it will produce a *subcritical* avalanche with a finite expected duration. Let $n_t(\rho)$ be the number of sites whose RV is smaller than ρ. An avalanche started at time t_0 in a site with with a RV $\epsilon_i = \rho$ will continue until $n_t(\rho) > 0$. The avalanche is critical if the average number of descendants of the initiator tends to one as $t \to \infty$

$$\bar{n}_t(\rho) = \langle n_t(\rho) \rangle \underset{t\to\infty}{\longrightarrow} 1 \tag{3.55}$$

where the average is performed on all the avalanche events with initiator $\epsilon_m = \rho$. The value of the limit is one here since the property $n_t(\rho)n_{t'}(\rho) = n_{t+t'}(\rho)$ is expected to hold for $t, t' \to \infty$. Then the possible values of the limit in eq. (3.55) are zero, that corresponds to a subcritical avalanche, ∞, for a super critical avalanche, and 1. Eq. (3.55) is the condition that, given $b_k(x)$, fixes the critical values of ρ. Note the similarity of this condition with eq. (4) of ref. [59]. Before going on, it is worth spending some words on a particular approach to the BS model that leads to a mapping to directed percolation [60].

3.3.1 The *Annealing* Approximation and the RTS Approach

In order to find $n_t(\rho)$ we introduce a representation in which a RV smaller than ρ or below threshold, is described as a particle. Borrowing the notations of second quantization, we introduce creation and annihilation operators, $a_i^\dagger$ and a_i, for a particle on the i^{th} site. Fermi statistics is assumed to ensure the single occupancy constraint. In the initial state, $|\psi_0\rangle \equiv a_0^\dagger|0\rangle$, there is only the initiator particle at $i = 0$. In the particle approximation the evolution of this state is given by $|\psi_t(\rho)\rangle = \hat{U}^t(\rho)a_0^\dagger|0\rangle$ where the operator

$$\hat{U}(\rho) = \frac{1}{2}\sum_{i,\delta=\pm1}(1-\hat{\rho}+\hat{\rho}a_{i+\delta}^\dagger)(1-\rho+\rho a_i^\dagger)(a_{i+\delta}+1-\hat{n}_{i+\delta})a_i \tag{3.56}$$

destroys a particle at site i, the one that bursts, and also one on the neighbor sites $i+\delta$, if it is there ($\hat{n}_i = a_i^\dagger a_i$ stands for the number operator on site i). Then it creates a particle at site i with probability ρ, that is just the probability for the new UDRV to be smaller than ρ, and one in the neighbor site with probability $\hat{\rho} = \int_0^\rho b(x)dx$. The average number of descendants of the initiator is

$$\bar{n}_t(\rho) = \langle\psi_t(\rho)|\sum_i \hat{n}_i\,|\psi_t(\rho).\rangle \tag{3.57}$$

There is a subtle approximation in what we have just said. Indeed the evolution of the probability distribution, under the conditional information acquired by the

system, suggests that particles should carry a second "quantum" number τ specifying the RTS of the RV on that site. This implies that a RV below threshold has a probability to be the smallest one that will differ from particle to particle. This probability, moreover, varies (i.e. it decreases) with time. Eq.(3.56), on the contrary, assumes that particles have the same probability to be selected. This point may change dramatically the nature of the model since the screening effect evidenced by the RTS is neglected. In ref. [60], assuming this *annealing* approximation, it was shown that a description at the mesoscopic level leads to the Reggeon field theory, a model that belongs to the directed percolation universality class. The claim that the BS model belongs to the directed percolation universality class was tested against numerical simulation. However the simulations were performed for the *annealed* model of eq. (3.56). The excellent agreement of the numerical results with directed percolation exponents may then have no relevance for the BS model.

Our intention is instead to take into full account the effect of different distributions in the RG transformation. The difference in the distribution does not arise only because a RV may be generated with density 1 or $b(x)$, but also because of the evolution of distributions, discussed in previous sections, under the information accumulated by the process [46, 61]. In the present case, the condition on the smallest RV must be supplemented with the condition that the event belongs to the avalanche. This in practice means that the smallest RV must be smaller than ρ. We briefly repeat the derivation of section 3.1.3 with this additional condition. Let $p_{i,t}(x)$ be the *run time statistics* of the i^{th} RV, i.e. its distribution at time t. The probability that the j^{th} RV is the smallest one, being smaller than ρ, is

$$\mu_{j,t}(\rho) = \int_0^\rho dx\, p_{j,t}(x) \prod_{i \neq j} \int_x^1 dy\, p_{i,t}(y). \tag{3.58}$$

With this probability the event at time t happens on site j. In this case the distribution of the j^{th} RV becomes

$$p_{j,t}(x) \to m_{j,t}(x) = \frac{\theta(\rho - x)}{\mu_{j,t}(\rho)} p_{j,t}(x) \prod_{i \neq j} \int_x^1 p_{i,t}(y) dy \tag{3.59}$$

that is just the density of ϵ_j conditional to the events $\epsilon_j = \min_i(\epsilon_i)$ and $\epsilon_j < \rho$. The same information acts conditionally on the distribution of other RV's (that were not the smallest at that time) that become

$$p_{i,t+1}(x) = A p_{i,t}(x) \int_0^x m_{j,t}(y) dy \tag{3.60}$$

where A is the normalization constant. These recursion relations for the probability densities enables us to study the deterministic process in a random media as an annealed process, that is one with a time dependent randomness. Note that there is no correlation between surviving RV's that remain mutually independent.

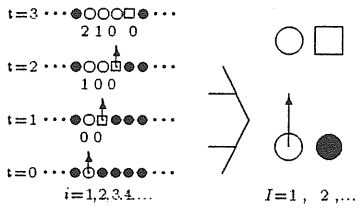

Figure 3.10: A simple path in one avalanche event. In the final configuration, at scale k, four states have been updated. This process (left) is mapped in the RSRG to a single selection–update event (right) at scale $k+1$. The different distributions of the RV's is also reported graphically: sites denoted by • have a RV larger than ρ and cannot take part in the avalanche; ○ (□) sites denote RV that were extracted from the uniform ($b(x)$) distribution. The number below each ○ or □ site indicate the RTS index τ which is the number of times the RV has been checked. The selection events, occurring on the minimum RV, are marked by an arrow.

3.3.2 Sketch of the Renormalization Procedure

Let us leave the problem of the solution of eq. (3.55) and, supposing for the moment to know the critical value of ρ, come to the renormalization scheme. This consists essentially in evaluating, from the knowledge of the distributions of RV at scale k, the distribution of those at scale $k+1$: $\epsilon_j(k+1) = f_k(\min\{\epsilon_{2j-1}(k), \epsilon_{2j}(k)\})$. Consider all paths α, as that shown in figure 3.10, in which the burst of the initiator leads, in the end, to a final configuration of four sites with updated RV's. Let t_α be the number of events occurred in this path ($t_\alpha = 3$ in fig. 3.10) and let the densities of the RV's in the final configuration be $p_i^{(\alpha)}(x) = p_{i,t_\alpha}(x)$ where $i = 1,2$ label sites in the cell $I = 1$ where the initiator was. while $i = 3,4$ label sites in the neighboring cell ($I = 2$). The RG transformation is carried out in three steps:

1. evaluate the distribution density of the minimum in each of the two cells in the final configuration

$$m_I^{(\alpha)}(x) = -\frac{d}{dx} \prod_{i=2I-1}^{2I} \int_x^1 p_i^{(\alpha)}(y)dy, \quad I = 1,2 \tag{3.61}$$

2. average over all possible paths:

$$\langle m_I(x) \rangle = \sum_\alpha w_\alpha m_I^{(\alpha)}(x), \quad I = 1,2. \tag{3.62}$$

The weights $w_\alpha = W\nu_\alpha$ of the paths are proportional the product ν_α of the probabilities $\mu_{j,t}(\rho)$, given by eq.(3.58), of the events that occur in that path. The proportionality constant $W = 1/\sum_\alpha \nu_\alpha$ is fixed by normalization;

3. transform variables in the unit interval ($x \to y$) in such a way that the RV in the $I = 1$ cell is uniformly distributed. This is simply accomplished if $y(x) = \int_0^x \langle m_1(x') \rangle dx'$ so that $\langle m_1(x) \rangle \to 1$ and

$$\langle m_2(x) \rangle \to b_{k+1}(y) = \frac{\langle m_2[x(y)] \rangle}{\langle m_1[x(y)] \rangle}. \tag{3.63}$$

With respect to the standard RG the first two steps perform a decimation of degrees of freedom in which small scale details are eliminated while the third one corresponds to the rescaling of block variables.

Let us now return to the problem of finding the critical value of ρ. Imagine to observe an avalanche spreading through the system. We can describe this event at any scale k. This implies that the number $\bar{n}_t^{(k)}(\rho)$ of cell variables smaller than ρ has the same asymptotic behavior as $t \to \infty$ for any k. In particular eq. (3.55) will be satisfied simultaneously for the same value of ρ at all scales. This statement is a consequence of the scale invariance of the critical state. Our RSRG enables us to evaluate a relation between $\bar{n}_t^{(k)}(\rho)$ and $\bar{n}_t^{(k+1)}(\rho)$ that reads

$$\bar{n}_t^{(k)}(\rho) = \frac{\sum_\alpha \nu_\alpha^{(k)} \sum_{i=1}^{4} \int_0^\rho p_i^{(\alpha)}(x) dx}{\rho + \int_0^\rho b_{k+1}(x) dx} \bar{n}_t^{(k+1)}(\rho) \tag{3.64}$$

and is derived by observing the same process (like that of figure 3.10) at two different scales. The avalanche at scale k produces, form one initiator site, an average number of particles (new RV smaller than ρ) equal to the numerator in eq. (3.64). The same event produces an average number $\rho + \int_0^\rho b_{k+1}(x) dx$ of particles at scale $k+1$. Eq. (3.64) can be iterated back to $k = 0$ and forth to any k. As $t \to \infty$, $n_t^{(k)}(\rho)$ will diverge, vanish or converge to a limit. simultaneously for all k. Then it will converge if and only if ρ is such that

$$\sum_\alpha \nu_\alpha^{(k)} \sum_{i=1}^{4} \int_0^\rho p_i^{(\alpha)}(x) dx = \rho + \int_0^\rho b_{k+1}(x) dx. \tag{3.65}$$

This is the condition that fixes ρ.

The distribution ν_α is defective; it is not normalized to one. The use of ν_α in the numerator of the l.h.s. eq. (3.64) is very important: the condition $\langle n_t(\rho) \rangle \to 1$ as $t \to \infty$ must be imposed averaging over the whole statistics of avalanches, including the finite ones, and not only on the infinite avalanches. Imposing normalization, with the substitution $\nu_\alpha \to w_\alpha$, we would average only over avalanches larger than 2^{k+1}. This average is appropriate for a different quantity

$$\tilde{n}_t^{(k)}(\rho) = \left\langle n_t^{(k)}(\rho) \,\middle|\, \xi \geq 2^{k+1} \right\rangle$$

that is the number of "particles" of size 2^k in an avalanche of size $\xi \geq 2^{k+1}$. This is exactly what we would measure in a box counting analysis of the particle distribution

inside the avalanche: the number of boxes of size 2^k which contains some particle. This number is expected to scale as $\tilde{n}_t^{(k)}(\rho) \sim \tilde{n}_t^{(0)}(\rho) 2^{-kD_f}$, where D_f is the fractal dimension of the particle distribution. At the critical point, eq. 3.64 implies that $\tilde{n}_t^{(k)}(\rho) = W \tilde{n}_t^{(k+1)}(\rho)$. Therefore

$$D_f = -\frac{\ln W}{\ln 2}. \tag{3.66}$$

In order to evaluate the dynamical exponent z, it is sufficient to note that the duration of an avalanche of size 2^k is $T_k = \prod_{j<k} t_j$ where t_j is the number of events at scale 2^j that produce one event at scale 2^{j+1}. The transformation from one scale to the next one, discussed previously, is realized in a number t_j of events at the smaller scale that is itself a random variable with a distribution that, under RSRG iteration, eventually converges to a fixed point distribution

$$P_f(t) = \sum_\alpha w_\alpha \delta(t - t_\alpha). \tag{3.67}$$

The most probable value of T_k is given by the law of large numbers: $T_k \cong \exp(k\langle \log t \rangle)$. The dynamical exponent is then

$$z = \frac{\langle \log t \rangle}{\log 2}. \tag{3.68}$$

In ref. [59] instead of the average of $\ln t$ the logarithm of the average of t was used to compute the exponent z. This method, in our opinion, has a weaker statistical justification and, as we shall see, it leads to an estimate of z which differs by a non negligible amount from that of eq. (3.68). In general, the difference in the two estimates of z is large if $P_f(t)$ has a long tail as in this case. Finally, the exponent of the avalanche size distribution can be derived computing [59]

$$\int_{2^k}^{\infty} P(\xi) d\xi = \prod_{j<k} (1 - K_j) \sim 2^{k(1-\tau)} \tag{3.69}$$

where K_j is the probability that the avalanche stops at size 2^j. For large j, if K_j converges under the RSRG iteration, to a fixed point value K^*, we find

$$\tau = \frac{\log K^*}{\log 2}. \tag{3.70}$$

In practice K^* is obtained summing the probabilities of all processes in which the activity occurs only on the same site $i = 0$, eventually for an infinite time.

Coming to the details of the calculation, it is instructive to evaluate explicitly the contribution of the realization shown in figure 3.10. The probability involved in the second event, at $t = 1$, is $\mu_{2,1}(\rho) = \int_0^\rho b(x)(1 - x)dx$ divided by 2 because of the choice of the neighbor. Correspondingly the density of the smallest RV becomes $m_{2,1}(x) = \theta(\rho - x)b(x)(1 - x)/\mu_{2,1}(\rho)$. The density of the RV on the initiator site

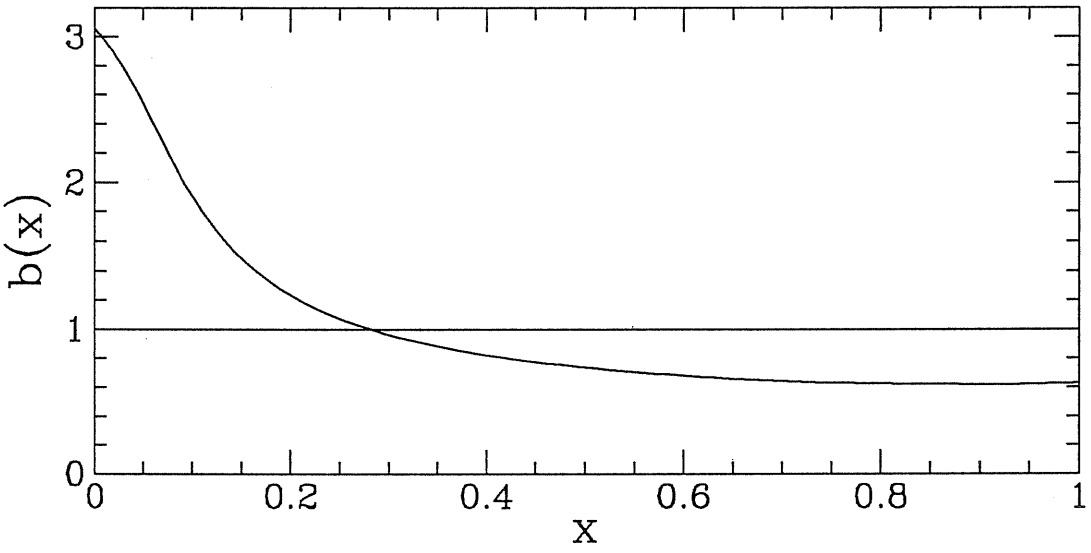

Figure 3.11: The fixed point density $b_\infty(x)$ for $T = 20$. The difference of this and $b_\infty(x)$ obtained for $T = 19$ is at most $\sim 0.01\%$.

at $t = 2$ is $p_{1,2}(x) \propto \int_0^x m_{2,1}(x')dx'$. The activity then moves on site $i = 3$ and the probability of this event is one half of $\mu_{3,2}(\rho) = \int_0^\rho b(x)(1-x)dx \int_x^1 p_{1,2}(x')dx'$. The distribution of the third RV, the smallest at this time, is $m_{3,2}(x) = \theta(\rho - x)b(x)(1-x)dx \int_x^1 p_{1,2}(x')dx'/\mu_{3,2}(\rho)$ and this is used to obtain the final densities on sites $i = 1, 2$ using again eq.(3.60). These with $p_{3,3}(x) = 1$ and $p_{4,3}(x) = b(x)$ are used in eq.(3.61) to find the contribution of this path to the distribution of the smallest RV in the two cells. This path will be summed with all other paths with its probability that is $w_1 = W\nu_\alpha = W\mu_{2,1}(\rho)\mu_{3,2}(\rho)$ where W is such that $\sum_\alpha w_\alpha = 1$.

Already for the simplest path the calculations are involved. For this reason the project outlined up to now was carried out numerically on a computer. Gaussian quadrature with 100 points was used to evaluate integrals. The process at the same scale was reproduced generating all configurations and calculating their weight, up to processes of order $T = 20$. The configurations occurring in the process are labeled by the four indices of the distributions on the four sites. To reduce the number of configurations and of different distributions occurring in the process, densities $p_{i,t}(x)$ with a L_1 distance less than ε were identified. The results are quite stable for changes of $\varepsilon < 5 \cdot 10^{-3}$. The criticality condition, eq.(3.65), was solved numerically. Under RG iteration, $b_k(x)$ converges rapidly to a fixed point $b_\infty(x)$ that is shown in figure 3.11. The attractive nature of the fixed point implies the lack of relevant parameters and can be read as a hallmark of self organization. As a manifestation of universality, we found that the same fixed point was reached for any starting $b_0(x)$. The enhancement of $b_\infty(x)$ for small x w.r.t. the uniform density indicate a tendency of activity to wander rather than to continue in the same region.

T	ρ	$\tilde{\rho}$	z	D_f	τ
12	0.541157	0.710563	2.339501	0.767690	1.269723
13	0.539545	0.709528	2.326541	0.762516	1.271850
14	0.539325	0.708022	2.316740	0.763463	1.273531
15	0.539235	0.707010	2.310200	0.764364	1.274623
16	0.539186	0.706358	2.305882	0.764985	1.275321
17	0.539157	0.705940	2.303040	0.765394	1.275767
18	0.539139	0.705672	2.301172	0.765659	1.276052
19	0.539127	0.705501	2.299945	0.765830	1.276234
20	0.539120	0.705391	2.299141	0.765938	1.276352
∞	0.539107	0.705198	2.297500	0.766125	1.276611

Table 3.2: Results of the RSRG calculation to order $T = 12, \ldots, 20$. Extrapolations were performed using the modified Romberg algorithm.

Table 3.2 lists the results for the exponents. The bottom line reports the results of sequence extrapolation using the modified Romberg algorithm [62]. D_f was evaluated, for any T, from the fixed point value of W and eq. (3.66). For the dynamical exponent, using the logarithm of the average of t [59] instead of $\langle \ln t \rangle$, as anticipated, we find a larger (extrapolated) value of the dynamical exponent $z' = \frac{\ln\langle t \rangle}{\ln 2} = 2.4505\ldots$. With respect to the τ exponent, K^* was evaluated numerically considering in detail the effect of different distributions occurring in the process. The extrapolated values of z and τ, in eq. (3.54), yield an exponent of the avalanche duration distribution $\tau_d \cong 1.1204\ldots$. The agreement of these values with those, obtained via numerical simulation, reported in ref. [45] is quite satisfactory.

3.3.3 The Relation with Directed Percolation

Our results are also in good agreement with the values obtained in ref. [60] from the mapping to directed percolation: $\tau_d^{DP} = 1.08 \div 1.11$ and $1/z \cong 0.4307$. This mapping, as well as these values of the exponents, rely on the annealing approximation.

Let us first analyze the relation between the BS model and directed percolation. By the experience with invasion percolation and the discussion in section 3.2.2, we may formulate an invasive version of directed percolation and argue that the local avalanche dynamics samples the cluster size distribution of directed percolation at the percolation threshold p_c. An avalanche event, in this model, will extend in the "time" direction for a length $\ell_{||}$ and in the spatial direction for a length $\ell_\perp$. These two lengths diverge as $\ell_i \sim |p_c - p|^{\nu_i}$ for $p \to p_c$ with exponents [63] $\nu_{||} \cong 1.733$, $\nu_{||} \cong 1.097$ respectively. $\ell_\perp = \xi$ will correspond to the space variable also for the BS model. The quotes on "time" mean that $\ell_{||}$ is not related to the time in the BS model. Indeed the latter is measured as the number of selection of the minimum RV. This definition of time, for our avalanche of directed percolation, corresponds to its

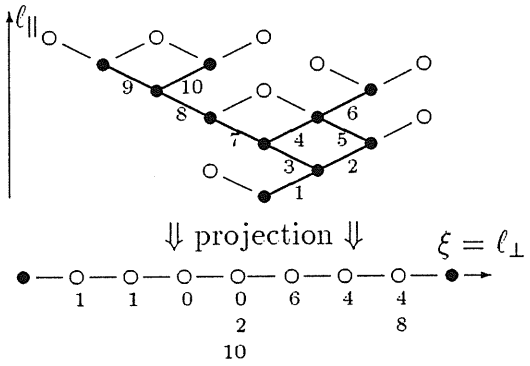

Figure 3.12: The relation between bond invasion directed percolation and the BS model. The bond variables are projected for each space coordinate in the time direction. As a result at each point x there are several variables. The BS model is obtained if only the younger variable is retained for each x. In the figure, the bonds of directed percolation are labeled by the time in which they have grown. Under the sites of the projection we report the RTS index τ for each bond variable.

mass s. Since in each "time" intersection there are a number $\ell_\perp^{D_f}$ of occupied sites, the mass of the avalanche will be $s = \ell_\parallel \ell_\perp^{D_f}$. Using the relation $\ell_\parallel = \ell_\perp^{\nu_\parallel/\nu_\perp}$ which relates the extension of the critical cluster, we find a relation between the time s and the size ξ of an avalanche for invasion directed percolation given by eq. (3.53) with

$$z^{DP} = D_f^{DP} + \frac{\nu_\parallel}{\nu_\perp}.$$

The exponent of the avalanche duration distribution is obtained by observing that the invasive growth process samples the duration s of the avalanches from the cluster size distribution of directed percolation at p_c. This implies an exponent $\tau_d^{DP} \simeq 1.11\ldots$.

A more direct relation between directed percolation and the BS models is sketched in figure 3.12. In the upper part it is shown a realization of directed bond invasion percolation. If we look at the dynamics projected on a "space" line, we find a process very similar to that modeled by Bak and Sneppen. Let us consider, on the projection line, an array of sites in correspondence of the bonds of the directed lattice. The dynamics we will see on this 1-dimensional lattice goes as follows. The smallest RV is selected and a new RV is generated in the same site and in one of its neighbors. However these do not substitute the other variables that were already on these sites. As a result on the same site of the line there will be more than one variable. At each selection on the site, or in one of its neighbors, a new RV will be added to list. The BS model has exactly the same dynamics except that only the most recent RV, on each site, will compete with the others in the search for the minimum. In other words only the last entry of the list of RV's is retained; the one with the smallest index τ the run time statistics. Furthermore note that the annealing approximation for

directed percolation is exact. If a RV on the perimeter $\partial\mathcal{C}_t$ of the cluster is smaller than p_c it will surely grow. It does not matter in what order the "particles" are selected in directed percolation since all of them will be selected sooner or later. In particular one can choose the prescription of directed invasion percolation by which the particle with the smallest RV is selected at each time. The particles can also be updated simultaneously. This is not so in the BS model. A "particle" may be replace by a RV larger than ρ before it is selected. Each different prescription for the order in which the particles are updated leads to a different evolution. The validity of the annealing approximation is therefore not obvious as in directed percolation. Whether these are relevant differences or not, for the determination of the universality class of the model, is not clear. Our numerical results suggest that the mapping to directed percolation [60], if not exact, is a very good approximation. The extension of the RSRG approach to the annealed model and to the projected directed invasion percolation model would probably clarify this issue.

Chapter 4

Self Organized Criticality

A large amount of efforts have been recently devoted to uncover the mechanism underlying the tendency of large statistical systems to self organize into a critical state [2, 66, 59, 49, 60]. This issue has a great relevance since self organized criticality manifests itself in a large variety of phenomena ranging from earthquakes [64] to magnetic systems [39, 52], from interface growth [35, 33] to biological evolution [45].

Much interest has focused on recently proposed models that involve quenched disorder [45, 35] and whose dynamics leads spontaneously to a self organized critical state. The occurrence of critical aspects in connection with a dynamics in a random environment is not a peculiarity of these models: invasion percolation [41] is known to reproduce the critical clusters of standard percolation right at the percolation threshold; non trivial space–time correlations also appear in spin glasses dynamics [52], charge density waves [37] and in zero temperature athermal dynamics of disordered magnetic systems [39, 40]. It has been recently recognized that these systems fit the description of self organized criticality. The latter is based on the concept of *avalanche* which may be defined as a macro event of evolution. The dynamics of a self organized critical system is a sequence of macro–events that are causally and spatially connected. The duration of these events and their size have no characteristic scale. The power law distribution of avalanche size (or duration) is the hallmark of self organized criticality. This is related to the hierarchical structure of avalanche events that extends from the microscopic scale up to the whole size of the system. Inside an avalanche we might identify smaller avalanches which in their turn contain even smaller avalanches and so on.

A peculiarity of systems involving quenched dynamics, apart their critical and self–critical aspects, is the presence of memory effects. Leaving for a later moment a more precise definition of memory, we will say a memory is present in the system if the dynamic of local variables is sensible to "long" period of the past history of the process.

This chapter inquires on the relation between dynamics in quenched disorder, mem-

ory effects and self organized criticality. We have already seen qualitatively and in some explicit example, that both memory effects and avalanche events arise in this dynamics. The main question we have enquired is whether the self organized critical behavior arises in these systems as a consequence of memory or not. The path to address this question we will be the following

1) discuss memory in quenched dynamics;

2) understand how to detect and measure memory in a system;

3) find a method to describe avalanche events without reference to the disorder and

4) generalize a model with quenched dynamics eliminating the disorder and retaining only memory effects. Finally we will analyze the model and find whether it can account for the self organized critical behavior of the corresponding model with quenched dynamics.

We will draw inspiration, in the definition of our model, from the two models already discussed in this thesis: the Bak–Sneppen (BS) model [45] and invasion percolation [41]. The models we will define make no reference to quenched random variables. For a particular value of the exponent α that tunes the effects of the past history on the evolution, we reproduce to some extent the critical behavior of the corresponding dynamics in quenched disorder. The most relevant difference concerns the self organized critical behavior. Avalanches in invasion percolation are not properly reproduced by our model when the exponent α is tuned to that observed in invasion percolation. This suggests that either the parametrization of memory effects in quenched dynamics used in our model is inappropriate or that there are features specific of quenched dynamics which are relevant for the self organized behavior observed. This point will be discussed in the final section. However the model we will define shows a rich scenario of self organized critical behavior. This includes stretched exponential avalanches distributions as well as power law distributions accompanied by a finite probability for infinite avalanches. This allows to conclude that self organized criticality is not a peculiarity of dynamics in quenched disorder. It arises in general as a result of memory effects.

4.1 Memory in Quenched Dynamics

Let us start from invasion percolation. The cluster $\mathcal{C}_t$ grows selecting at each time step the minimum RV among those on the perimeter $\partial\mathcal{C}_t$. This site is included in the cluster $\mathcal{C}_{t+1}$ while the set of perimeter sites is updated to $\partial\mathcal{C}_{t+1}$ adding the sites the cluster has reached with this growth event. We have already seen that, with this rule, the system self organizes to a "critical" state: almost all RV's in $\partial\mathcal{C}_t$ are above a certain threshold value p_c and long range correlations, both in space and in

time, appear. As shown in the previous chapter, this rule is equivalent to a stochastic dynamics. While the original rule is based on (taking the minimum among) the values of the RV, the latter is defined in terms of the distributions of the RV's. The relevant index in the stochastic rule is the number τ of times the RV has been checked in the search for the minimum RV. τ_i, as we have seen, is the "lifetime" of the RV on site i. It is a counter variable which is increased by one each time the RV is not selected and its value is zero for a new uniformly distributed RV. This variable will be a central quantity in this chapter. In order not to confuse it with the avalanche exponent, we shall slightly change notations, using the letter k for counter variables.

In a system that evolves probing a random environment, as the BS model and invasion percolation, it is natural to think that the evolution will take place more often on recently updated regions than in older ones. This is because a site whose RV has been checked a large $k_i \gg 1$ number of times in the search for the minimum RV will probably have a large RV. It still has a probability of being the smallest in the future but this probability gets smaller and smaller as time goes on. This implies that the probability that a site with a counter equal to k is selected decreases with k. In the previous chapter we have shown that it is possible [61], keeping track of the evolution of the statistics of the RV on each site, to pursue this argument further and to evaluate the probability of each growth event. The probability that a random variable ϵ_i is the smallest one depends on k_i. Under approximations of mean field type, for invasion percolation

$$\text{Prob}\{\epsilon_i = \min[\epsilon_j;\, \forall j]\} \equiv \mu_{k_i,t} \sim k_i^{-\alpha} \tag{4.1}$$

for $t \gg k_i \gg 1$ with $\alpha = 2$. It is worth to stress here that $\mu_{k,t}$ is *not* a function of k alone in models like invasion percolation. In a single realization it actually depends on finer details of the past history. However, on average, it displays a fairly stable power law dependence on k as shown in figure 4.1. We postpone a discussion of this figure and how it has been obtained to the last section. For the moment it is important to stress that the qualitative behavior of $\mu_{k,t}$ is correct: it has a power law dependence on the counter variable k. We shall see that exactly this behavior, using approximations of the same nature, can account for the power law in the avalanche size distribution.

4.1.1 Counter Variables and Memory

Before discussing the characterization of avalanche events in terms of counter variables, let us discuss memory effects. For a generic growth process defined in terms of lattice variables ϵ_i we can assign to each site i a counter variable k_i. These are initially set to zero on the whole lattice. The variables k_i starts increasing when the site i is first reached by the growing cluster $\mathcal{C}_t$. The variables k_i of perimeter sites $i \in \partial\mathcal{C}_t$ are increased by one unit at each time step unless they are selected in the growth event. In this way $k_i(t)$ is the time spent by the site i on the perimeter of

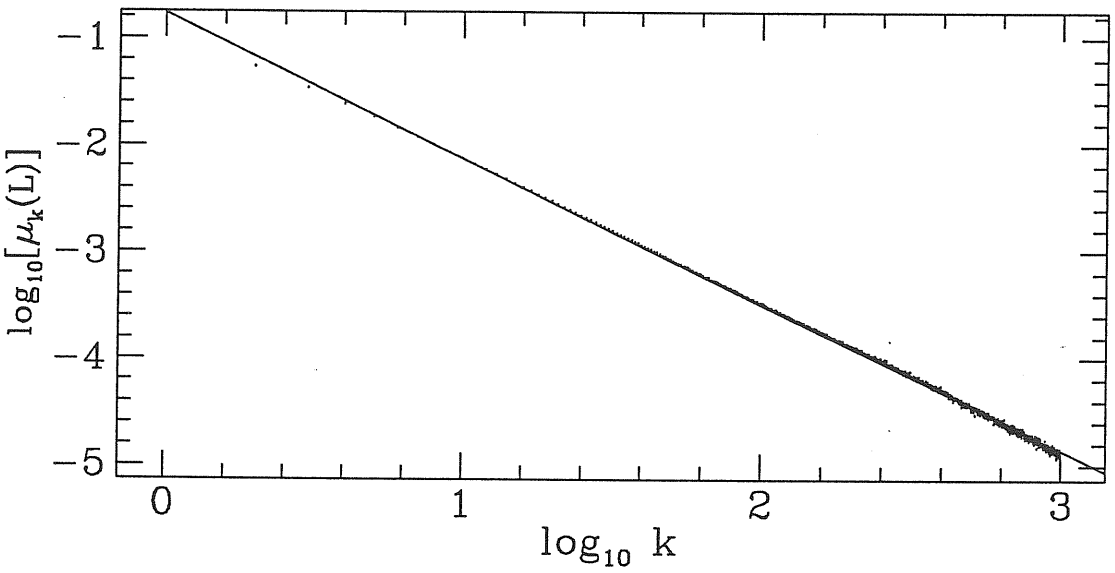

Figure 4.1: The distribution $\mu_{k,t}$ measured in clusters of invasion percolation of $t = 8192$. The power law fit yields an exponent $\alpha_{IP} = 1.35 \pm 0.01$.

the cluster. The distribution $\mu_{k,t}$ can be defined in general as a frequency in terms of counter variables. $\mu_{k,t}$ is a directly accessible quantity in a computer simulations. Indeed the fraction of times selection occurs on a site with $k_i = k$ will be $n_{k,t}\mu_{k,t}$, where $n_{k,t}$ is the number of sites with counter $k_i(t) = k$ at time t. These satisfy the normalization conditions $\sum_k \mu_{k,t} n_{k,t} = 1$ and $\sum_k n_{k,t} = N_t$ which is the number of sites in $\partial\mathcal{C}_t$.

A measure of the effect of memory is given by the first moment of the distribution $n_{k,t}$

$$T_t = \frac{1}{N_t} \sum_{k=0}^{\infty} k\, n_{k,t} \sim t^{\varsigma}. \tag{4.2}$$

On the average the local dynamic of the variable on site i is sensible to a period of length T_t of the past history of the process. The exponent ς is an indicator of the presence of memory effects. Indeed $\varsigma = 1$ implies that the dynamics at time t "remembers" a number of events that is of the order of the "age" of the whole cluster. The local dynamics is sensible to the previous state of the process. Conversely $\varsigma < 1$ implies that the dynamics depends only on the current configuration of the interface.

It is instructive to discuss the above quantities for some examples of cluster growth processes. Let us first discuss the Eden model [67, 24]. In this case $\mu_{k,t}$ is a constant and the resulting distribution $n_{k,t}$ decays exponentially with a rate proportional to N_t^{-1}. The Eden clusters are compact so $N_t \sim \sqrt{t}$ in $D = 2$, and $\varsigma = 1/2$. The surface to volume ratio tends to zero as $t \to \infty$, which is the appropriate thermodynamic limit for all compact clusters. Instead, processes that generate fractal patterns, often lead

to a finite surface to volume ratio for the infinite cluster. This is the case for invasion percolation, where this ratio is related to the percolation threshold [50]. Accordingly we find that T_t is proportional to the volume. Thus we find $\varsigma = 1$. As shown in figure 4.1, $\mu_{k,t}$ decays as a power law in k. As $k < t \to \infty$ $n_{k,t}$ reaches a constant value $n_{\infty,\infty}$ which is the surface to volume ratio. The behavior of $\mu_{k,t}$ embodies the screening effect which produces fractal structures. The screening effect is also present in other models, as diffusion limited aggregation [68] and the self avoiding walk [55]. In the former $\mu_{k,t}$ decays exponentially, as a consequence of the screening induced by the Laplace equation. In the latter $\mu_{k,t} = \delta_{k,0}$ since growth is allowed only at the ends of the walk. Both models have a finite surface to volume ratio and $\varsigma = 1$.

For a system of finite size L (with periodic boundary conditions), the process will reach a stationary state. This is a slightly different situation and it requires a little change in our notations. In the steady state the above distributions attain a constant value $\mu_k(L)$ and $n_k(L)$. These satisfy the normalization conditions $\sum_k \mu_k(L) n_k(L) = 1$ and $\sum_k n_k(L) = L^d$ for a system of linear size L. The equivalent of eq. (4.2) is

$$T_t(L) = \frac{1}{L^d} \sum_{k=0}^{\infty} k\, n_k(L) \sim L^{d(1+\zeta)}. \tag{4.3}$$

As ς, the exponent ζ is an indicator of the presence of memory effects. On the average the local dynamic of the variable on site i is sensible to a period of the past history of the process. If the length of this period, measured in units of L^d individual events, increases with L, i.e. if $\zeta > 0$, the state of the infinite system will depend on the whole history. If $\zeta = 0$ we can say that no memory effect is present.

As an example, consider the Metropolis dynamics [6] of the Ising model. A variable is selected on average once every L^d attempts. With a probability that does not depend on L the move is accepted and the spin flipped. Thus we expect $\zeta = 0$ for this model and in general for equilibrium dynamics. Consider next the prototype model of self organized criticality, the sandpile model [2]: sand is added on randomly chosen sites. A site cannot store more than $2d - 1$ grains and it "topples" when it receives the $2d^{\text{th}}$ one, i.e. it distributes one grain to each of its neighbor sites causing eventually "toppling" on these sites as a result. After a toppling a site is empty. Before it will topple again it needs to store enough sand. Thus the probability that it will topple after k toppling events grows with k and on the average it will topple once every L^d toppling events. Then $\zeta = 0$ also in this case. This result is consistent with the abelian nature of this model [65]. Coming to the quenched disorder, figure 4.2 shows that the situation is different for the Bak Sneppen model [45]. $\mu_k(L)$ decays as a power law in k with an exponent $\alpha_{BS} = 1.31 \pm 0.01$ and $n_k(L)$ satisfies the scaling behavior

$$n_k(L) = k^{-\beta} f\left(k/L^{1+\varsigma}\right) \text{ for } k > 0 \tag{4.4}$$

with $\beta_{BS} = 0.58 \pm 0.01$. The scaling function $f(x)$ drops quickly to zero for large arguments and tends to a constant $f(0) \cong n_1(L)$ for $x \to 0$. The assumption of a single time scale $T_\infty(L)$ for a given size is implicit in (4.4). If $\beta < 1$, the normalization

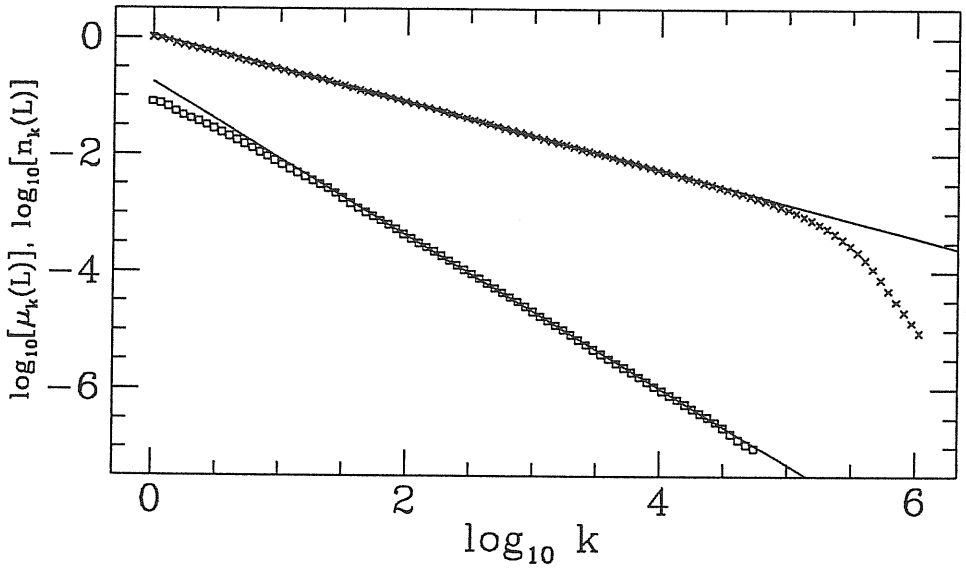

Figure 4.2: The distributions $n_k(L)$ and $\mu_k(L)$ measured from simulations of the BS model.

condition on $n_k(L)$ easily yields the exponent relation

$$\zeta = \frac{\beta}{1-\beta}. \tag{4.5}$$

This yields $\zeta_{BS} \simeq 1.44$ in fair agreement with the direct measure $\zeta_{BS} = 1.46 \pm 0.03$ using eq.(4.3).

The conclusion we have reached is that quenched dynamics implies memory.

4.1.2 Counter Variables and Self Organization

If ζ or ς are the indicators of the relevance of memory, the self organized nature is usually related to the occurrence of avalanche events. An avalanche event is made of a spatially and causally connected series of events.

Let us recall the definition of avalanches in quenched dynamics. This dynamics is based on the selection of the minimum RV. The event on a site at time t may generate RV's in its neighborhood, that are smaller than the one that has just been selected. The evolution will naturally select these RV at time $t+1$. The same may happen for a certain period and as a result selection events will be localized in a small region. This sequence of local causally connected events is an avalanche. At each time one avalanche starts, so a number of nested avalanches are active at each time. In the self organized critical state, the duration s of an avalanche follows a power law distribution $P_d(s) \sim s^{-\tau_d}$ that defines the exponent τ_d.

Up to now and in the previous chapter, we have defined avalanches in processes involving quenched disorder in terms of the sequence $p(t)$ of minimum RV selected during the evolution. If the minimum RV $\epsilon_m = p(t+1)$ at time $t+1$ is smaller than the one $p(t)$ that has been selected previously, the two events are causally connected. This is obvious because the RV selected at time $t+1$ must have been generated in the growth event at time t. At that time in fact the minimum RV was $p(t)$ and not $p(t+1)$. However it might also occur that a RV generated in the event at time t turns out to be the smallest one even though it is larger than $p(t)$. The above criterion would say the two events are not causally connected, while actually they are. The larger is the number of sites N_t or L on which the dynamics searches for the minimum the smaller is the probability of the occurrence of this event.

This problem does not occur if we use counter variable to define avalanche events. The definition of an avalanche is particularly simple in terms of the variables k_i. Indeed the event at time $t+1$ will be causally connected to that occurred at time t if and only if the counter variable of the site selected at time $t+1$ is $k=0$. This argument establishes also the causal connection on a longer period s of time. Consider the avalanche started at time t_0. This will be active at time t_0+s if all sites $i(t)$ selected at times $t_0 < t \leq t_0+s$ had a counter $k_{i(t)}(t) \leq t-t_0$. Indeed this means that all the sites $i(t)$ for $t_0 < t \leq t_0+s$ have entered the set of active sites $\partial\mathcal{C}_t$ after the avalanche began. On the other hand the selection of a site with a counter k at time t terminates all avalanches that started after time $t-k$. Moreover the size of an avalanche that lasts for s time steps is simply evaluated as the size of the region with counters smaller than $k_i \leq s$.

We will assume that this definition of avalanche events, that fully reflect the causality relation that binds individual events into an avalanche, is equivalent to that based on the values of the smallest RV at each time.

In order to discuss the behavior of the avalanche distribution[1] it is convenient to generalize it to account for infinite avalanches

$$P_d(s) = (1-N_\infty)P_d^{(f)}(s) + N_\infty \delta_{s,\infty} \tag{4.6}$$

where N_∞ is the fraction of avalanches that never stop. An avalanche that lasts a time s is terminated when a site with $k_i > s$ is selected. For a finite system of size L, if $k_{\max}(t) = \max[k_i(t), i=1,\ldots,L]$, all the avalanches that began before time $t-k_{\max}(t)$ will never be terminated. These will contribute to N_∞. In general, the probability that the avalanche stops at time t after s events, for what we have said previously, is

$$P_{\text{stop}}(s,t) = \sum_{k>s} n_{k,t}\mu_{k,t}. \tag{4.7}$$

[1]In the remaining of this chapter we will study the statistics of the duration of avalanches. Implicitly, in the following, the avalanche distribution will refer to the duration.

An avalanche will still be active after s events at time t with a probability

$$P_{\rm act}(s,t) = \prod_{k=1}^{s} \left[1 - P_{\rm stop}(s-k, t-k)\right]. \tag{4.8}$$

These two equations provide a relation between the distributions $\mu_{k,t}$, $n_{k,t}$ and the distribution of finite avalanches. This is because the probability to observe an avalanche of duration s is the probability that this avalanche is active after s events times the probability that it stops at time t:

$$P_d^{(f)}(s,t) = P_{\rm act}(s,t) P_{\rm stop}(s,t). \tag{4.9}$$

The contribution of infinite avalanches is instead given by

$$N_\infty = \lim_{t>s\to\infty} P_{\rm act}(s,t). \tag{4.10}$$

It is worth stressing that $P_d^{(f)}(s,t)$ can be factorized as long as the events at time t and $t-k$ for $k<s$ are statistically independent. This is the case for most models of fractal growth [67, 68, 41] and holds also for quenched dynamics as shown in the previous chapter. Note that the growth probability distribution (GPD) $\{\mu_{k,t},\, n_{k,t}\}$ depends on time. More precisely the GPD is itself a random quantity which depends on the past history of the process. The analysis of equation (4.9) involves the problem of evaluating the averages of a product of correlated random variables. Neglecting this correlations and using the product of the average values instead of the average of the product we found the behavior of $\mu_{k,t}$ in eq. (4.1). Before we apply the same approximation to eq. (4.9), it is important to emphasize a further point. A self organized critical behavior can result only if the dependence on t is irrelevant. In other words we will be interested in the distribution $P_d(s) \equiv \lim_{t\to\infty} P_d(s,t)$. This limit is the $L\to\infty$ limit in finite size systems. We will assume this limit situation if the dependence on t (or L) is not explicit in the following. Regarding $P_{\rm stop}(s,t) = P_{\rm stop}(s)$ as a fixed quantity, let us first consider infinite avalanches. These will occur when the infinite product in eq. (4.8) for $t\to\infty$, will converges to $N_\infty > 0$. The criterion for the convergence of infinite product implies that this will occur when the series $\sum_s P_{\rm stop}(s)$ converges to a finite value. This will be the case for the SAW where $P_{\rm stop}(s) = 0$ for $s>0$ and for the DLA where it decays exponentially. Indeed in the former model all the events are causally connected while in the latter infinite avalanches occur as a result of the Laplace screening. When $P_{\rm stop}(s) \sim s^{-\vartheta}$ decays as a power law the sum will diverge for $\vartheta \le 1$. It is interesting to note that, within the same approximation, in section 3.1.6, we have derived relations for $\mu_{k,t} \simeq k^{-2}/\gamma_t + O(k^{-3})$ and $n_{k,t} \simeq \gamma_t + O(k^{-1})$ which lead to $P_{\rm stop}(s) \simeq \kappa s^{-1} + O(s^{-2})$. This is exactly the limiting case $\vartheta = 1$ and the coefficient is $\kappa = 1$. Pursuing this approximation it is not difficult to find in the end that $P_d(s) \sim s^{-\kappa-1}$. The correct power law behavior of the avalanche distribution for invasion percolation is properly reproduced. The value of the exponent is however wrong. $\tau_d = \kappa + 1$ should be compared with the exponent

of the cluster size distribution of percolation at p_c. This is $\tau_d^{IP} = 1.05\ldots$ instead of 2.

If $\vartheta > 1$, apart from a finite contribution of infinite avalanches N_∞, we find a power law distribution for finite avalanches: $P_d^{(f)}(s) \sim s^{-\vartheta}$. For $\vartheta < 1$ finally, our brute approximation suggests a stretched exponential behavior for the avalanche distribution: $P_d^{(f)}(s) \sim \exp(-as^{1-\vartheta})$.

The simplest method to go beyond the approximation used above, is to devise a simple model that may scan the various situations occurring in a process with a memory. This will be the subject of the next section.

4.2 The Generalized BS Model

The key points we have reached up to now with the introduction of counter variables are: *i)* dynamics in quenched disorder leads to memory effects. For a finite size system the model is characterized by power law behavior in both $\mu_k(L)$ and $n_k(L)$ (see fig. 4.2). *ii)* the mechanism of self organization is not the same in sandpile models [2], that display no memory effect, and in the BS model. *iii)* We can describe both memory effects and avalanche events in terms of counter variables alone. These observations motivates the introduction of a new model defined in terms of counter variables to study the interplay between the effects of memory and self organization.

Let us consider again the BS model [45], which is perhaps the simplest model of dynamics in quenched disorder, and repeat briefly its definition: assign a uniformly distributed RV ϵ_i on each site i of a d–dimensional lattice. At each time step select the smallest RV and replace it and the RV's on the neighboring sites with newly extracted uniform RV's. Figure 4.2 suggests a natural generalization of this model which is the following: assign a counter variable k_i to each site $i = 1, \ldots, L$ of a 1 dimensional lattice. At each time step one site is selected, with a probability μ_{k_i} that depends on the value of the counter

$$\mu_k = \mu_0(k+1)^{-\alpha}. \tag{4.11}$$

If site i is selected, its counter variables and that of its neighbor sites are set to zero. All other variables are increased by one:

$$k_{i+\delta}(t+1) = 0 \qquad \text{for } \delta = 0, \pm 1 \tag{4.12}$$

$$k_j(t+1) = k_j(t) + 1 \qquad \text{else.} \tag{4.13}$$

The dependence of the selection probability on k is devised to generalize the situation occurring when the dynamics is driven by the extreme statistics of a random field. This is the simplest way to account for a dependence of the local dynamics on the history of the process. The larger the time a region has been tested for selection

the smallest the probability it will be selected. The rules of the model apply to situations without disorder but with the same screening effect in time. In particular it relies on a stochastic description which is often preferable to the deterministic nature of quenched dynamics. For example, the present model yields a description of biological evolution that differs from that of the original BS model [45]: a specie has a probability to undergo a mutation which is given by (4.11). This probability is consistent with the fact that the longer a specie has not undergone mutations the more it fits its environment. However it still has a probability to mutate and this depends on a stochastic event. Mutations may depend on variables that are not explicitly present in the model and not only on the fitness of the specie. Events like glaciations, fall of asteroids, large scale forest fires or sudden changes of the climate are best taken into account by a stochastic description. In the present model a mutation in one specie can be induced also by mutation in "neighboring" species, as in the BS model. We might also think to other situations this model may describe. Our concern however is mostly on the statistical properties of this model so we will refrain our fantasy.

For a finite L the system reaches to a steady state that is characterized by a distribution of counters $n_k(L)$ for which we shall assume the scaling form eq.(4.4). Of course $n_0(L) = 3$ since three counters are updated at each time step. The normalization of the selection probability $\sum_{k=0}^{\infty} n_k(L)\mu_k(L) = L$ fixes the value of $\mu_0^{(\alpha)}(L)$:

$$\mu_0^{(\alpha)}(L) = \frac{1}{3 + \sum_{k=1}^{\infty} n_k(L)(k+1)^{-\alpha}}. \tag{4.14}$$

Let us start the discussion of the model from the $\alpha = 0$ case. Clearly $\mu_0^{(0)}(L) = 1/L$ at all times. The distribution $n_k(L)$ instead decays exponentially. A simple explanation of this comes from the relation between the number of sites with $k_i(t+1) = k+1$ and $k_i(t) = k$. In the steady state this reads $n_{k+1}(L) = n_k(L)(1 - 3/L)$. This immediately yields $n_k(L) \cong 3\exp(3k/L)$ and $\zeta(\alpha = 0) = \beta(\alpha = 0) = 0$. Of course the probability of a connected event of s steps also goes to zero exponentially with s, i.e. $\tau_d(\alpha = 0) = 0$. In conclusion neither memory nor avalanches are present in the model for $\alpha = 0$. The same behavior is expected to persist for small values of α. Let us focus on a site with $k_i = k$ and consider the probability $p_k(s)$ that it will not be selected in the next s steps, under the condition that in this period it will not be updated because of its neighbors. Clearly $p_k(s) = \prod_{j=k+1}^{k+s}(1 - \mu_0 j^{-\alpha})$. It is not difficult to check that, if $\alpha < 1$, $p_k(s) \to 0$ as $s \to \infty$ while it tends to a constant if $\alpha > 1$. So this site, if it is not updated by its neighbors, will surely be selected sooner or later. This suggests that for $\alpha < 1$ the average time $T_\infty(L)$ between two updates of the same site stays finite and $\zeta(\alpha < 1) = \beta(\alpha < 1) = 0$ (see eq.(4.5)). The occurrence of self organized criticality can be excluded as well for $\alpha < 1$. The probability of local, causally connected events (the avalanches) depends on $\mu_0(L)$. The existence of such events on all length and time scale requires this probability to stay finite independent of L. Supposing the scaling form (4.4) for $n_k(L)$ in eq.(4.14),

α	β	ζ
1.10	0.3 ± 0.1	0.5 ± 0.2
1.20	0.48 ± 0.01	0.90 ± 0.04
1.30	0.58 ± 0.01	1.40 ± 0.06
1.40	0.619 ± 0.005	1.53 ± 0.03
1.50	0.613 ± 0.005	1.47 ± 0.03
1.75	0.571 ± 0.005	1.31 ± 0.03
2.00	0.545 ± 0.005	1.17 ± 0.02
2.50	0.510 ± 0.005	1.06 ± 0.02

Table 4.1: The results of numerical simulation for the exponents β and ζ. The model was simulated for the values of α reported on a finite size lattice of width $L = 32$–256.

it is easy to see that if $\alpha + \beta \geq 1$, as $L \to \infty$, $\mu_0(L) \to \mu_0(\infty) > 0$, while in the opposite case $\mu_0(\infty) = 0$.

Let us now consider the opposite case: $\alpha = \infty$. In this case $\mu_k = 0 \ \forall k > 0$ and $\mu_0 = 1/3$. The model describes a random walk on a $d = 1$ lattice. It is not difficult to find $\zeta(\infty) = 1$ and a distribution $n_k(L)$ that follows eq. (4.4) with $\beta(\infty) = 1/2$. With respect to self organized criticality, the evolution is a single connected event: every avalanche lasts for an infinite time. Thus $N_\infty = 1$ in eq. (4.6).

For a finite, large $\alpha > 1$, supposing again eq.(4.4) for $n_k(L)$, the sum in eq. (4.7) yields $P_{\text{stop}}(s) \lesssim s^{1-\alpha-\beta}$. Thus $P_{\text{act}}(s)$ will converge to a finite limit $N_\infty > 0$ as long as $\alpha + \beta > 2$. Under the hypothesis that $\alpha + \beta$ is a monotonic function of α we define α_c as the solution of $\alpha + \beta(\alpha) = 2$. For $\alpha > \alpha_c$ a finite fraction $N_\infty > 0$ of avalanches will never stop and the distribution of finite avalanches will behave as a power law with exponent $\tau_d = \alpha + \beta(\alpha) - 1$.

Below α_c the probability of infinite avalanches goes to zero. The approximation discussed in the previous section would yield a stretched exponential avalanche distribution.

Let us now come to the result of numerical simulation. For $\alpha < 1$, as expected, $\mu_0(L) \sim L^{-\omega}$ vanishes with $\omega(\alpha) \approx 1 - \alpha$ and $T_\infty(L)$ converges to a finite value as $L \to \infty$. For $\alpha = 1$ the best fit suggests $T_\infty(L) \sim \log L$. Table 4.1 lists the values obtained for the exponents β and ζ by numerical simulations of the model for sizes up to $L = 256$ and $\alpha > 1$. The statistical uncertainty gets large as $\alpha = 1$ is approached from above. The relation (4.5) is satisfied fairly well. $\alpha + \beta(\alpha)$ gets bigger than 2 for $\alpha \approx 1.4$. Correspondingly $\beta(\alpha)$ reaches a maximum and, as expected, N_∞ becomes positive. This is shown in fig. 4.3 where we report also the estimate of the exponent τ_d obtained for $L = 128$ and 256. For these sizes the distribution $P_d^{(f)}(s)$ is not still relaxed to its asymptotic behavior and the reported values are upper bounds to the true τ exponent. For small α the statistics of avalanches was too poor to extract a reliable estimate of $\tau_d(\alpha)$. For large α, where a stable behavior of $P_d^{(f)}(s)$ was found with L, the difference between $\tau_d(\alpha)$ and $\alpha + \beta(\alpha) - 1$ is small. The character of the

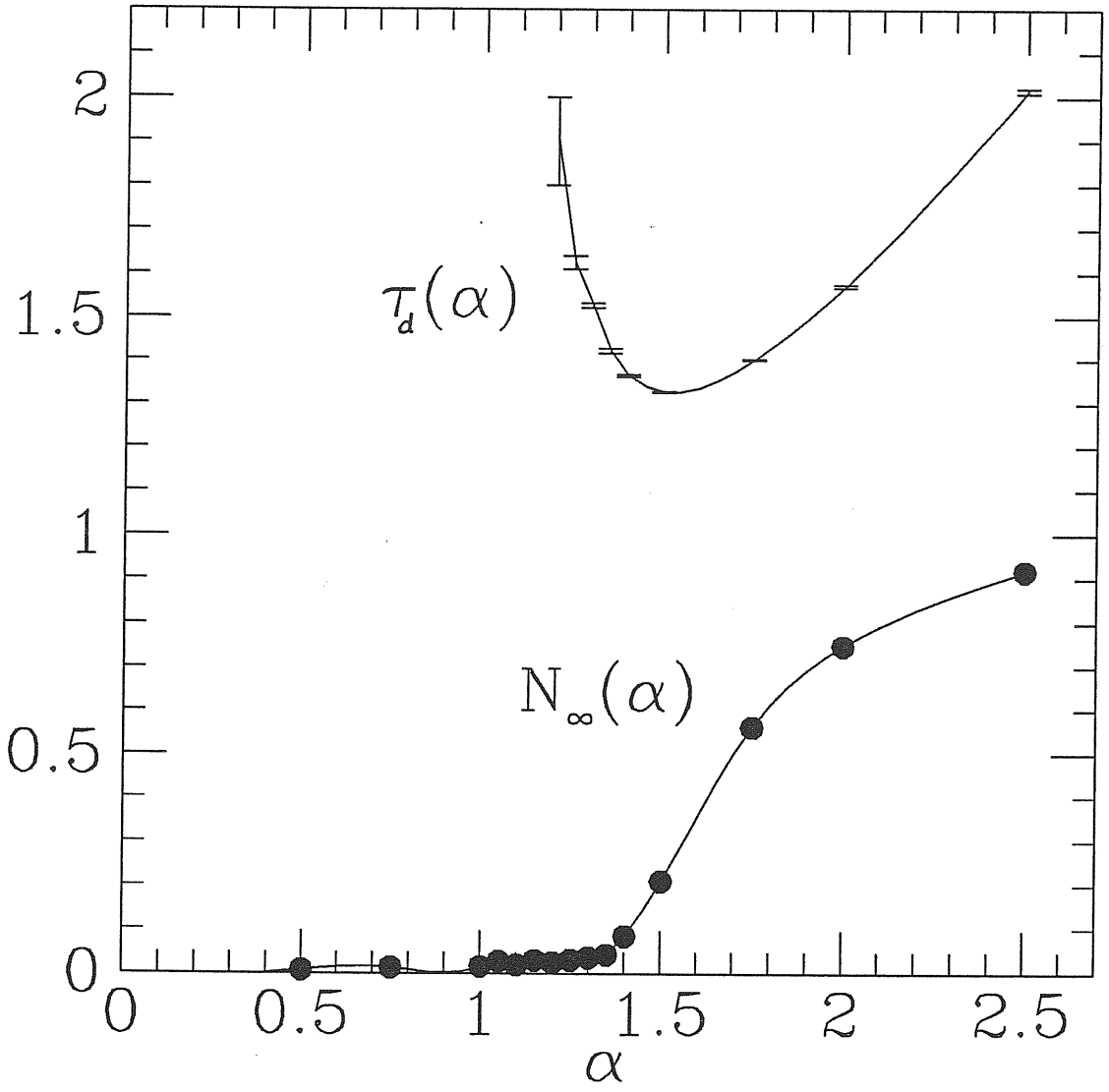

Figure 4.3: The measured values of N_∞ and τ_d for $\alpha > 1$.

$\tau_d(\alpha)$ curve, however, is quite evident: τ_d reaches a minimum approximately in the same region where $\alpha + \beta \approx 2$ and N_∞ starts to increase.

We performed simulations on the BS model as well. The agreement of $\beta(1.30)$ and $\zeta(1.30)$ with the exponents measured for the BS model is remarkable. For the avalanche statistics, the latter model displays a much better scaling behavior than our model. This enabled us to conclude that $N_\infty(L) \sim L^{-0.98}$ vanishes indeed. A direct measure of the τ_d exponent for $L = 128$ yields a value $\tau_d \cong 1.38$ that is 0.3 larger than the best estimates [60]. The claim, $\min_\alpha\{\tau_d(\alpha)\} = 1$, suggests a systematic error of the same magnitude. These considerations suggest that the mechanism of self organization of the BS model, being similar to that of our model, is related to memory effects rather than to the presence of quenched disorder.

We have assumed in our numerical simulation a power law behavior for the avalanche distribution also for $\alpha < \alpha_c$. The approximation discussed previously implies a stretched exponential behavior in this region. Our numerical data did not allow us to distinguish clearly between these two behaviors. For small $\alpha > 1$ the stretched exponential behavior is more evident while if α is close to α_c a power law behavior is more likely. Thus we cannot definitely establish whether the self organized critical behavior of our model coincides or not with that of the BS model.

4.3 Cluster Growth with Memory

The second model we discuss is a generalization of the invasion percolation model. To each site i of a D dimensional infinite lattice is assigned a counter variable k_i which is initially set to zero. Growth starts from one seed site $i(0) = \mathcal{C}_0$ and after a time t it produces a cluster $\mathcal{C}_t = \{i(s),\ s = 0, \ldots, t-1\}$ with the following rule: one of the sites in the perimeter $\partial\mathcal{C}_t$ of the cluster is selected with a probability which depends on its counter variable

$$\text{Prob}\{i \text{ is selected}\} = \mu_{k_i} = \mu_0(t)(k_i + 1)^{-\alpha}. \tag{4.15}$$

The counter variable of the site $i(t)$ which has been selected will remain unchanged in the future. The site is included in the cluster $\mathcal{C}_{t+1} = \mathcal{C}_t \bigcup \{i(t)\}$. The counter variable $k_j(t)$ of all the other sites $j \in \partial\mathcal{C}_t$, $j \neq i(t)$, will be increased by one: $k_j(t+1) = k_j(t) + 1$. At each time step one only site grows. This is enforced by the normalization condition that yields

$$\mu_0(t) = \left[\sum_{k=0}^{\infty} n_{k,t}(k+1)^{-\alpha}\right]^{-1} \tag{4.16}$$

Depending on the value of α we expect different behavior as for the model of the previous section. In particular for $\alpha = 0$ we recover the Eden [67] model. For $\alpha \to \infty$ growth will occur only at the sites with $k = 0$. These are those reached by the cluster,

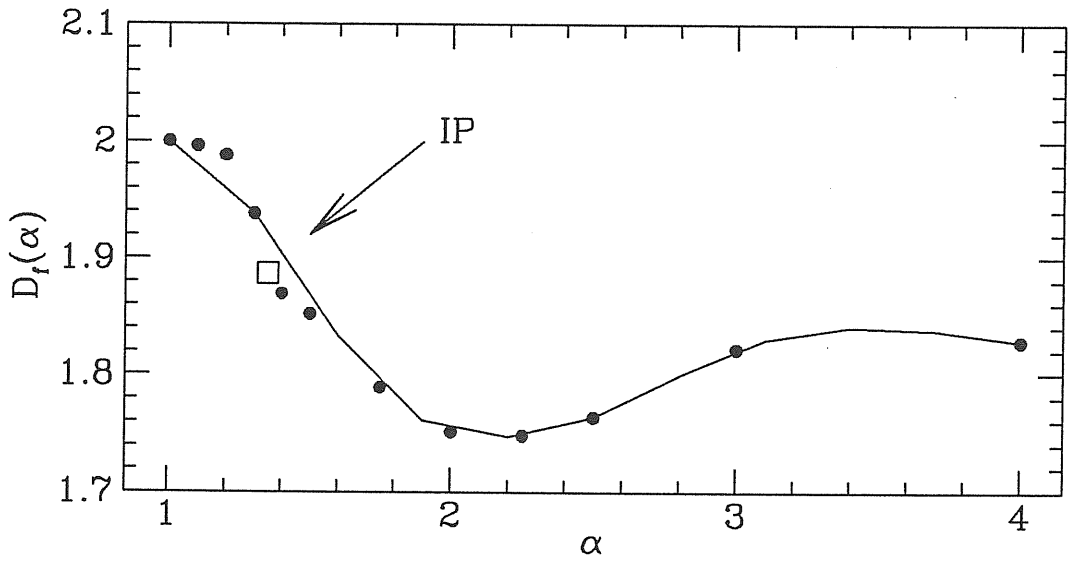

Figure 4.4: The fractal dimension $D_f(\alpha)$ as a function of α (•). The solid line is a spline interpolation intended only to guide eyes. The □ point is the measured fractal dimension of invasion percolation $D_f^{IP} \simeq 1.89$.

for the first time, at the previous growth event. The rule than reduces to that of the self avoiding random walk [55]. The model is expected to interpolate between these two models and to reproduce to some extent the properties of invasion percolation. The latter model has indeed a $\mu_{k,t}$ of the form (4.15). The exponent, read off from figure 4.1, is $\alpha_{IP} = 1.35 \pm 0.01$. The approximation discussed in section 3.1.6 yields $\alpha_{IP}^{\text{app}} = 2$ which differs substantially from the numerical result.

We shall shortly repeat some of the arguments of the previous section for this model together with some preliminary results of numerical simulation. Even though we cannot draw definite conclusions it seems that the α–model misses the structure of avalanche events of invasion percolation. In this sense it is likely that these models display different self organized critical properties.

As in the previous section we can conclude that for $\alpha < 1$ growth will occur in a Eden like fashion. We can indeed assert that all the sites in the perimeter $\partial\mathcal{C}_t$ will surely grow sooner or later. Indeed by eq. (4.16) $\mu_0(t) \sim t^{-\gamma_\mu}$ can eventually vanish with an exponent that is at most $\gamma_\mu \leq 1 - \alpha$. The probability that a site will not grow for s time steps after it has entered the interface is $P_0(s) = \prod_{k<s}[1 - \mu_0(t_0 + k)(k+1)^{-\alpha}]$. If the series $\sum_k \mu_0(t_0 + k)(k+1)^{-\alpha}$ diverges the limit of the product will be zero. This happens for $\gamma_\mu + \alpha \leq 1$ which, as observed before, is always the case for $\alpha < 1$. The probability that a site spends a time s in the set of perimeter sites goes to zero as $s \to \infty$ for $\alpha < 1$. The same argument suggests that clusters will grow compact, that the surface to volume ratio will vanish asymptotically and

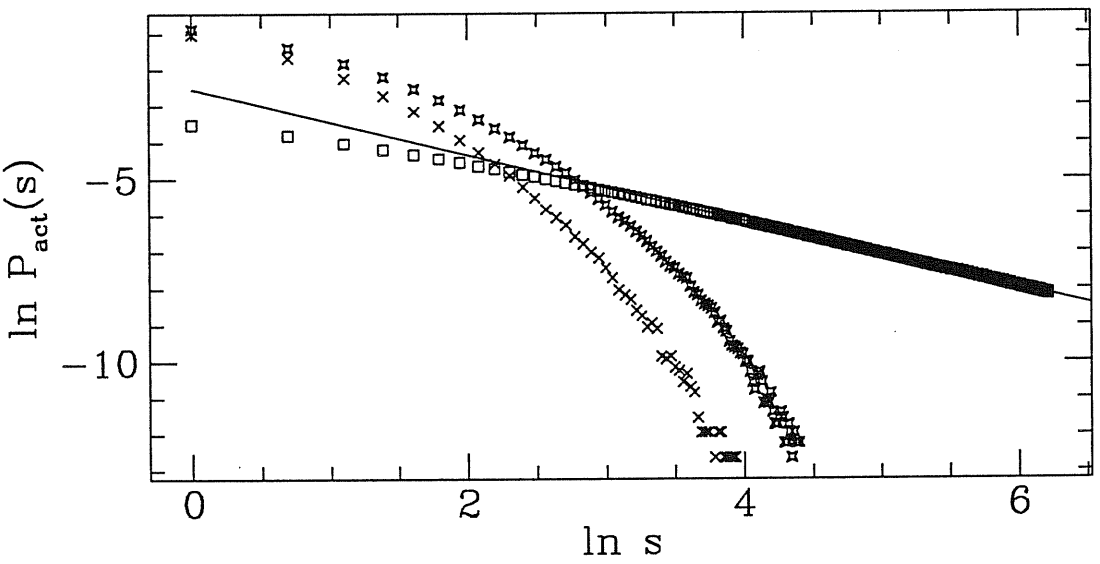

Figure 4.5: The probability $P_{\rm act}(s)$ for $\alpha = 1.30, 1.40$ ($\times$) and for invasion percolation ($\square$). The solid line has a slope $\gamma = -0.90$.

that the average value of k will scale with an exponent $\varsigma < 1$ in eq. (4.2). The latter occurrence implies that no memory is present in the process. Finally no self organized critical behavior occur. In fact the fact that $\mu_0(t) \to 0$ precludes the possibility of a local dynamics such as that of avalanches. This scenario for $\alpha < 1$ is confirmed quite well by numerical simulation.

For $\alpha > 1$ instead we find $\varsigma = 1$ as an indication of the presence of memory effects. Both the surface to volume ratio and $\mu_0(t)$ converge to a finite value as $t \to \infty$. The former implies that the growth process produces a fractal cluster. Preliminary results for the fractal dimension are shown in figure 4.4. The latter suggests that avalanches have a well defined distribution. For $1 < \alpha < 2$, the previously discussed approximation, implies a stretched exponential distribution. This is roughly confirmed by the numerical data shown in figure 4.5. The distribution of avalanches for the α–model is consistent with a stretched exponential behavior since $P_{\rm act}(s) \sim \exp(-as^{2-\alpha})$. Conversely for invasion percolation $P_{\rm act}(s)$ is a fairly stable power law with an exponent $\gamma \approx 0.9$ which is roughly consistent with the value of $\tau_d = \alpha + \gamma - 1 \simeq 1.05\ldots$. For $\alpha = 2$ the stretched exponential behavior of $P_d^{(f)}(s)$ turns into a power law and for $\alpha > 2$ a finite probability for infinite avalanches appears.

4.4 Discussion

Let us summarize the results we have reached in this section. First of all we have seen that the introduction of counter variables allows both to detect memory and to characterize completely the avalanche behavior. The causal relation between individual events is more transparent in terms of counter variables than in terms of the succession of minimum RV selected during quenched dynamics. Moreover the same definition in terms of counter variables extends to more general situations. Regarding the self organized critical nature of processes involving quenched dynamics, we have seen that a model that accounts in the most simple way for the memory effects can reproduce the "standard" critical properties. These are in the BS model the exponents β and ζ, in invasion percolation the surface to volume ratio and the fractal dimension (see fig. 4.4). In both models the presence of memory ($\zeta > 0$ or $\varsigma = 1$) comes along with critical properties such as fractality in cluster growth. The presence of memory is also accompanied by the presence of well defined local events (avalanches). The avalanche distribution has a power law character, which is the hallmark of standard self organized criticality, for $\alpha \geq \alpha_c$. In this region of α there is a finite probability to observe endless avalanches. This probability vanishes at α_c. For $1 < \alpha < \alpha_c$ a simple approximation suggests a stretched exponential distribution for avalanche events. We could not clarify this issue for the generalized BS model. Our numerical data did not allow for a definite characterization of the avalanche distribution. For values close to $\alpha_c \approx 1.4$, as is the value measured in the BS model $\alpha_{BS} \approx 1.3$, a power law character was found to fit well the data, while closer to $\alpha = 1$ the stretched exponential form seems to be more appropriate.

In cluster growth with memory, where $\alpha_c = 2$, the stretched exponential behavior suggested by the above mentioned approximation, is more suited in the region $1 < \alpha < \alpha_c$. A suggestive similarity between the two models comes from the comparison of the β data and figure 4.4. In both cases the exponent attains an extreme value at α_c (which is 2 in fig. 4.4).

With respect to the relation with quenched dynamics the failure of our model in reproducing correctly avalanche events for the appropriate value of α can be read in one of two ways: *1)* the modelling of memory effects in the corresponding model involving quenched dynamics is not appropriate; *2)* there are features of quenched dynamics which has nothing to do with memory and which are relevant for the self organized critical behavior. A shortcoming of our model, as well as of the approximation we have discussed, is that the selection of a variable has the same conditional effect on the remaining ones *irrespectively* of the value of its counter variable. In the model counters are increased of one unit no matter what value of k has been selected. In the approximation the average distribution of the minimum variable is used instead of the distribution of the RV that is actually selected (which is conditional to the fact that *this* variable was the smallest). In quenched dynamics, the longer the selected RV has been in the set of the perimeter sites the closer it will be to the threshold

value. The selection of an old RV will have a strong conditional *screening* effect on the other variables. This effect may account for the mismatch between the approximation and the simulation in the α exponent for invasion percolation. It might also be responsible for the markedly different behavior in the avalanche distribution shown in figure 4.5.

A more complete understanding of the behavior of models with memory and of its capability of reproducing features of quenched dynamics necessitates a more sensible theoretical approach. The simplicity of the models discussed in this chapter suggest that it should be a feasible project to uncover in more detail the very rich behavior discussed so far.

Chapter 5

Acknowledgements

In the long list of the acknowledgements, the first entry is surely Trieste. Its particular atmosphere and the mood it produces, *la Bora* in clear sunny days, the romantic cloudy days and the stormy ones. The sea, every day of a different colour. The individuality of its inhabitants and their *cold* friendship. Their being Mittle–european an therefore always *lontano da dove*. And the friends, social assistants, postwomen, lady writers and journalists, bankers, singers, physicians and nurses, violin players, who will never be cited in physics even though their help has been essential.

I have also greatly benefited of the many opportunities Trieste can offer to a student in physics. The very warm and informal atmosphere of the S.I.S.S.A. have greatly facilitated my acquaintance with the physicists community. In my particular experience, the influence of Erio Tosatti has been priceless. I have largely benefitted of his time and patience in the first two years of my stay at S.I.S.S.A. I am also deeply grateful to Amos Maritan. In spite of the poorness of my experience in physics, his attitude to place on my same level has made me feel at my ease in our collaboration. I have to thank Jayanth R. Banavar for very stimulating discussions and encouragements.

I have to acknowledge Luciano Pietronero for his disposability throughout this period and for frequent help. A large part of this thesis draws inspiration from the discussions I had with him and the students of the room "003" in Rome. Among these I should remember the members of Little Italy, Alessandro Vespignani, Massimo Vergassola and Stefano Zapperi, Vittorio Loreto, the inexhaustible Raffaele Cafiero, Andrea Gabrielli and Marina Piccioni (and his ...). "Piovra" Claudio Grimaldi and Patrizia Benedetti have contributed more with their madness and friendship respectively, than with equations.

I have to acknowledge also Giancarlo Jug, Attilio Stella, Y. C. Zhang and Stefano Galluccio, Umberto Marini Bettolo and Luca Peliti for fruitful discussions and collaborations.

Last but not least, the members of the room 239. The former ones, "mamma" Michela Di Stasio and Guido Goldoni, and the present ones Michele Vendruscolo and Guido Caldarelli, with whom I have coloured in red & green some epic moments.

Appendix A

Elements of Differential Geometry and Derivation of Reparametrization Invariant Growth Equations

A.1 Differential Geometry

An orthonormal basis is assumed in the $D+1$ dimensional space and Greek letters are used for the vector components. Instead latin letters index refer to the components of vectors in the D dimensional parameterization space. s^i are general curvilinear coordinates that label points on the D dimensional surface. The notation $\partial_i = \partial/\partial s^i$ is used for covariant derivatives. Summation over repeated indexes is always assumed. Lastly for the scalar product in both spaces a dot is used while $\times$ denotes the vector product.

The distance between infinitesimally close points on the surface is given by the first fundamental quadratic form

$$|d\vec{r}|^2 = \partial_i \vec{r} ds^i \cdot \partial_j \vec{r} ds^j = g_{i,j} ds^i ds^j. \tag{A.1}$$

This defines the metric tensor $g_{i,j} = \partial_i \vec{r} \cdot \partial_j \vec{r}$. $g = \det\{g_{i,j}\}$ denotes its determinant while $g^{i,j}$ is the inverse, $g_{i,k} g^{k,j} = \delta_i^{j}$[1], and also defines the contravariant derivative $\partial^i = g^{i,j} \partial_j$.

The only restriction on the choice of the parameterization is that $g \neq 0$, i.e. that $g_{i,j}$ is invertible, and this implies also $\partial_i \vec{r} \neq 0$. The vectors $\partial_i \vec{r}$ lie in the tangent

[1]The symbol δ is used here for the Kronecker delta. It will also be used for the Dirac delta function and for functional differentiation.

hyperplane so that the normal versor is given by $\hat{n} = g^{-1/2}\partial_1\vec{r} \times \partial_2\vec{r} \times \ldots \times \partial_D\vec{r}$ where $g^{-1/2}$ ensures normalization.

The invariant surface element is given by $d\sigma = d^D s\sqrt{g}$ and this implies that the invariant form of the delta function in parameter space is

$$\delta_0(\underline{s} - \underline{s}') = \frac{\delta(\underline{s} - \underline{s}')}{\sqrt{g}} \tag{A.2}$$

where $\delta(\underline{s})$ is the usual delta function in D dimensional space.

For differential calculus, invariant forms of the gradient, divergence and curl are obtained requiring the transformation properties of tensors to apply. The gradient of a scalar S is simply given by $\partial_i S$ while the divergence of a vector is

$$\mathrm{div}\underline{v} = \frac{1}{\sqrt{g}}\partial_i\sqrt{g}v^i$$

Taking the divergence of the contravariant gradient yields the reparametrization invariant generalization of the laplacian operator in curved spaces

$$\underset{\sim}{\Delta} = \frac{1}{\sqrt{g}}\partial_i\sqrt{g}\partial^j = \frac{1}{\sqrt{g}}\partial_i\left(\sqrt{g}g^{i,j}\partial_j\right) \tag{A.3}$$

which is known as the Beltrami Laplace operator.

The curvature κ of the surface along a curve $\underline{s}(\ell)$ is given by the second fundamental quadratic form

$$\kappa = -\partial_j\hat{n} \cdot \partial_i\vec{r}(\underline{s}(\ell))\frac{ds^i}{d\ell}\frac{ds^j}{d\ell} = b_{i,j}\frac{ds^i}{d\ell}\frac{ds^j}{d\ell} \tag{A.4}$$

This defines the principal curvatures (directions) as the eigenvalues λ_i (vectors) of b_i^j. These are invariant under reparametrization. The mean curvature H is the sum of these and then equals the trace of b_i^j[2]

$$H = b_i^i = \sum_{i=1}^{D}\lambda_i = -\partial_i\hat{n} \cdot \partial^i\vec{r}. \tag{A.5}$$

Another useful definition of H comes from observing that, since $\hat{n} \cdot \partial^i\vec{r} = 0$, $\partial_i\sqrt{g}\hat{n} \cdot \partial^i\vec{r} = \sqrt{g}(\partial_i\hat{n}) \cdot \partial^i\vec{r} + \hat{n} \cdot \partial_i\sqrt{g}\partial^i\vec{r} = 0$. This implies

$$H = -\partial_i\hat{n} \cdot \partial^i\vec{r} = \hat{n} \cdot \underset{\sim}{\Delta}\,\vec{r} \tag{A.6}$$

The Gaussian curvature is instead defined as $K = \det\{b_i^j\} = \prod_i \lambda_i$.

[2]actually the mean curvature should contain a factor $1/D$ that we disregard for convenience.

With respect to the dynamic we note that the time derivative of $\vec{r}$ has to be parallel to the normal of the surface, as stated in Eq.(2.2). This is because $t = s^0$ can be regarded as the $D + 1^{\text{th}}$ coordinate, and $(\underline{s}, s^0)$ is a curvilinear coordinate system. If the growing surface invades the $D + 1$ dimensional space, this parameterization is legitimate since the metric tensor is positive definite. However s^0 is the absolute time, and changes of parameterization cannot involve this variable. This is satisfied only if the elements $g_{0,i} \equiv \partial_t \vec{r} \cdot \partial_i \vec{r}$ vanish, that implies that $\partial_t \vec{r} \perp \partial_i \vec{r}$ for all $i = 1, \ldots, D$.

A.2 The Monge Form

A particular choice for the parameterization is the Monge form

$$\vec{r} = (\underline{x}, h(\underline{x})) \tag{A.7}$$

where $\underline{x}$ is a vector in the D dimensional substrate plane and $h(\underline{x})$ is the height of the surface in the direction $\hat{z}$ perpendicular to this plane. Use of this parameterization implies that no overhangs are present in the surface otherwise $h(\underline{x})$ would not be single valued. In this parameterization the metric tensor has the form $g_{i,j} = \delta_{i,j} - \partial_i h \partial_j h$,

$$g = 1 + (\underline{\nabla} h)^2 \text{ and } \hat{n} = \frac{1}{\sqrt{g}}(-\underline{\nabla} h, 1). \tag{A.8}$$

Finally the mean curvature is given by

$$H = \underline{\nabla} \frac{\underline{\nabla} h(\underline{x})}{\sqrt{g}}. \tag{A.9}$$

The equation for $h(\underline{x}, t)$ is obtained from (2.2) considering the various components of $\vec{r}$. Take $\vec{r}(\underline{s}, t) = (\underline{x}(\underline{s}, t), h(\underline{s}, t))$, then for components we have

$$\begin{aligned} \partial_t h(\underline{s}, t) &= n^z \mathcal{G} \\ \partial_t x^i(\underline{s}, t) &= n^i \mathcal{G} \end{aligned}$$

where n^i (n^z) is the component of the normal in the direction $\hat{x}^i$ ($\hat{z}$). These derivatives are evaluated at constant $\underline{s}$ while we are interested in the derivative of h at constant $\underline{x}$, that is

$$\partial_t h(\underline{x}, t) = \partial_t h(\underline{s}, t) + \frac{\partial h}{\partial x^i} \partial_t x^i(\underline{s}, t)$$

that, using the above equations and $\hat{n} = (-\underline{\nabla} h, 1)/\sqrt{g}$, readily yields the deterministic part of eq. (2.3).

A.3 Equations derived from a potential in the Monge representation

The property that the functional derivative is orthogonal to the vector $\partial_i \vec{r}$ translates into

$$\frac{\delta \mathcal{H}}{\delta h} \partial_i h + \frac{\delta \mathcal{H}}{\delta x^i} = 0.$$

This allows to eliminate the functional derivative w.r.t. x^i in

$$\mathcal{G} = \hat{n} \cdot \frac{\delta \mathcal{H}}{\delta \vec{r}} = n^z \frac{\delta \mathcal{H}}{\delta h} + n^i \frac{\delta \mathcal{H}}{\delta x^i}$$

and to find Eq. (2.5).

A.4 Derivation of the Growth Term Due to Surface Energy

In the functional derivative of g w.r.t. $\vec{r}$, in eq. (2.6), we use the fact that g is a determinant and the property

$$\delta \ln \det \hat{M} = \delta \mathrm{tr} \ln \hat{M} = \mathrm{tr} \hat{M}^{-1} \delta \hat{M}$$

that holds for variations of a matrix $\hat{M}$. This allows to write

$$\delta \int d^D s \sqrt{g} = \frac{1}{2} \int d^D s \sqrt{g} g^{i,j} \delta g_{j,i} = - \int d^D s \partial_i \sqrt{g} g^{i,j} \partial_j \vec{r} \cdot \delta \vec{r}$$

for a variation $\delta \vec{r}$ of $\vec{r}$, which readily yields Eq. (2.6).

A.5 Curvature Dependent Potential

For a variation $\delta \vec{r}$ in $\vec{r}$, $\hat{n}$ changes to $\hat{n} + \delta \hat{n}$. Since $\delta(\hat{n} \cdot \hat{n}) = 0$, the variation $\delta \hat{n}$ is normal to $\hat{n}$. Take Eq. (A.6) for H; then in

$$\delta H = \delta \hat{n} \cdot \underset{\sim}{\Delta} \vec{r} + \hat{n} \cdot \delta(\underset{\sim}{\Delta} \vec{r})$$

the first term in the r.h.s. vanishes since $\underset{\sim}{\Delta} \vec{r}$ is parallel to $\hat{n}$. The variation of $\underset{\sim}{\Delta} \vec{r}$, by simple arithmetic, is

$$\begin{aligned} \delta \underset{\sim}{\Delta} \vec{r} &= \delta \frac{1}{\sqrt{g}} \partial_i \left(\sqrt{g} g^{i,j} \partial_j \right) \vec{r} \\ &= \left(\partial_i \frac{\delta \sqrt{g}}{\sqrt{g}} \right) \partial^i \vec{r} + \underset{\sim}{\Delta} \delta \vec{r} + \frac{1}{\sqrt{g}} \partial_i \left[\sqrt{g} (\delta g^{i,j}) \partial_j \right] \vec{r}. \end{aligned}$$

The first term in the last line, being proportional to $\partial^i\vec{r}$, vanishes once it is multiplied by $\hat{n}$. For the same reason the only contribution that survives in the last term is obtained when the derivative ∂_i acts on $\vec{r}$. The variation $\delta g^{i,j}$ is expressed in terms of $\delta\vec{r}$ taking the variation of $g^{i,k}g_{k,j} = I^i_j$ so that finally

$$\delta H = \hat{n}\cdot\underset{\sim}{\Delta}\,\delta\vec{r} - 2\left(\partial^i\delta\vec{r}\partial^j\vec{r}\right)(\hat{n}\cdot\partial_i\partial_j\vec{r})\,.$$

The variation of $\mathcal{H}_{c,1} = -\kappa_1\int d^Ds\sqrt{g}H$ w.r.t. $\delta\vec{r}$ involves the variation δH and the variation of $\sqrt{g}$, which is evaluated as before. The functional derivative of the first term is evaluated from the above equation with a partial integration

$$-\frac{1}{\sqrt{g}}\frac{\delta\mathcal{H}_{c,1}}{\delta\vec{r}} = k_1\left\{-H\underset{\sim}{\Delta}\,\vec{r} - \partial^i\vec{r}\partial_i H + \underset{\sim}{\Delta}\,\hat{n} + 2\frac{1}{\sqrt{g}}\partial_i\left[\sqrt{g}(\hat{n}\cdot\partial^i\partial_j\vec{r})\partial^j\vec{r}\right]\right\}.$$

On multiplication of the above equation with $\hat{n}$ to find $\mathcal{G}_{c,1}$, the property $\hat{n}\cdot\partial_i\vec{r} = 0$ can be used again to show that the second term gives no contribution and to perform the derivative in the last term that becomes $b^i_j b^j_i$. This is the trace of the square of the matrix of the coefficients of the second fundamental form. Finally we have to compute $\hat{n}\cdot\underset{\sim}{\Delta}\,\hat{n}$. Using the facts that $\hat{n}\perp\partial^i\hat{n}$ and that $\partial_i\hat{n} = -b_i^j\partial_j\vec{r}$, we easily find

$$\hat{n}\cdot\underset{\sim}{\Delta}\,\hat{n} = -\partial_i\hat{n}\cdot\partial^i\hat{n} = -b_i^j b_j^i = -\sum_{i=1}^{D}\lambda_i^2. \tag{A.10}$$

Collecting the various terms we get the result displayed in Eq. (2.13) that is clearly fully R–invariant.

The chain rule of differentiation, applied to $\mathcal{H}_{c,p} = -\kappa_p\int d^Ds\sqrt{g}H^p$, also gives Eq. (2.15), where the second term, as before comes from the variation of $\sqrt{g}$ while the others come from $\delta H^p = pH^{p-1}\delta H$. This needs also the straightforward generalization of Eq. (A.10) to

$$\hat{n}\cdot\underset{\sim}{\Delta}(F\hat{n}) = \left(\underset{\sim}{\Delta} - \sum_{i=1}^{D}\lambda_i^2\right)F$$

for a generic R–invariant function $F(\underline{s})$.

Appendix B

Dynamic Renormalization Group for Growth from an Inclined Flux

B.1 The Dynamic Renormalization Group

Let us consider the Langevin equation

$$\partial_t h(\underline{x},t) = \hat{\mathcal{L}}\{h(\underline{x},t)\} + \hat{\mathcal{N}}\{h(\underline{x},t)\} + \eta(\underline{x},t)$$

where $\hat{\mathcal{L}}$ ($\hat{\mathcal{N}}$) is a linear (nonlinear) differential operator in the $\underline{x}$ variable and

$$\langle \eta(\underline{x},t)\eta(\underline{x}',t)\rangle = 2\Delta\delta^D(\underline{x}-\underline{x}')\delta(t-t'). \tag{B.1}$$

The first step for the dynamic renormalization group (DRG) analysis, following Ma and Mazenko [11, 9], is to transform the equation in the Fourier space:

$$\tilde{h}(\underline{k},\omega) = \int d^D x\, dt\, h(\underline{x},t)\epsilon^{-i\underline{k}\cdot\underline{x}}$$

$$\tilde{\eta}(\underline{k},\omega) = \int d^D x\, dt\, \eta(\underline{x},t)\epsilon^{-i\underline{k}\cdot\underline{x}}$$

$$-Q_k\tilde{h}(\underline{k},\omega) = \int d^D x\, dt\, \hat{\mathcal{L}}\{h(\underline{x},t)\}\epsilon^{-i\underline{k}\cdot\underline{x}}$$

where Q_k is a function of k whose form depends on the combination of differential operators in $\hat{\mathcal{L}}$. For a quadratic nonlinear term, the equation can be cast in the form

$$\begin{aligned}\tilde{h}(\underline{k},\omega) &= G_0(\underline{k},\omega)\tilde{\eta}(\underline{k},\omega) \\ &+ G_0(\underline{k},\omega)\int_{S(\Lambda)}\frac{d^D q}{(2\pi)^D}\int_{-\infty}^{\infty}\frac{d\nu}{2\pi}\Gamma(\underline{k},\underline{q})\tilde{h}(\underline{q},\nu)\tilde{h}(\underline{k}-\underline{q},\omega-\nu)\end{aligned} \tag{B.2}$$

where $G_0(k,\omega) = 1/(Q_k - i\omega)$ is the bare propagator and Γ is the bare vertex function. $S(\Lambda)$ is the domain of integration with Λ being the momentum cutoff. The

renormalization of the propagator and of the vertex (or of the coefficients that appear in them) and of the amplitude Δ of the noise correlation is given by the variation of these functions under an enlargement of scale. The change of scale is done in two steps: *i)* elimination of "fast" degrees of freedom (that describe the system at small scales) by eliminating the variables whose momentum lies in the shell $S(\Lambda)/S(e^{-l}\Lambda) = \{\underline{k} \in S(\Lambda), \underline{k} \notin S(e^{-l}\Lambda)\}$. *ii)* rescaling of the variables $\underline{k} \to e^{-l}\underline{k}$, $t \to e^{zl}t$ and $h \to e^{\alpha l}h$ in such a way as to recover, in the new variables, the original cutoff Λ. The renormalization scheme is successful if after these two steps the equation can be cast in the form (B.3) with a new propagator G_0' and a new vertex function Γ'. The equations of the RG flow are obtained, for $0 < l \ll 1$, by evaluating the variation of G_0 and Γ to first order in l. The fixed point solutions are eventually obtained by setting these variations to zero, thus requiring scale invariance of the equation. In order to carry out the first step, the elimination of fast degrees of freedom, it is helpful to adopt the following graphical representation of eq. (B.3):

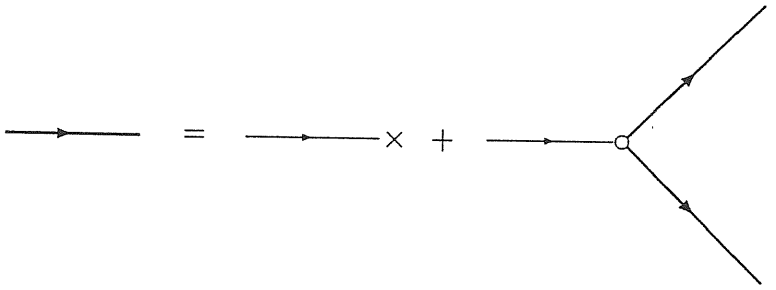

$\tilde{h}$ is denoted by a solid thick line and G_0 by a thin one. The cross stands for a noise term $\tilde{\eta}$ and the vertex Γ is graphically represented by an open dot o. It is also useful to use a different notation for the degrees of freedom that we are going to eliminate. A slash on a thick (thin) line represent a $\tilde{h}$ (G_0) with $\underline{k}$ in the shell. So the equation for h for $k \in S(e^{-l}\Lambda)$ is given by the full equation a) in figure B.1 while eq. b) applies to h for k in the shell. Note that, since we are interested in the $k \to 0$ limit, the term in which the h's going out of the vertex are in $S(e^{-l}\Lambda)$ can be neglected in the equation b using moment conservation. Equation b) is solved iteratively in powers of Γ. The zeroth order term, with no vertex, is just the first term of equation b): $G_0\tilde{\eta}$. The first order is obtained obtained by substituting the zeroth order solution in equation b) (i.e. changing all slashed full lines with a $G_0\tilde{\eta}$ term). This solution in used back in equation b) to get the second order solution (that contains two factors Γ) and so on. In this way $\tilde{h}(\underline{k}, \omega)$ for $\underline{k}$ in the shell is expressed as a function of $\tilde{h}(\underline{k}, \omega)$ for $\underline{k} \in S(e^{-l}\Lambda)$. This solution is then substituted to the slashed thick lines in eq. a). At this point we take the average over the noise with momentum in the shell. Since the noise is gaussian this amounts in pairwise contracting external lines of the type $G_0\tilde{\eta}$ in all possible ways. A contraction of two $\tilde{\eta}$ is shown as a $\square$. The graphs with an odd number of $\tilde{\eta}$ with moments in the shell vanishes. At the end of the calculation, considering only one loop corrections, the equation for $\tilde{h}(k \in S(e^{-l}\Lambda))$ is as shown in figure B.2. The explicit form of the terms appearing in figure B.2 is obtained by the following Feynman rules:

—— is equivalent to a factor $G_0(\underline{k},\omega)$. If the line is slashed then $\underline{k}$ lies in the shell.

• implies a factor $\Gamma(\underline{k},\underline{q})$, where $\underline{k}$ is the incoming momentum and an integration on $d^Dq/(2\pi)^D$ and on the frequency ν. Momentum and frequency must be conserved at the vertex.

□ stands for the factor $2\Delta\delta(\underline{q}+\underline{q}')\delta(\nu+\nu')$ that results from contraction of $\tilde{\eta}(\underline{q},t)$ and $\tilde{\eta}(\underline{q}',t')$.

The multiplicity of the graph, that is shown in figure B.2, is the number of ways in which it can be obtained.

For example, the self energy insertion Σ in the second line of figure B.2 is given by

$$\Sigma_k(\omega) = 4\int_{\text{shell}}\frac{d^dq}{(2\pi)^d}\int_{-\infty}^{\infty}\frac{d\nu}{2\pi}\Gamma(k,q)G_0(\underline{k}-\underline{q},\omega-\nu)G_0(\underline{q},\nu)2\Delta G_0(-\underline{q},-\nu)\Gamma(\underline{k}-\underline{q},-\underline{q}).$$

This term will provide a renormalize the propagator G_0 while the other terms in the bottom line of figure B.2 will renormalize the vertex function.

We finally have to take into account of the renormalization of the noise. This comes from the last term of equation a) of figure B.1 when we substitute $G_0\tilde{\eta}$ to both legs with $\underline{k}$ in the shell. This graph and the first term of equation a) can be absorbed in the definition of the new term $G_0'\tilde{\eta}'$. Graphically

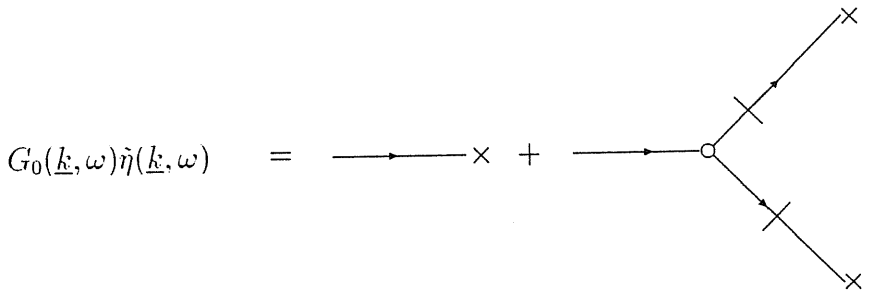

Under the hypothesis that the noise is still gaussian one has only to evaluate the coefficient of the delta functions in eq. (B.1). This amounts in evaluating $\langle\tilde{\eta}'(\underline{k},0)\tilde{\eta}'(\underline{-k},0)\rangle$ which yields the correction to Δ.

B.2 Calculations for the Growth Equation with an Inclined Flux

For eq. (2.44) we have to consider a different renormalization of the length scales in the different directions ($k_{\|} \to k_{\|}e^{-l}$, $k_{\perp} \to k_{\perp}e^{-l\zeta}$ and $h \to he^{l\alpha}$) and of the time

scale $t \to te^{lz}$. The most general form of Q_q consistent with the anisotropy and eq. (2.44) is

$$Q_q = \mu_{||} q_{||}^4 + \mu_\perp q_\perp^4 + \mu_d q_{||}^2 q_\perp^2 \tag{B.3}$$

which is the inverse of the propagator at zero frequency. This is because the anisotropy in the nonlinear term renormalizes differently the three terms of Eq. (B.3).

Also for the vertex function a second parameter is necessary

$$\begin{aligned}\Gamma(k,q) &= \Gamma_{||}(k,q) + \Gamma_{||}(k,q) \\ &= \left(-i\frac{\lambda}{2}\right) k_{||} q_{||} (k_{||} - q_{||}) + \varphi \left(-i\frac{\lambda}{2}\right) \left[q_{||}(k_\perp - q_\perp)^2 + (k_{||} - q_{||}) q_\perp^2\right]\end{aligned}$$

to account for different scaling properties of $\lambda_{||} = \lambda$ and $\lambda_\perp = \lambda\varphi$.

Propagator Renormalization

The self energy correction to the free propagator Q_k at $\omega = 0$ has two contributions. One ($\Sigma_k^{\rm scal}$) coming from the bare scaling of x, t and h, the other resulting from the integration in the momentum shell $\Lambda e^l < |q_{||}| < \Lambda$, $\Lambda^\varsigma e^{\varsigma l} < |q_{||}| < \Lambda^\varsigma$. The latter, after integration on the internal frequency, reads

$$\begin{aligned}\Sigma_k^{\rm shell} &= -4\Delta \int_{\rm shell} \frac{d^D q}{(2\pi)^D} \frac{\Gamma(k,q)\Gamma(k-q,-q)}{Q_q\,(Q_q + Q_{q-k})} = \\ &= -4\Delta \int_{\rm shell} \frac{d^D q}{(2\pi)^D} \frac{\Gamma(k,q)\Gamma(k-q,-q)}{2Q_q^2} \left\{1 + \left[\frac{\underline{k}\cdot\underline{\nabla}}{2} - \frac{(\underline{k}\cdot\underline{\nabla})^2}{4} + \ldots\right] \ln Q_q\right\}.\end{aligned} \tag{B.4}$$

Expanding in power of k,

$$\Sigma_k = \Sigma_k^{\rm scal} + \Sigma_k^{\rm shell} = \left[\nu_{||} k_{||}^2 + \nu_\perp k_\perp^2 + \sigma_{||} k_{||}^4 + \sigma_d k_{||}^2 k_\perp^2 + \sigma_\perp k_\perp^4 + \ldots\right] l \tag{B.5}$$

where l is the scale factor. Since there is no term proportional to $k_\perp^2$, the term $q_\perp^2$, which is absent from the bare propagator, will not be generated. On the contrary a contribution $k_{||}^2$ exists so the term $q_{||}^2$ in Q_q is generated by iteration of the DRG. Our results will hold as long as this term is negligible. The product of the two Γ in eq. (B.4) is

$$\begin{aligned}-4\Delta\Gamma(k,q)\Gamma(k-q,-q) = &- \lambda^2\Delta \left[k_{||}^2 q_{||}^2 (k_{||} - q_{||})^2 + 2\varphi k_\perp k_{||} k_\perp q_{||}^2 (k_{||} - q_{||})(k_\perp - q_\perp)\right. \\ &\left. - \varphi^2 (k_{||} q_\perp^2 - k_\perp^2 q_{||})(k_{||} q_\perp^2 - 2k_\perp q_{||} q_\perp + k_\perp^2 q_{||})\right],\end{aligned}$$

then the other coefficients in eq. (B.5) are:

$$\sigma_{||} = z - 4 + \frac{\lambda^2\Delta}{2} \int_{\rm shell} \frac{d^D q}{(2\pi)^D} \left\{\frac{q_{||}^4 - \varphi^2 q_\perp^4}{4Q_q^2} \partial_{||}^2 \ln Q_q + \frac{q_{||}^3}{Q_q^2} \partial_{||} ln Q_q - \frac{q_{||}^2}{Q_q^2}\right\},$$

$$\sigma_\perp = z - 4\zeta + \lambda^2\Delta\varphi^2 \int_{\text{shell}} \frac{d^D q}{(2\pi)^D} \frac{q_{||}^2}{2Q_q^2} \left\{ c^2 q_\perp \partial_\perp \ln Q_q - 1 \right\}$$

and

$$\begin{aligned} \sigma_d = z - 2 - 2\zeta \;+\; & \frac{\lambda^2\Delta}{2} \int_{\text{shell}} \frac{d^D q}{(2\pi)^D} \left[\frac{q_{||}^4 - \varphi^2 q_\perp^4}{4Q_q^2} \partial_\perp^2 \ln Q_q \right. \\ & + \varphi c^2 \frac{q_{||} q_\perp (q_{||}^2 + \varphi q_\perp^2)}{Q_q^2} \partial_{||} \partial_\perp \ln Q_q \\ & \left. + \varphi \frac{q_{||}^2}{Q_q^2} \left(q_{||} \partial_{||} \ln Q_q + c^2 q_\perp \partial_\perp \ln Q_q - 2 \right) \right]. \end{aligned}$$

Vertex Renormalization

The product of three Γ entering the renormalization of the vertex is instead

$$\begin{aligned} \Gamma(k,q)\,[\Gamma(q,k-k')\Gamma(q-k+k',k') \;+\; & \Gamma(q,k')\Gamma(q-k',k-k') \\ + \; & 2\Gamma(q,k')\Gamma(k-q,k-k')] = \\ = \; & \Gamma_{||}(k,k')(q_{||}^2 - \varphi q_\perp^2)(q_{||}^2 + \varphi q_\perp^2)^2 + \dots \end{aligned}$$

No contribution of the form $\Gamma_\perp$ arises so that

$$\frac{\partial \ln \lambda_\perp}{\partial l} = z + \alpha - 1 - 2\zeta.$$

For $\lambda_{||} = \lambda$, the integral on the internal frequency yields a factor $\Delta/(4Q_q^3)$, that, combined with the degeneracy (4) of the graphs gives

$$\frac{\partial \ln \Gamma_{||}}{\partial \ln \Lambda} = z + \alpha - 3 + \lambda^2\Delta \int_{\text{shell}} \frac{d^D q}{(2\pi)^D} \frac{(q_{||}^4 - \varphi^2 q_\perp^4)(q_{||}^2 + \varphi q_\perp^2)}{Q_q^3}. \qquad \text{(B.6)}$$

The evaluation of the integrals is straightforward but tedious. In terms of the adimensional parameters of eq. (2.54) we find

$$\begin{aligned} \frac{\partial \ln \rho}{\partial l} &= \frac{1}{4}(\sigma_\perp - \sigma_{||}) \\ \frac{\partial \ln r_\mu}{\partial l} &= \left(\sigma_d - \frac{1}{2}\sigma_\perp - \frac{1}{2}\sigma_{||} \right) \\ \frac{\partial \ln r_\lambda}{\partial l} &= z + \alpha - 1 - 2\zeta - \frac{\partial \ln \lambda}{\partial l} - \frac{1}{2}(\sigma_\perp - \sigma_{||}) \end{aligned}$$

that finally yield eq.(2.55).

Finally, it is easy to see that, since the vertex $\Gamma(k,q)$ is proportional to the parallel component $k_{||}$ of the incoming momentum, the correction to Δ is proportional to $k_{||}^2$. Therefore there is no **noise renormalization.**

A Note on the Domain of Integration

The integrals on the momentum shell $\Lambda e^{-l} < |q_{\|}| < \Lambda$ and $\Lambda^{\zeta} e^{-\zeta l} < |q_{\perp}| < \Lambda^{\zeta}$ can be performed in the following way (up to orders l^2)

$$\int_{\text{Shell}} \frac{d^D q}{(2\pi)^D} \Psi\left(q_{\|}, q_{\perp}\right) = l \frac{\partial}{\partial \ln \Lambda} \int_{S(\Lambda)} \frac{d^D q}{(2\pi)^D} \Psi\left(q_{\|}, q_{\perp}\right) \equiv l \frac{\partial}{\partial \ln \Lambda} F(\Lambda)$$

where

$$S(\Lambda) = \left\{ \left|q_{\|}\right| < \Lambda;\ |q_{\perp}| < \Lambda^{\zeta} \right\}.$$

In the evaluation of the integrals one often has the additional condition that also $\underline{q} - \underline{k} \in S(\Lambda)$. This additional condition is easily dealt with[1] introducing a θ function in the integrals and expanding it in powers of k:

$$\begin{aligned} F(\Lambda) &\equiv \int_{\underline{q}, \underline{q}-\underline{k} \in S(\Lambda)} \frac{d^D q}{(2\pi)^D} \Psi(q) = \int_{S(\Lambda)} \frac{d^D q}{(2\pi)^D} \theta\left[(q-k)^2 - \Lambda^2\right] \Psi(q) \\ &= \int_{S(\Lambda)} \frac{d^D q}{(2\pi)^D} \left[1 - 2qk\delta\left(q^2 - \Lambda^2\right) + k^2 \left(1 + 2q^2 \frac{\partial}{\partial q^2}\right) \delta\left(q^2 - \Lambda^2\right) \ldots \right] \Psi(q). \end{aligned}$$

The terms containing a delta function only involve the integration on the angular variable. It is easy to see that, since $\Psi(bq) = b^{-D_c} \Psi(q)$ with $D_c = 6$ in our case, the integral on $S(\Lambda)$ of these terms is proportional to Λ^{D-D_c}. Upon differentiation w.r.t. $\ln \Lambda$ we find that their contribution vanishes at $D = D_c$. In conclusion in the evaluation of the integrals the domain can be safely neglect the condition $\underline{q} - \underline{k} \in S(\Lambda)$ as long as one is interested in first order correction in the $\epsilon = D_c - D$ expansion.

[1] We discuss, for the sake of simplicity, the isotropic case where $S(\Lambda) = \{|q| < \Lambda\}$. The generalization to the non isotropic case is straightforward and only involves longer formulas.

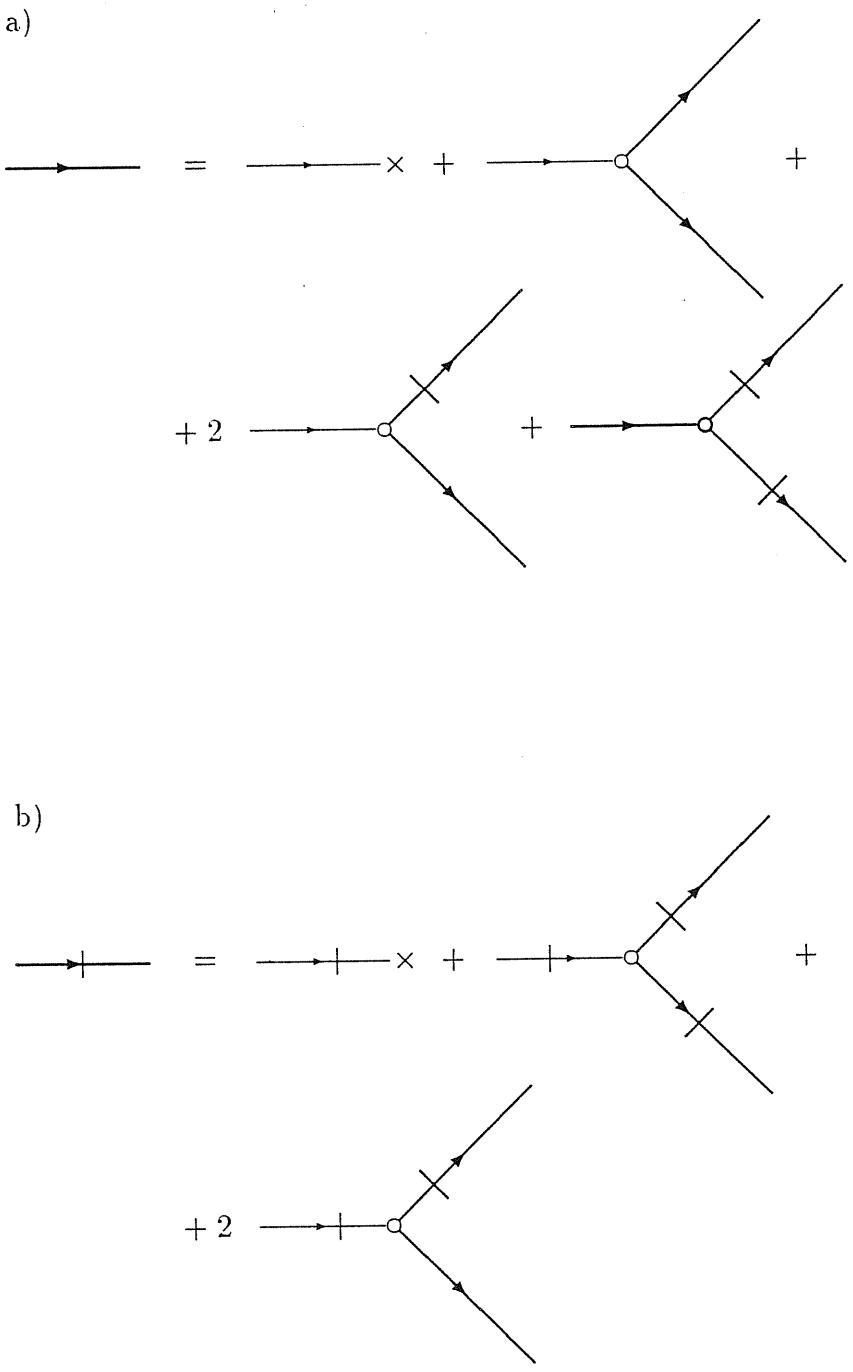

Figure B.1: Feynman diagram for a quadratic Langevin equation a) for $k \in S(\epsilon - l\Lambda)$, b) for k in the shell.

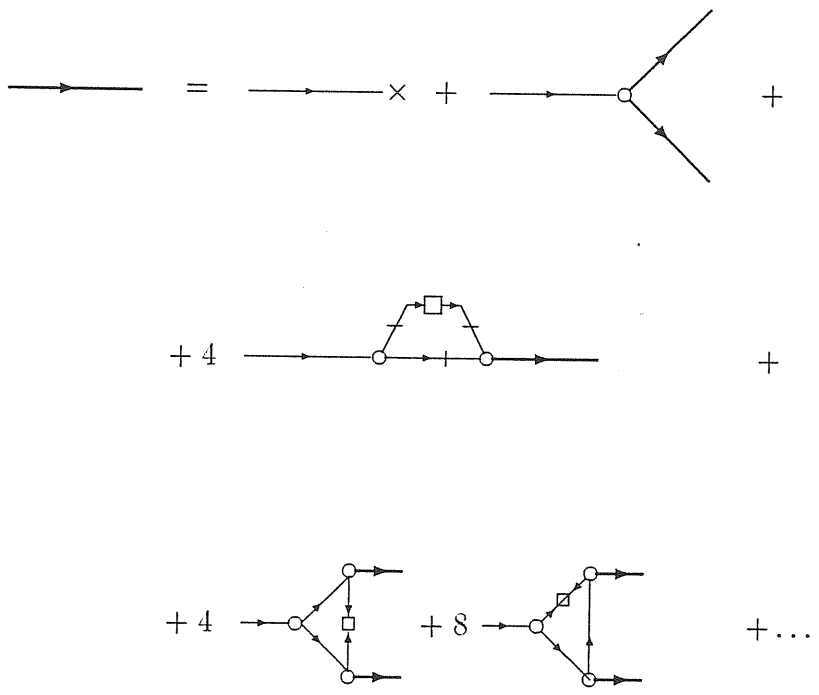

Figure B.2: Renormalized equation at 1 loop order for $\tilde{h}(k,\omega)$. The graph of the second line is absorbed in the renormalization of the propagator. Those in the last line yield the renormalization of the vertex.

Appendix C

Notes on the Run Time Statistics

C.1 The Poisson transformation.

The average of $Z_t(x)$ on the realizations $\mathcal{C}_t$ is given by

$$\langle Z_t(x)\rangle = \sum_{\{\mathcal{C}_t\}} \mathcal{W}(\mathcal{C}_t) Z_t(x, \mathcal{C}_t)$$

where $\mathcal{W}(\mathcal{C}_t)$ is the probability of a given cluster. The dependence of $Z_t(x)$ on $\mathcal{C}_t$ comes primarily because of the explicit exponents $n_{\tau,t}$ in Eq.(3.5). Neglecting other dependencies, that comes in the functions $P_{\tau,t}(x)$ through $M_t(x|\tau)$ see Eq.(3.7), the average can be performed on the probability $\mathcal{P}\{n_{\tau,t}\}$ of a given set $\{n_{\tau,t}\}$ (note that $P_{\tau,t}$ does not depend on the distribution of times $\{n_{\tau,t}\}$ at the same time). The average is easily evaluated using the Poisson transformation [54]

$$\mathcal{P}\left(\mathcal{C}_{t-1}, \{n_{\tau,t}\}\right) = \int \mathcal{F}\left(\mathcal{C}_{t-1}, \{\alpha_\tau\}\right) \prod_k d\alpha_k \frac{\alpha_k^{n_{k,t}}}{n_{k,t}!} e^{-\alpha_k}$$

where the new variables α_k have of the meaning of the average value of $n_{k,t}$. With this transformation the sum on $n_{k,t}$ can be performed explicitly in evaluating the averages with the result

$$\langle h_t(x)\rangle_{\mathcal{C}_t} = \sum_\tau \langle \alpha_\tau \rangle P_{\tau,t}(x) = N_t \phi(x,t)$$

and

$$\langle Z_t(x)\rangle_{\mathcal{C}_t} = \left\langle \exp\left[-\sum_\tau \alpha_\tau P_{\tau,t}(x)\right]\right\rangle = \left\langle \exp\left[-\int_0^x h_t(y)dy\right]\right\rangle .$$

In the average also the term $n_{\tau,t} = 0$ for all τ is considered in the average and this makes $\langle Z_t(1)\rangle = e^{-N_t} \neq 0$.

C.2 The Order Statistics

Let ϵ_i, $i = 1 \ldots, L$, be a random variables with distribution $P_i(x)$ and density $p_i(x)$. Define the permutation π_k^* in such a way that $\epsilon_{\pi_k^*} < \epsilon_{\pi_{k+1}^*}$ for all k. The distribution density of the k^{th} order statistics, that is $\epsilon_{\pi_k^*}$, is given by

$$\theta_k(x) = \frac{1}{(L-k)!(k-1)!} \sum_{\vec{\pi}} \left[\prod_{i=1}^{k-1} P_{\pi_i}(x) \right] p_{\pi_k}(x) \prod_{j=k+1}^{L} \left[1 - P_{\pi_j}(x) \right] \tag{C.1}$$

where the sum is over all permutations $\vec{\pi} = \{\pi_i,\, i = 1 \ldots, L\}$ of L indices. This just expresses the fact that among the L variables, $k-1$ must be smaller than the k^{th} order statistics while $L-k$ must be larger.

The function $\theta_k(x)$ can be derived from the generating function

$$Z_\lambda(x) = \frac{1}{\lambda} \prod_{i=1}^{L} [1 - \lambda P_i(x)] \tag{C.2}$$

by differentiating $k-1$ times w.r.t. λ

$$\theta_k(x) = -\partial_x \left| \frac{(-1)^{k-1} \partial_\lambda^{k-1}}{(k-1)!} Z_\lambda(x) \right|_{\lambda=1} \tag{C.3}$$

as it is easily seen by interchanging the order of the derivatives. Note that for $k = 1$ eq. (C.3) yields the same expression found before for the distribution $m(x)$ of the minimum variable. A direct consequence of eq. (C.3) is that the distribution function $\Theta_k(x) = \int_0^x \theta_k(x')dx'$ is related to the expansion of $Z_\lambda(x)$ in powers of $\eta = 1 - \lambda$:

$$Z_{1-\eta}(x) = \sum_{k=1}^{L} [1 - \Theta_k(x)] \eta^{k-1}.$$

The distribution of order statistics can be evaluated explicitly within the approximation presented in section 3.1.3: the generating function is

$$Z_\lambda(x) \cong \frac{1}{\lambda} \left[\frac{\gamma + 1 - \gamma\phi}{(L-\gamma)\phi} \right]^\lambda \tag{C.4}$$

and

$$\theta_k(x) \cong (\gamma + 1 - \gamma\phi) \frac{(-1)^{k-1}}{(k-1)!} \left[\ln \frac{\gamma + 1 - \gamma\phi}{(L-\gamma)\phi} \right]^{k-1}. \tag{C.5}$$

Bibliography

[1] B. B. Mandelbrot, *The Fractal Geometry of Nature* (Freeman, San Francisco 1982).

[2] P. Bak, C. Tang and K. Weisenfeld, Phys. Rev. Lett. **59**, 381, (1987); Phys. Rev. **A 38**, 364, (1988).

[3] P. C. Hohemberg and B. I. Halperin Rev. Mod. Phys. **49**, 435, (1977).

[4] A. Maritan, F. Toigo, J. Koplik and J. R. Banavar Phys. Rev. Lett. **69**, 3193, (1992).

[5] M. Kardar, Turkish J. of Phys. **18**, 221 (1994).

[6] N. Metropolis, A. W. Rosenbluth, M. N.Rosenbluth, A. M. Teller, and E. Teller: J. Chem. Phys. **21**, 1087 (1953).

[7] L. Pietronero, A. Erzan and C. Evertsz: Phys. Rev. Lett. **61**, 861 (1988), Physica **A 151**, 207 (1988).

[8] M. Kardar, G. Parisi and Y. C. Zhang Phys. Rev. Lett. **56**, 889, (1986).

[9] D. Forster, D. R. Nelson and M. J. Stephen, Phys. Rev. **A 16**, 732, (1977).

[10] D. A. Huse and C. Henley, Phys. Rev. Lett. **54**, 2708, (1985); M. Kardar, Phys. Rev. Lett. **55**, 2235, (1985); J. M. Kim, A. J. Bray and M. A. Moore, Phys. Rev. **A 44**, 2345, (1991).

[11] S. K. Ma and G. F. Mazenko, Phys. Rev. B11, 4077 (1975).

[12] T. Sun, H. Guo and M. Grant, Phys. Rev. **A 40**, 6763, (1989).

[13] Z. W. Lai and S. Das Sarma, Phys. Rev. Lett. **66**, 2348, (1991).

[14] J. M. Kim and S. Das Sarma, Phys. Rev. Lett. **72**, 2903, (1994)

[15] B. Grossmann, H. Guo and M. Grant, Phys. Rev. **A 43**, 1727, (1991).

[16] L.–H. Tang, B. M. Forrest and D. E. Wolf Phys. Rev. **A 45**, 7162, (1992).

[17] J. Krug J. Phys. **A 22**, L769, (1989), J. Krug, H. Spohn in *Solids Far From Equilibrium: Growth, Morphology and Defects* ed. Godrèche (Cambridge University Press 1990).

[18] A. Mazor, D. J. Srolovitz, P. S. Hagan and B. G. Bukiet Phys. Rev. Lett. **60**, 424, (1988).

[19] J. Villain, J. Physique **I 1**, 19, (1991)

[20] L. Golubović and R. P. U. Karunasiri, Phys. Rev. Lett. **66**, 3156, (1991).

[21] T. Sun and M. Plischke Phys. Rev. Lett. **71**, 3174, (1993).

[22] *Molecular Beam Epitaxy 1990*, edited by C. W. Tu and J. S. Harris, Jr. (North-Holland, Amsterdam, 1991).

[23] R. C. Salvarezza, L. Vasquez, P. Herrasti, P. Ocón, J. M. Vara and A. J. Arvia, Europhys. Lett. **20**, 727 (1992), P. Herrasti, P. Ocón, L. Vasquez, R. C. Salvarezza, J. M. Vara and A. J. Arvia, Phys. Rev. **A 45**, 7440, (1992).

[24] For a comprehensive review see: P. Meakin, Phys. Rep. **235**, 189 (1993).

[25] A. Mazor, D. J. Srolovitz, P. S. Hagan, and B. G. Bukiet, Phys. Rev. Lett. **60**, 424, (1988).

[26] M. Siegert and M. Plischke, Phys. Rev. Lett. **68**, 2035, (1992); J. Physique **I 3**, 1371, (1993).

[27] T. Sun and M. Plischke, Phys. Rev. Lett. **71**, 3174, (1993).

[28] D. E. Wolf and J. Villain, Europhys. Lett. **13**, 389 (1990).

[29] S. Das Sarma and P. Tamborenea, Phys. Rev. Lett. **66**, 325 (1991).

[30] S. Das Sarma and S. V. Ghaisas, Phys. Rev. Lett. **69**, 3762 (1992).

[31] S. F. Edwards and D. R. Wilkinson, Proc. R. Soc. London A **381**, 17 (1982).

[32] L. Golubović and R. Bruinsma, Phys. Rev. Lett. **66**, 321 (1991).

[33] S. V. Buldyrev, A.-L. Barabási, F. Caserta, S. Havlin, H. E. Stanley and T.Vicsek: Phys. Rev. A **45**, R8313 (1992), L.-H. Tang and H. Leshhorn: Phys. Rev. A **45**, R8309 (1992).

[34] S. Galluccio and Y. C. Zhang *Driven Interfaces in Quenched Disorder at Critical Depinning*, preprint (1994).

[35] K. Sneppen: Phys. Rev. Lett. **69**, 3539 (1992), **71**, 101 (1993).

[36] L.–H. Tang and H. Leschhorn Phys. Rev. Lett. **70**, 3832, (1993); Z. Olami, I. Procaccia and R. Zeitak, Phys. Rev. **E 49**, 1232, (1994); H. Leschhorn and L.–H. Tang, Phys. Rev. **E 49**, 1238, (1994).

[37] G. Kriza and G. Mihàli: Phys. Rev. Lett. **56**, 2529 (1986); R. M. Fleming and L. F. Schneemeyer: Phys. Rev. B **33**, 2930 (1986); G. Gruner: Rev. Mod. Phys. **60**, 1129 (1988).

[38] G. Parisi and L. Pietronero, Physica A **179**, 16 (1991).

[39] J. P. Sethna, K. Dahmen, S. Kartha, J. A. Krumhansl, B. W. Roberts and J. D. Shore Phys. Rev. Lett. **70**, 3347 (1993) and references therein.

[40] R. Bruinsma and G. Aeppli: Phys. Rev. Lett. **52**, 1547 (1984); J.Koplik and H. Levine: Phys. Rev. B **32**, 280 (1985); B. Koiller, H. Ji and M. O. Robbins: Phys. Rev. B **46**, 5258 (1992).

[41] R. Lenormand and S. Bories: C. R. Acad. Sci. **291**, 279 (1980), R. Chandler, J. Koplick, K. Lerman, J. F. Willemsen: J.Fluid Mech. **119**, 249 (1982), D. Wilkinson and J. F. Willemsen: J. Phys. A **16**, 3365 (1983).

[42] M. Cieplak and M. O. Robbins, Phys. Rev. Lett. **60**, 2042, (1988); N. Martys, M. O. Robbins and M. Cieplak Phys. Rev. **B 44**, 12294, (1991);

[43] L. de Arcangelis, A. Hansen, H. J. Herrmann and S. Roux: Phys. Rev. B **40**, 877 (1989), E. Luis and F. Guinea: Europhys. Lett. **3**, 871 (1987).

[44] A. Hansen, E. L. Hinrichsen, S. Roux, H.J. Herrmann and L. de Arcangelis: Europhys. Lett. **13**, 341 (1990).

[45] P. Bak and K. Sneppen: Phys. Rev. Lett. **71**, 4083 (1993), H. Flyvbjerg, K. Sneppen and P. Bak: Phys. Rev. Lett. **71**, 4087 (1993).

[46] L. Pietronero, W. R. Schneider and A. Stella: Phys. Rev. A **42**, R7496 (1990), L. Pietronero and W. R. Schneider: Physica **A 170**, 81 (1990).

[47] M. Marsili, A. Gabrielli, R. Cafiero and L. Pietronero in preparation.

[48] L. Furnberg, J. Feder, A. Aharony and T. Jossang, Phys. Rev. Lett. **61**, 2117, (1988); S. Roux and E. Guyon J. Phys. **A 22**, 3693, (1989).

[49] M. Marsili: *Renormalization Group approach to the self organization of a simple model of biological evolution* submitted to Europhys. Lett. 1994.

[50] J. T. Chayes, L. Chayes and C. M. Newman: Commun. Math. Phys. **101**, 383 (1985).

[51] J. P. Bouchaud, A. Comtet, A. Georges and P. Le Doussal, Ann. Phys. **201**, 285 (1990).

[52] M. Lederman, R. Orbach, J. M. Hamman, M. Ocio and E. Vincent: Phys. Rev. B **44**, 7403 (1991) and references therein.

[53] E. Marinari and G. Parisi, *On Toy Aging*, preprint, Roma La Sapienza 962–93.

[54] C. W. Gardiner and S. Chaturvedi: J. Stat. Phys. **17**, 429 (1977); see also D. Elderfield: J. Phys. A **18**, L773 (1985).

[55] P. G. de Gennes: *Scaling Concepts in Polymer Physics* (Cornell University Press, Ithaca, 1979).

[56] T. S. Ray and N. Jan, Phys. Rev. Lett. **72**, 4045, (1994).

[57] A. Erzan, L. Pietronero and A. Vespignani, preprint to appear in Rev. Mod. Phys. (1995).

[58] R. De Angelis, M. Marsili, L. Pietronero, A. Vespignani and H. J. Wiesmann Europhys. Lett. **16**, 417, (1991).

[59] L. Pietronero, A. Vespignani and S. Zapperi, Phys. Rev. Lett. **72**, 1690 (1994).

[60] M. Paczuski, S. Maslov and P. Bak *Field Theory of Self Organized Criticality* preprint.

[61] M. Marsili: *Run Time Statistics in Models of Growth in Disordered Media.* To appear in Nov. 1994 issue of J.Stat.Phys.

[62] F. Beleznay, J. Phys. **A19**, 33 (1986).

[63] J. W. Essam, A. J. Guttmann and K. De Bell J. Phys. **A 21**, 3815, (1988).

[64] J. M. Carlson and J. S. Langer: Phys. Rev. Lett. **62**, 2632 (1989)

[65] D. Dhar : Phys Rev. Lett. **64**, 1613 (1990)

[66] T. Hwa, M. Kardar: Phys. Rev. Lett. **62**, 1813 (1989)

[67] M. Eden *Fourth Berkeley Symposium on Mathematics, Statistics and Probability* Vol. 4, ed. F. Neyman (Berkeley, CA: Univ. of California, 1961).

[68] T. A. Witten L. M. Sander, Phys. Rev. Lett. **47**, 1400, (1981).